Cell

Extracellular pectin-RALF phase separation mediates FERONIA global signaling function

Graphical abstract

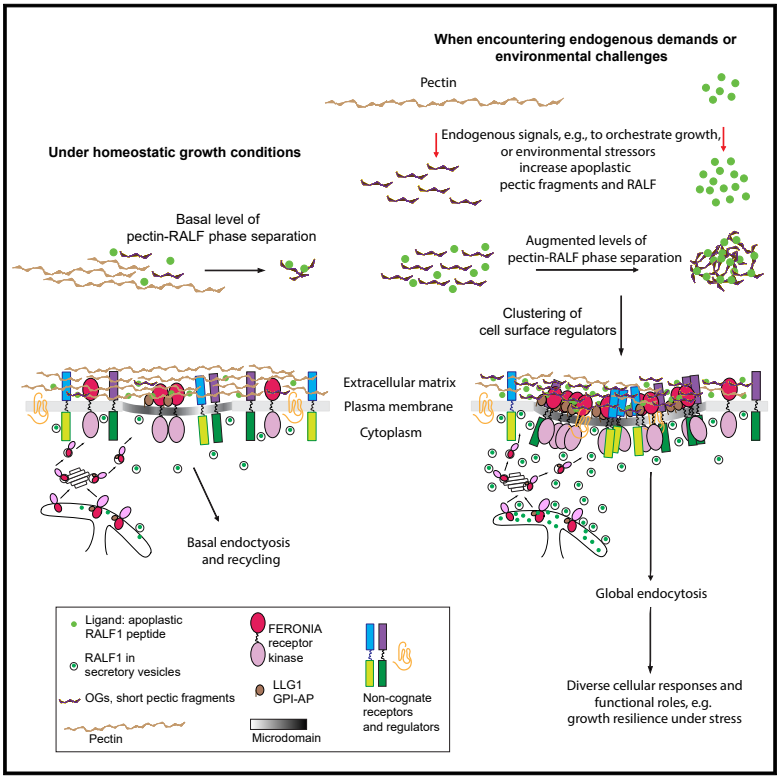

Highlights

- Cell surface pectin-RALF1 phase separation recruits FERONIA-LLG1 into condensates
- RALF induces FERONIA-LLG1-dependent promiscuous receptor clustering and endocytosis
- RALF1-pectin molecular condensates function as surface sensors for stress signals
- FERONIA-LLG1-mediated global endocytosis ensures plant resilience under stress

Authors

Ming-Che James Liu, Fang-Ling Jessica Yeh, Robert Yvon, ..., James Chambers, Hen-Ming Wu, Alice Y. Cheung

Correspondence

hmwu@biochem.umass.edu (H.-M.W.), acheung@biochem.umass.edu (A.Y.C.)

In brief

In deciphering the global signaling capacity of FERONIA receptor kinase, Liu, Yeh, et al. discovered an extracellular phase separation process driven by FERONIA peptide ligand RALF-cell wall polysaccharide pectin interaction, which leads to cognate and non-cognate receptor clustering and promiscuous endocytosis as a coping mechanism in response to environmental stressors.

Liu et al., 2024, Cell *187*, 312–330
January 18, 2024
https://doi.org/10.1016/j.cell.2023.11.038

CellPress

CellPress

Cell

Article

Extracellular pectin-RALF phase separation mediates FERONIA global signaling function

Ming-Che James Liu,[1,5] Fang-Ling Jessica Yeh,[1,4,5] Robert Yvon,[1,2,6] Kelly Simpson,[1,2] Samuel Jordan,[1,7] James Chambers,[3] Hen-Ming Wu,[1,2,*] and Alice Y. Cheung[1,2,4,8,*]

[1]Department of Biochemistry and Molecular Biology, University of Massachusetts, 710 N. Pleasant St., Lederle Graduate Tower, Amherst, MA 01003, USA

[2]Molecular and Cell Biology Program, University of Massachusetts, Amherst, MA 01003, USA

[3]Light Microscopy Core Facility, Institute of Applied Life Sciences, University of Massachusetts, Amherst, MA 01003, USA

[4]Plant Biology Graduate Program, University of Massachusetts, Amherst, MA 01003, USA

[5]These authors contributed equally

[6]Present address: Department of Chemistry and Chemical Biology, Harvard University, Cambridge, MA 02138, USA

[7]Present address: FOG Pharma, 30 Acorn Park Drive, Cambridge, MA 02140, USA

[8]Lead contact

*Correspondence: hmwu@biochem.umass.edu (H.-M.W.), acheung@biochem.umass.edu (A.Y.C.)

https://doi.org/10.1016/j.cell.2023.11.038

SUMMARY

The FERONIA (FER)-LLG1 co-receptor and its peptide ligand RALF regulate myriad processes for plant growth and survival. Focusing on signal-induced cell surface responses, we discovered that intrinsically disordered RALF triggers clustering and endocytosis of its cognate receptors and FER- and LLG1-dependent endocytosis of non-cognate regulators of diverse processes, thus capable of broadly impacting downstream responses. RALF, however, remains extracellular. We demonstrate that RALF binds the cell wall polysaccharide pectin. They phase separate and recruit FER and LLG1 into pectin-RALF-FER-LLG1 condensates to initiate RALF-triggered cell surface responses. We show further that two frequently encountered environmental challenges, elevated salt and temperature, trigger RALF-pectin phase separation, promiscuous receptor clustering and massive endocytosis, and that this process is crucial for recovery from stress-induced growth attenuation. Our results support that RALF-pectin phase separation mediates an exoskeletal mechanism to broadly activate FER-LLG1-dependent cell surface responses to mediate the global role of FER in plant growth and survival.

INTRODUCTION

The collective activities orchestrated by diverse cellular processes support and regulate growth and development. In times of danger, life forms from microbes to multicellular organisms react rapidly to deploy various and often interconnected stress responses to cope and survive.[1] Plants, unable to move, have evolved elaborate strategies on the genetics and epigenetics, cellular, molecular, and biochemical levels in response to environmental stressors, such as heat, drought, and high salinity.[2] Rapid deployment of these strategies is critical to reduce irreversible damage. Growth is often attenuated, allowing plants to adapt, become resilient, and maintain the capacity to recover when more favorable conditions return. How to orchestrate a coordinated response from numerous cellular pathways to achieve a life-sustaining response is complex and far from understood. FERONIA (FER) receptor kinase in the model plant *Arabidopsis* has emerged in recent years as a prime candidate for a regulator of a plethora of cellular and molecular responses to ensure growth and survival,[3] offering an excellent opportunity to explore how coordinated control of multiple and diverse cellular pathways might be achieved.

FER and its co-receptor LLG1 (LORELEI-LIKE glycosylphosphatidylinositol-anchored protein [GPI-AP] 1) profoundly impact a broad range of processes throughout the plant life cycle.[3–5] Functioning with their peptide ligand rapid alkalinization factor (RALF),[6,7] the RALF-FER-LLG1 signaling module[3,8,9] (Figures S1A–S1D) has been linked to growth regulation and intersects multiple major hormone-regulated processes,[10–13] reproduction,[14–19] and responses to environmental stresses such as high salinity,[20,21] high light,[22] and pathogens.[8,23,24] The FER cytoplasmic domain interacts directly with guanine exchange factors to activate RAC/ROPs (RHO GTPases of plants)[10] and signal nicotinamide adenine dinucleotide phosphate (NADPH) oxidase-dependent production of reactive oxygen species (ROS)[9,10,15,18,19] (Figure S1B). Similar to their counterparts, RHO GTPases in animals and yeast, RAC/ROPs are major molecular switches controlling myriad signaling pathways in

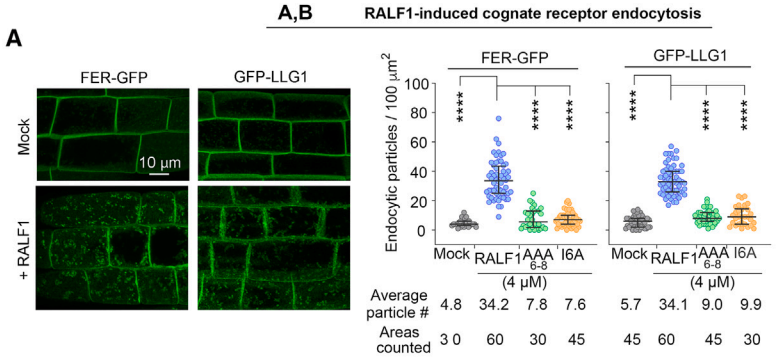

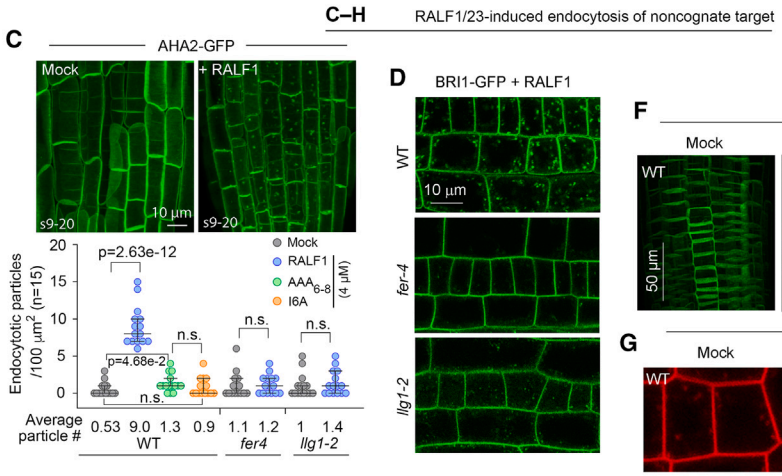

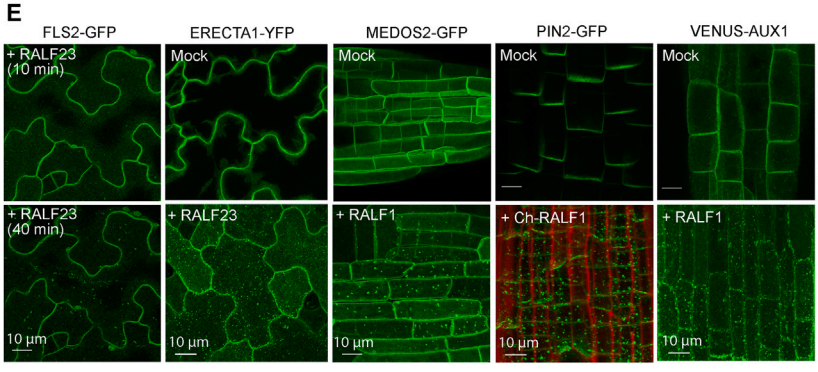

H

Target	Function	Response to RALF1/23
FER-GFP GFP-LLG1	Co-receptors[9]	Endocytosed
AHA2-GFP	H^+-ATPase[47]	Endocytosed
BRI1-GFP	Brassinosteroid receptor[48,54]	Endocytosed
FLS2-GFP	Immunity receptor[23,24]	Endocytosed
ERECTA-YFP	Stomagen receptor for epidermal patterning[49]	
MEDOS-GFP	FER-related, immunity signaling[50]	Endocytosed
PIN2-GFP	Auxin transport (efflux)[11]	Endocytosed
VENUS-AUX1	Auxin transport (influx)[11]	Endocytosed
REM1.2-YFP	Microdomain-associated[51,52]	Endocytosed
FM4-64	Plasma membrane dye[53]	Endocytosed
LTI1.6-YFP	Membrane marker protein[20]	Not-endocytosed

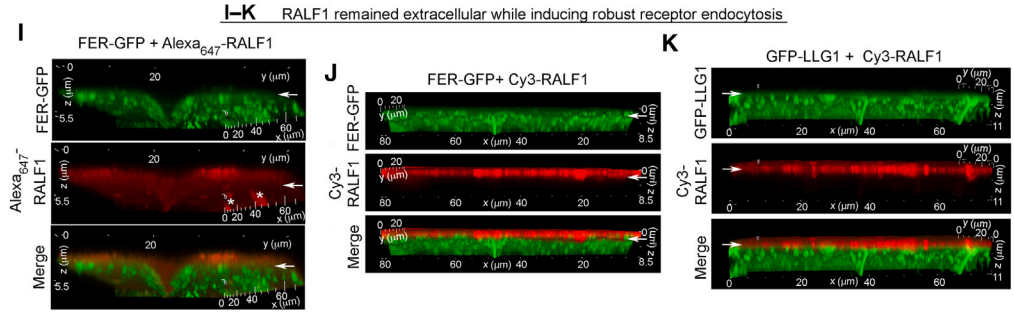

(legend on next page)

plants and ROS are ubiquitous second messengers.[25] This core FER-LLG1-RAC/ROP-ROS signaling pathway allows for expansive functional diversification, from polarized cell growth[9,10,26] to male-female interaction.[15–18] FER also impacts a complex network of cytoplasmic and nuclear pathways,[27] including processes controlled by phytochrome, the photoreceptor and key regulator of growth and development.[21] However, an overarching view of how FER-LLG1 achieves its broad functional range remains unclear.

Several considerations prompted our search for a mechanism that enables the immense functional versatility of FER-LLG1 at the cell surface, the frontline of signal perception. GPI-APs are important for signaling regulation and, as a class, are known to be localized in membrane microdomains where regulatory molecules concentrate.[28] LLG1 chaperones FER to its functional location, presumably positioning FER-LLG1 in LLG1-destined membrane subdomains.[9] The plant cell wall maintains tight linkages with the cell membrane and impinges on its biological activities.[29,30] Pectin, a major polysaccharide in the cell wall, is indispensable to plant growth and survival.[31,32] The FER extracellular domain (FERecd), characterized by homology with the animal diglucose-binding protein Malectin[4,5,33] (Figure S1A), binds pectin.[20,26] This interaction impacts cell wall quality and several FER-controlled biological processes.[18,20,26] FERecd and RALF also interact with leucine-rich repeat extensins, which tightly associate with the cell wall and participate in growth regulation.[34–36] FER also intersects cell wall remodeling and defense-related processes linked to lignin, an important polymer in secondary cell walls.[37]

Liquid-liquid phase separation (LLPS) is emerging as a major mechanism controlling diverse biological processes.[38–40] They occur in the nucleus or cytoplasm and involve multivalent molecules, such as nucleic acid. Intrinsically disordered proteins are structurally flexible and have the propensity to interact with and recruit diverse molecules through specific and multivalent interactions, concentrating them into molecular condensates to potentiate the activation of specific biological processes. RALFs are intrinsically disordered peptides.[6,7] Pectin, with its homogalacturonan, or polygalacturonic acid (PGA), backbone (Figure S1E), is well known to have the capacity for phase transitions in response to changing conditions in its environment.[31,32,41] *In planta*, this capacity might be key to unique decorations of certain plant cell surfaces, such as the elaborate sculpting of the pollen coat, and modifications of cell walls in response to cellular demands or environmentally induced challenges.[41] Here, we report that RALF and pectic fragments phase separate at the cell wall-cell membrane interface, forming RALF-pectin condensates to mediate a mechanism that enables the global signaling role of FER-LLG1. We show that RALF induces FER and LLG1 clustering and endocytosis and promiscuously induces widespread non-cognate receptor clustering and endocytosis in a FER- and LLG1-dependent manner, fitting of the broad biological roles played by FER-LLG1. We show further that RALF-pectin phase separation responds to high salt and elevated temperatures, providing an extracellular sensing mechanism to trigger promiscuous FER- and LLG1-dependent cell surface responses and activate a coping strategy to ensure resilience against environmental stresses.

RESULTS

RALF induces promiscuous endocytosis but remains extracellular

We first examined how RALF impacts its cognate coreceptors FER and LLG1. We used RALF1[42] and RALF23[23,34] since they are closely related and each is best characterized in its predominantly expressed location, root and aerial tissues, respectively, and ascertained that their biological activities are comparable[7] (Figures S1F and S1G). Typical of ligand-receptor interaction,[43–45] recombinant RALF1, RALF23, and synthetic RALF1 induced FER and LLG1 endocytosis[46] (Figures 1A and S2A–S2F). The N-terminal $YISY_{5–8}$ motif is conserved in a subset of RALFs (Figure S1D).[6–8] RALF1(I6A), traditionally used in RALF studies,[6,42] did not notably impact binding to FERecd but substantively reduced interaction with LLG1 (Figures S2G–S2J).[8] I6A was severely impaired in its capacity to induce medium alkalinization or inhibit root growth (Figures S1F, S1H, and S1I),[6,7,42] as did and the mutant $ISY_{6–8} \rightarrow AAA_{6–8}$. These N-terminal RALF1 mutants also failed to trigger FER and LLG1 endocytosis (Figures 1A, 1B, and S2K–S2M). These results established that ligand-receptor interaction, in particular via the interaction between the RALF1 YISY region and LLG1, as suggested by crystallographic data,[8] was critical for ligand-triggered cognate receptor endocytosis, connecting ligand-modulated receptor density to the cell growth-regulatory activities of RALFs.

Figure 1. RALF induces promiscuous endocytosis but itself remains extracellular

4-day-old *Arabidopsis* seedlings expressing various fluorescent protein (FP)-tagged cell membrane proteins were used. Figures S1F–S1K shows representative RALF preparations. Unless otherwise indicated, treatment conditions were 1–4 μM peptide, for 30–40 min. Figures S2A–S2D shows pilot experiments.

(A and B) RALF1 but not N-terminal mutants I6A, $AAA_{6–8}$ induced FER-GFP, and GFP-LLG1 endocytosis. (B) Comparative time courses. See also Figures S2A–S2M.

(C–H) RALF induced endocytosis of non-cognate targets[11,23,47–53] (C–F) and uptake of endocytic dye FM4-64[53] (G). (H) Cognate and non-cognate RALF targets examined and summary responses. See also Figures S2N–S2Q.

(I–K) 3D views of $Alexa_{647}$ (sulfonylated[54]) RALF1 and Cy3-RALF1-induced FER-GFP and GFP-LLG1 endocytosis. Figures S2R and S2S shows Ch-RALF1 also remained extracellular.

(D and G) Single sections (0.25 μm). (A, C, E, and F) Maximum projections of sections covering similar tissue thickness for comparative samples. (I–K) 3D reconstructions from maximum projections. Quantification (A and C), ≥3 replicate seedlings per treatment, 3–5 100 μm^2 from each seedling were quantified for particles (≥0.5 μm); scatter-dot plots are from one representative experiment; center, upper and lower lines indicate median, upper and lower quartiles. In (B), total intracellular GFP signals (from 166 μm^2 areas) were quantified by Image J. Data = average signal intensity ± SD, (n = 5–6 cells); *$p < 0.05$,**$p < 10^{-2}$,***$p < 10^{-3}$,****$p < 10^{-4}$ by Student's t tests, two-tailed, and paired; n.s, non-significant. All experiments were repeated at least three times with comparable results. See STAR Methods for details.

	Experiment	Sample
B	Endocytosis response of cognate receptors to RALF1 and RALF1(I6A)	Seedlings
C,D	Dynamics of cognate receptor clustering and endocytosis response by TIRFm	Seedlings
E	Clustering respoose of cognate receptors to RALF1 and RALF1(I6A)	Agroinfiltrated leaves
F	Colocalization of ligand and co-receptors in RALF1-induced receptor clusters	Agroinfiltrated leaves
G	Clustering response of FER and FLS2 to RALF1 and immunity elicitor flg22	Agroinfiltrated leaves
H	Clustering response of FLS2 and BRI1 to RALF1 aand RALF1(I6A)	Agroinfiltrated leaves

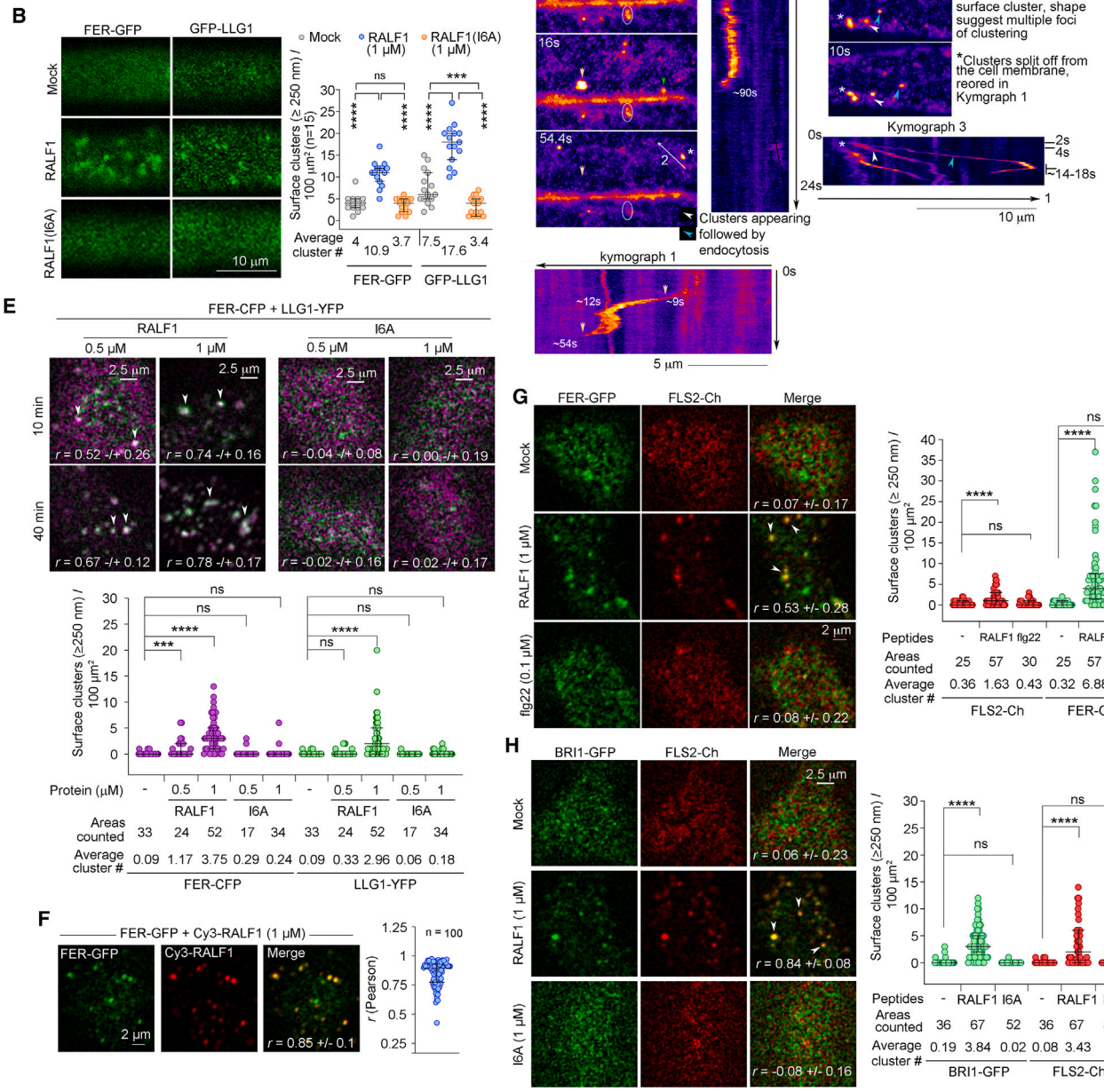

(legend on next page)

We extended the analysis to other key cell surface regulators of growth and immunity. We examined the *Arabidopsis* H^+-ATPase AHA2 first because its H^+-efflux activity acidifying the apoplastic space is central to cell growth,[47] RALFs induce medium alkalinization[6,7] and RALF1 affects the phosphorylation state of AHA2,[42] albeit not at the penultimate phospho-target site known to be key for activation.[47] We observed that RALF1, but not the N-terminal mutants, induced AHA2-GFP endocytosis (Figures 1C and S2N). Thus RALF1-induced reduction of AHA2 abundance in the cell membrane could be among the underlying factors for its medium alkalinization and growth-inhibition activities. Furthermore, RALF1 and RALF23 triggered robust endocytosis of a variety of fluorescent protein (FP)-tagged cell surface regulators[45,48–53] and augmented the uptake of the general endocytic marker dye FM4-64[53] into the cytoplasm (Figures 1D–1H, S2O, and S2P). Results based on FM4-64 uptake imply that the impact could be widespread. However, an often-used cell membrane marker protein[20] was not affected (Figure S2Q), indicating that while promiscuous, RALF-induced endocytosis was not without selectivity.

The RALF1 capacity to induce endocytosis of cognate and non-cognate targets was exceptional to typical ligand-induced endocytosis, which specifically targets the ligand-bound cognate receptor for endocytosis to modulate the activated signaling response.[43–45] We examined whether the RALF-induced endocytosis of non-cognate targets was connected to its interaction with FER-LLG1. For the regulators examined and FM4-64 uptake, their endocytic response to RALF was severely hampered in *fer-4* and *llg1-2* mutants (Figures 1C, 1D, 1F, 1G, S2N, and S2O), showing that the RALF1-triggered endocytosis of non-cognate targets was dependent on the presence of its cognate coreceptors.

In ligand-induced receptor endocytosis, ligands are typically internalized with the bound receptors.[43–45,54] However, Cherry (Ch)-RALF1 and various small fluorochrome-labeled peptides (Figures S1J–S1M) were not taken up into the cell while actively inducing FER and LLG1 endocytosis (Figures 1I–1K, S2R, and S2S). Since FER binds pectin[20,26] and RALF binds FER,[23,42] the extracellular retention of RALF1 might involve interactions with the cell wall, preventing its extraction by the endocytic machinery. Together, results here uncovered a RALF-triggered FER-LLG1-dependent mechanism at the cell surface that is unconventional but capable of simultaneously impacting multiple functional pathways upon ligand binding, thus enabling the multifaceted biological roles of FER-LLG1.

RALF recruits and induces multiple receptor clustering in the cell membrane

We then explored the mechanism that enables RALF-triggered FER- and LLG1-dependent promiscuous endocytosis (Figure 2A). Imaging tangential sections of seedling root cells showed wild-type (WT) but not I6A mutant RALF1 stimulated FER-GFP and LLG1-GFP clustering in the cell membrane (Figure 2B), correlating with their differential capacity in inducing receptor endocytosis (Figures 1A and 1B) and growth-regulatory activities (Figures S1H and S1I). Total internal reflection fluorescence microscopy (TIRFm)[51,55,56] showed the dynamics of RALF1-triggered FER-GFP and GFP-LLG1 clustering in the cell membrane, followed by their excision and endocytosis (Figures 2C and 2D; Videos S1, S2, S3, and S4), consistent with ligand-induced receptor clustering and endocytosis being in a continuum of cell surface receptor responses upon ligand binding.[43,57–59]

With an intact cell wall, agroinfiltration transformed *Nicotiana benthamiana* leaf epidermal cells is broadly used in signal transduction studies due to their versatility and reliability in reflecting *in planta* phenomena, including studies related to the organization of co-expressed receptors in the cell membrane.[51,52,55] Using agroinfiltration, we determined that RALF1 (Figures 2E and S3D–S3F) and RALF23 (Figure S3I) induced FER and LLG1 co-clustering in the leaf cell surface while RALF1(I6A) was severely hampered in this activity. Application of Cy3-RALF1 to FER-GFP-expressing cells revealed the peptide ligand also colocalized with the receptor clusters (Figure 2F), implying a tripartite RALF-FER-LLG1 complex[8,9] before receptor endocytosis. We then examined whether RALF would induce clustering of other non-cognate targets using Brassinosteroid Insenstivie 1 (BRI1)[54] and Flagellin-sensitive 2 (FLS2)[45] as representatives because RALF1 impacts BRI1 signaling[6,48] and FLS2 intersects RALF-FER-LLG1 signaling.[23,24] BRI1 and FLS2 share the same co-receptor and some downstream signaling components.[60] Studies in transformed *Arabidopsis* seedlings and transiently transformed *N. benthamiana* leaf cells showed that BRI1 and FLS2 formed distinct, non-overlapping nanodomains in response to their respective ligands brassinosteroid (BR) and flagellin 22 (flg22).[55] Here, we observed that RALF induced co-clustering of FER-GFP and FLS2-Ch (Figures 2G and S3J), FER-GFP and BRI1-CFP (Figure S3K). However, unlike flg22,[55] RALF also induced co-clustering of BRI1-GFP and FLS2-Ch and their endocytosis (Figures 2H and S3L); RALF1(I6A) lacked this activity (Figure 2H, bottom row). When BRI1-GFP and

Figure 2. RALF induces clustering of cognate and non-cognate cell surface receptors

(A) List of experiments and samples.

(B–D) *Arabidopsis* seedlings. (B) RALF1 but not I6A mutant induced FER-GFP and GFP-LLG1 clustering. (C and D) TIRFm of RALF-induced receptor clustering and endocytosis showed a continuum of receptor clustering (arrowheads) to endocytosis (*); some clusters were less dynamic (ellipse). Numbered arrows designate kymographs. See Videos S1, S2, S3, and S4. Figures S3A and S3B shows control.

(E and F) *N. benthamiana* (Figure S3C show workflow). (E and F) Ligand-induced clustering of cognate receptors. (E) WT but not I6A mutant RALF1 induced FER-CFP and LLG1-YFP co-clustering. (F) Ligand and receptor colocalization and (*r*), Pearson's colocalization coefficient.

(G) RALF1 induced co-clustering of cognate FER-GFP and non-cognate FLS2-Ch receptor; immunity elicitor flg22 did not.

(H) RALF1 but not I6A induced co-clustering of non-cognate receptors BRI1-GFP and FLS2-Ch.

Figures S3D–S3H shows related RALF1-treatment data; Figures S3I–S3M show results from RALF23. (*r*) in panels, average Pearson's correlation coefficients of colocalization. Images (B) and (E)–(H) are single surface sections (0.25 μm); images and data plots are from 30 to 40 min samples. Cluster (arrowheads) quantification (≥0.25 μm in 100 μm^2 areas) followed that described in Figure 1. *r* analyses were from ≥20 equal-sized regions of interest from three replicate samples for each treatment in one experiment and used FIJI according to Bücherl et al.[55] Random analysis of entire areas shown in images (NIS, NIKON) yielded similar results. *p, as designated in Figure 2; n.s., non-significant.

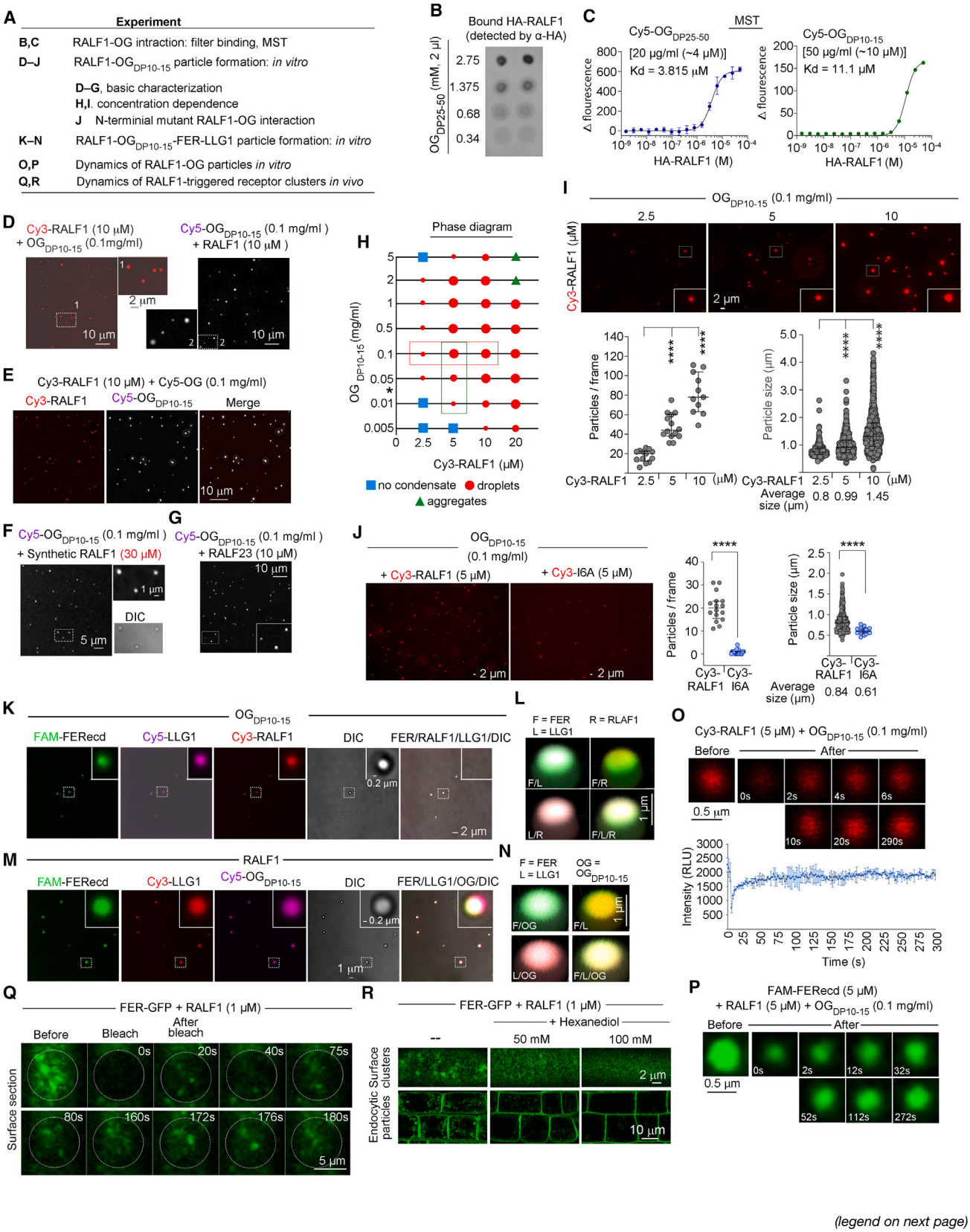

(legend on next page)

FLS2-Ch were co-expressed in *fer-4* and *llg1-2* mutant seedlings, RALF1-triggered co-clustering was notably subdued than when expressed in wild-type (Figure S3N). Taken together, these observations support the notion that RALF-induced non-cognate receptor clustering depended on RALF interaction with the cognate receptors FER and LLG1.

Together, these results established that RALF triggers the clustering of cognate and non-cognate receptors, concentrating them into nano- to microsized membrane subdomains. These would potentiate not only the activation of FER-LLG1 signaling but also signaling from the non-cognate BRI1 and FLS2 receptors. These results also underscore a key difference between RALFs from ligands that typically act only on their cognate receptors, such as flg22 and BR, a mechanism attributed to maintaining specificity in signaling.[55] It is plausible that partnering with an intrinsically disordered peptide ligand with the capacity for multivalent interactions represents a design evolved to enable FER-LLG1 for diverse functional roles. Furthermore, the RALF-triggered recruitment of FLS2 to FER (Figures 2G and S3J) and endocytosis could contribute to sequestering FLS2 from activation by its cognate ligand, providing a mechanistic linkage to how RALF23 negatively regulates flg22-triggered FLS2 signaling.[23]

RALF-pectin phase separation promotes the assembly of pectin-RALF-FER-LLG1 condensates *in vitro* and *in planta*

We speculated that RALF retention extracellularly while inducing robust endocytosis (Figures 1I–1K) might be due to physical interactions between RALF and cell wall matrix molecules, pectin in particular since it has major involvements in FER-LLG1/LORELEI functions.[18,20,26] Indeed, binding assays detected RALF1 interaction with de-esterified pectin of variant sizes, with degree of oligogalacturonide (OG) polymerization (DP) between 10 and 15 ($OG_{DP10–15}$), which are biologically active,[61–63] 25–50 ($OG_{DP25–50}$) and longer fragmented PGA (f-PGA) (Figures 3A–3C and S4A–S4C, left). We reaffirmed pectin-FERecd interaction (Figure S4C, right) and established that pectin did not bind LLG1 (Figure S4D).

RALF1 is predicted to be largely disordered (from Predictor of Natural Disordered Region, http://www.pondr.com). While there are many examples of disordered proteins that undergo phase separation,[38–40] RALF1 alone did not form typical phase-separated condensates *in vitro* (Figure S4E). Pectin is prone to undergo phase transition,[41] but short pectic fragments on their own did not form notable congregates *in vitro* (Figure S4E). However, when combined, RALF1 and $OG_{DP10–15}$ assembled into congregates readily detected by light microscopy (Figures 3D and 3E). Synthetic RALF1 and recombinant RALF23 also assembled with $OG_{DP10–15}$ (Figures 3F and 3G). We refer to these RALF-pectin congregates interchangeably as particles, clusters, or condensates from hereon. We determined that the assembly was dependent on RALF1 and $OG_{DP10–15}$ concentrations (Figures 3H, 3I, S4F, and S4G). It was impacted by the conserved N-terminal YSIY motif since the mutant I6A showed diminished capacity in the assembly, producing significantly fewer and smaller particles with $OG_{DP10–15}$ (Figure 3J).

We next investigated how RALF, pectin, FER, and LLG1 might interact together since *in vivo* they occur together in the extracellular milieu. Combining differentially labeled RALF1, FER-ecd, LLG1 with $OG_{DP10–15}$, $OG_{DP25–50}$, or f-PGA (Figure S4A), we observed that FER and LLG1 readily assembled with RALF1 and varying sizes of pectic fragments into particles that comprised all four components (Figures 3K–3N, S4H, and S4I). We also determined that both RALF1 and pectin were required for the assembly of these pectin-RALF1-FER-LLG1 particles (Figure S4J), indicating that RALF-pectin complexes nucleated these molecular condensates. Pectin-RALF self-assembly and the formation of pectin-RALF-FER-LLG1 particles suggest a spontaneous demixing process akin to LLPS driving the formation of molecular condensates, often a highly dynamic process.[38–40] Fluorescence recovery after photobleaching (FRAP), often used in phase separation studies,[38–40] showed rapid fluorescence recovery from bleached pectin-RALF1 and pectin-RALF1-FERecd condensates (Figures 3O and 3P; Video S5), reflecting a dynamic recruitment process akin to LLPS had supported their formation.

RALF1-pectin phase separation contributes to RALF1-triggered biological responses

The high local concentrations of molecules congregated into phase-separated condensates could potentiate biological

Figure 3. Pectin-RALF phase separation and assembly of pectin-RALF-FER-LLG1 condensates *in vitro* and *in vivo*

(A) List of experiments.

(B and C) RALF1-pectin binding *in vitro*. (B) Dot blot with immobilized $OG_{DP25–50}$; (C) MST using Cy5-$OG_{DP25–50}$ or Cy5-$OG_{DP10–15}$ as targets for HA-RALF1 binding. Figures S4A–S4D shows related studies.

(D and E) Pectic fragments and RALF1 assembly. Labeled and unlabeled RALF1 and OG are as indicated, yielding comparable results. Alone, neither form notable condensates (Figure S4E).

(F and G) Synthetic RALF1 and RALF23 assembly with Cy5-$OG_{DP10–15}$.

(H and I) Concentration dependence of RALF-OG assembly. (H) Phase map showing concentration dependence on both RALF and $OG_{DP10–15}$. Droplets sizes = condensate numbers. *OG concentration used in fluorescence anisotropy analyses (see below). Figure S4F shows representative images. (I) Representative data of assembly dependence on RALF1 concentration; Figure S4G shows representative data for dependence on OG concentration.

(J) Mutant I6A-$OG_{DP10–15}$ assembly.

(K–N) *In vitro* assembly of $OG_{DP10–15}$-RALF1-FER-LLG1 nanoparticles. (K and L) unlabeled $OG_{DP10–15}$ (0.1 mg/mL) and fluorescence tagged RALF1 (10 μM), FERecd (5 μM), LLG1 (5 μM). (M and N) unlabeled RALF1 (10 μM), and fluorescence tagged $OG_{DP10–15}$ (0.1 mg/mL), FERecd (5 μM), LLG1 (5 μM). (L) and (N) are cross-sections from a 3D reconstruction of particles from (K) and (M). Figures S4H–S4J shows various combinations of pectic fragments and RALF1s all yielding comparable results.

(O and P) FRAP of Cy3-RALF1-$OG_{DP10–15}$ condensates (O; Video S5) and RALF1-$OG_{DP10–15}$-FAM-FERecd condensates (P).

(Q) FRAP of RALF1-induced surface receptor clusters in FERp:FER-GFP seedling root cell surface.

(R) Hexanediol inhibited RALF1-induced receptor clustering and endocytosis; Figure S4K shows quantified data. Figure S4L shows hexanediol effect on *in vitro* assembled Cy3-RALF1-$OG_{DP10–15}$ particles.

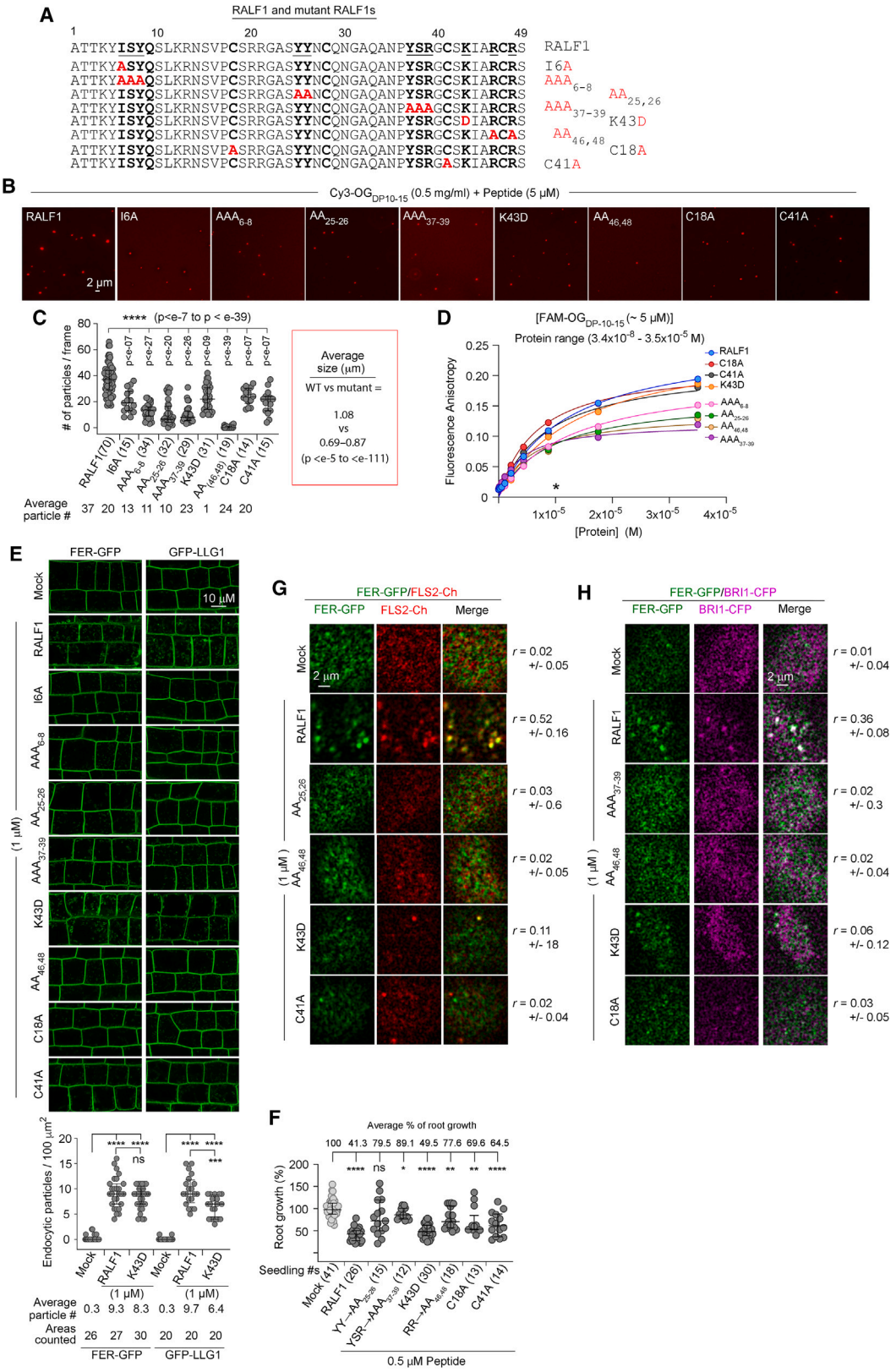

(legend on next page)

processes *in vivo* by activating constituent activities.[38–40] RALF1 triggers cytoplasmic [Ca^{2+}] spike in a FER-dependent manner[42] and the activity was dependent on the N-terminal YISY motif (Figures S5A–S5C). We ascertained that RALF1 and pectin are biologically connected because chemically disrupting the normal pectic environment in seedlings[29] obliterated the RALF1-induced response (Figure S5D), and similar to RALF1, $OG_{DP10–15}$ also triggered FER-dependent [Ca^{2+}] spike (Figure S5E). We then asked whether RALF and pectin also phase separate to form RALF-pectin condensates along the cell surface and whether the phenomenon could be linked to RALF-triggered receptor clustering. When we photobleached RALF1-induced FER-GFP receptor clusters, rapid FRAP followed reflecting a dynamic receptor recruitment process *in vivo* (Figure 3Q). Moreover, hexanediol, another often-used reagent to interfere with LLPS in biological studies,[38–40] severely hampered RALF1-induced FER-GFP clustering and endocytosis (Figures 3R and S4K). However, *in vitro*, the impact of hexandiol was more limited resulting only in reducing the number and sizes of $OG_{DP10–15}$-RALF1 condensates (Figure S4L). The differential *in vitro* and *in vivo* responses to hexanediol interference suggest additional parameters were likely involved in the *in vivo* RALF-triggered receptor clustering and endocytosis.

To further explore the biological significance of RALF-pectin interaction, we generated additional RALF1 mutants (Figure 4A) to examine how the mutations might impact RALF1-OG phase separation *in vitro* and RALF1-triggered responses *in planta*. Similar to RALF1(I6A) (Figure 3J) and relative to WT RALF1, these mutants were impaired in forming peptide-$OG_{DP10–15}$ condensates, producing significantly fewer and smaller particles (Figures 4B, 4C, and S4N). Importantly, mutations in the C-terminal region arginine residues ($RR_{46,48}$AA) profoundly impacted the mutant RALF1 ability to form condensates with $OG_{DP10–15}$, and those in tyrosine residues ($ISY_{6–8}$AAA, $YY_{25,26}$AA, $YSR_{37–39}$AAA) also significantly reduced the peptide efficacy in this process. These observations were consistent with the positively charged C-terminal region being important for interaction with the negatively charged pectin and aromatic π-π interaction mediated by tyrosine residues being important for RALF1-pectin phase separation. The K43D mutant was the least affected; we note that the lysine 43 position is often replaced by an uncharged amino acid,[7] e.g., in RALF23 (Figure S1D). Interestingly the two mutations at C18 and C41, which are predicted to form disulfide bridges with C28 and C46, respectively, only moderately impacted the activity of the C18A and C41A mutant RALF1.

Consistent with these results from peptide-OG condensation, fluorescence anisotropy analysis also clustered the RALF1 mutants into two groups, the tyrosine residue and terminal arginine mutants displayed more notably reduced anisotropy from WT RALF1 while the remaining mutants showed anisotropies closer to that of the WT peptide (Figures 4D and S4O). The higher fluorescence anisotropies generated by WT RALF1-$OG_{DP10–15}$ interaction reflected slower tumbling of complexes relative to those formed with mutant RALF1s, thus consistent with the reduced capacity of the mutant RALFs to form larger-sized complexes.

To explore the connection between RALF-pectin condensation and RALF-pectin-triggered biological responses, we compared the capacity of WT and mutant RALF1s in inducing FER and LLG1 endocytosis and root growth inhibition. The RALF1 mutants were considerably compromised in triggering receptor endocytosis and inhibiting root growth (Figures 4E and 4F). They were also hampered in their capacity to induce the coalescence of non-cognate and cognate receptors to form co-receptor clusters on the plant cell surface (Figures 4G, 4H, and S4P). Consistent with the *in vitro* peptide-OG interaction, the K43D mutant was the least impacted in these biological assays. These results together further support the importance of the OG-RALF1 condensates in nucleating multivalent interactions with multiple cell surface molecules to broadly impact diverse biological processes.

Pectin status is crucial for RALF-triggered receptor clustering and endocytosis

We then pursued a series of experiments to solidify the conclusion that RALF-pectin interaction is crucial for RALF-triggered clustering of its cognate receptors and their endocytosis and that this process also extends to non-cognate targets (Figure 5). Pectin is the most dynamic component of the plant cell wall and its homeostasis is regulated by many pectin-modifying and degradative agents[31,32,61–63] (Figure 5A). For instance, methyl-esterified pectin secreted by the cell is de-esterified by cell wall-located pectin methylesterases (PMEs), which are inhibited by cell-wall-located enzymes PME inhibitors (PMEIs). Pectin degradative enzymes, such as polygalacturonase ADPG1,[32,64] degrade de-esterified pectin to pectic fragments of varying sizes, including biologically active OGs, which are inactivated by OG oxidases, such as OGOX1.[65] Epigallocatechin gallate (EGCG) is an often-used chemical inhibitor of PMEs to perturb pectin status *in planta*[29,66–68]; EGCG suppressed RALF1-induced clustering of FER-GFP in the cell membrane and its endocytosis (Figure 5B). Seedlings that over-expressed PMEI5 (PMEI5oe) have reduced de-esterified pectin accumulation in the cell surface[67–70] and were less sensitive to RALF-induced root growth inhibition than WT seedlings (Figures S5F–S5I).

Figure 4. Analysis of mutant RALF1s

(A) RALF1 mutant amino acid sequences.

(B and C) Assembly of $OG_{DP10–15}$ with WT and mutant RALF1s *in vitro* and quantified data; (#) number of frames analyzed. Figure S4N shows full data on size quantification.

(D) Fluorescence anisotropy. *Approximates the optimum RALF1-$OG_{DP10–15}$ assembly condition (indicated by * in Figure 3H). See also Figure S4O.

(E and F) Seedling responses to peptide treatments. (E) FER-GFP and GFP-LLG1 endocytosis in seedlings. Endocytic particles (≥0.5 μm) were quantified as described in Figure 1. Except for RALF1 and RALF1(K43D), cytoplasmic puncta in other mutant RALF1-treated seedlings were below the size threshold for measurement. Images were brightness and contrast adjusted as one panel. (F) Root growth; K43D was most comparable with RALF1 activity. *$p < 0.05$, **$p < 10^{-2}$, ****$p < 10^{-4}$; ns, non-significant.

(G and H) Co-clustering response of FER-GFP with non-cognate receptor FLS2-Ch (G) and BRI1-CFP (H) to WT and mutant RALF1 in *N. benthamiana* leaf cells. $AA_{25,26}$ and $AAA_{37–39}$ behaved similarly; C18A and C41A behaved similarly. (*r*) average Pearson's coefficient of colocalization; Figure S4P shows full *r* data.

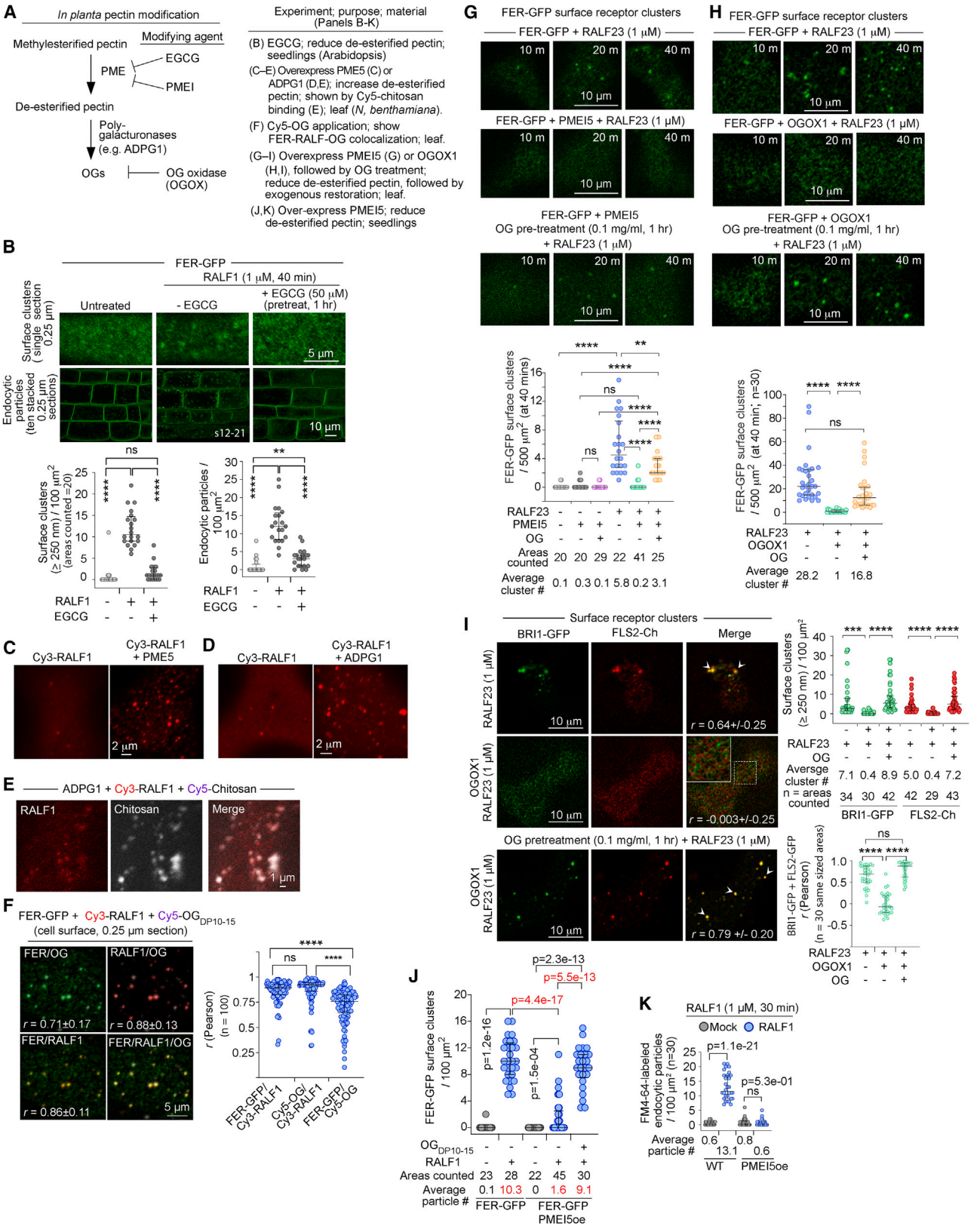

(legend on next page)

These observations indicate that an intact cell wall and properly regulated pectin status are crucial for RALF-signaled responses, from the early response of cytosolic [Ca^{2+}] spike (Figures S5D and S5E) to more sustained receptor and plant growth responses.

To ascertain the involvement of pectic fragments in RALF-triggered receptor clustering, we manipulated the pectin status in the cell wall matrix by transiently expressing in *N. benthamiana* leaves ADPG1 (Figure 5A) to increase the level of pectic fragments in the cell wall.[64] Application of Cy3-RALF1 revealed a small number of nano-sized Cy3-RALF1 surface clusters in control cells whereas they were dramatically increased in cells over-expressing PME5 or ADPG1 (Figures 5C and 5D). The increases in Cy3-RALF1 clusters reflected the impact of more de-esterified pectin and fragmented pectin, including biologically active OGs, in augmenting pectin-RALF condensation. To demonstrate that the augmented Cy3-RALF1 condensates were indeed the product of elevated pectic fragments, we used chitosan decoration as a diagnostic. Chitosan oligosaccharides, derivatives of chitin (polymer of N-acetylglucosamine) bind de-esterified pectin with high affinity[71] (Figure S5F) and have been used to probe the level of de-esterified pectin *in vivo*.[68] We determined that Cy5-$Chitosan_{DP12–20}$ binds *in vitro* assembled RALF-pectin condensates (Figures S5J–S5L). When applied to Cy3-RALF1-treated ADPG1-expressing leaves, Cy5-chitosan decorated the induced Cy3-RALF1 clusters, revealing the ADPG1-driven RALF clusters were indeed RALF-pectin condensates in the cell surface (Figure 5E). Applied Cy5-$OG_{DP10–15}$ was also incorporated into Cy3-RALF1 triggered-FER-GFP cell surface particles (Figure 5F), further supporting that they were assembled from the recruitment of FER-GFP into phase-separated RALF-pectic fragments to assemble into condensates of pectin-RALF-receptor conglomerates *in vivo* along the cell wall-cell membrane interface.

We then directly probe the importance of de-esterified pectic fragments in RALF-induced receptor clustering and endocytosis (Figure 5A). First, we co-expressed FER-GFP with either PMEI5[67] or OGOX1[65] in *N. benthamiana* leaf cells. Both conditions resulted in the suppression of RALF-induced FER-GFP clustering and endocytosis (Figures 5G, 5H upper and middle rows, and S5N). These results were consistent with the prediction that over-expressing PMEI5 would reduce the accumulation of de-esterified pectin, whereas OGOX1 would inactivate biologically active de-esterified pectic fragments in the cell wall matrix (Figure 5A). To further support these notions, the FER-GFP and PMEI5 or FER-GFP and OGOX1 co-expressing leaves were pretreated with $OG_{DP10–15}$ before RALF application. Augmenting the OG level in the cell wall counteracted the inhibitory effects of PMEI5 and OGOX1, restoring RALF-induced receptor clustering and endocytosis (Figures 5G, 5H, and S5N, bottom rows). Similarly, when co-expressed with BRI1-GFP and FLS2-Ch, OGOX1 suppressed RALF-induced co-clustering of these receptors and their endocytosis, and the inhibition was also reversed by $OG_{DP10–15}$ pre-treatment before RALF application (Figures 5I and S5O). Aligned with observations in transiently transformed leaf cells, stably transformed PMEI5oe[67] seedlings that co-expressed FER-GFP were severely deficient in RALF-induced FER-GFP endocytosis, while pre-treatment with $OG_{DP10–15}$ restored the response to mimic that observed in FER-GFP seedlings that lacked the PMEI5oe transgene (Figures 5J and S5P). Furthermore, RALF1-stimulated FM4-64 uptake, and therefore elevated overall endocytosis, was also suppressed in PMEI5oe seedlings (Figures 5K and S5Q). Together these observations provide compelling evidence for biologically active de-esterified pectic fragments being critical for RALF-triggered and pectin-RALF phase separation-mediated clustering of cognate and non-cognate receptors on the cell surface and their ensued endocytosis.

Pectin-RALF-FER-LLG1 mediates downstream signaling and buffers against stress

We next sought evidence for the biological significance of RALF-pectin interaction in FER-LLG1 controlled processes (Figure 6A). We first examined whether RALF and pectin impact the FER to ROS pathway (Figure S1B).[9,10,15,19] We observed that relative to WT seedlings, root ROS level was significantly reduced not only in *fer-4*[10] and *llg1-2*,[9] but also in seedlings with reduced levels of RALF1 (*ralf1-3*, *ralf1-4*) or inhibited in pectin de-esterification (PMEI5oe) (Figures S6A–S6C). RALF1 and $OG_{DP10–15}$ both stimulated ROS levels in WT seedlings and the response was dependent on FER, LLG1, and unperturbed apoplastic

Figure 5. Pectin and RALF coordinately control RALF-triggered FER- and LLG1-dependent responses *in planta*

(A) Experimental rationales and schemes. (Left column) Chemical and biological means for pectin modification. PME de-esterifies native methyl-esterified pectin secreted to the cell wall; EGCG is a chemical inhibitor of PME,[29,66–68] which de-esterifies native pectin; PMEI inhibits PME; ADPG1 is a polygacturonase degrading pectin,[62] and OG oxidase (OGOX) inactivates biologically active fragmented pectin.[32,65] (Right column) List of experiments.

(B) EGCG inhibited RALF1-induced FER-GFP clustering (top) and endocytosis (bottom). Figure S5D shows EGCG inhibition of RALF1-signaled cytosolic [Ca^{2+}] spike.

(C–I) Experiments in *N. benthamiana* (Figure S3C shows workflow). (C–E) RALF and pectic fragments together drive pectin-RALF assembly. (C) PME5[68] and (D) ADPG1[62] over-expression stimulated Cy3-RALF1-surface clusters. (E) Cy5-chitosan[71] decorated Cy3-RALF1 and ADPG1-driven RALF1 surface clusters, confirming they were condensates of RALF and de-esterified pectin. Figures S5F, S5J, and S5K shows chitosan-pectin interaction, its binding to *in vitro* phase-separated pectin-RALF condensates. Cy5-chitosan binding also confirmed reduced de-esterified pectin status in PMEI5ox seedlings[64,66] (Figure S5G).

(F) Cy5-$OG_{DP10–15}$, Cy3-RALF1, and FER-GFP colocalized to RALF1-induced FER-GFP clusters.

(G–I) Pectic fragments are crucial for RALF-induced surface receptor clustering. The impact from PMEI5 (G) and OGOX1 (H): top two rows, their expression inhibited RALF23-triggered FER-GFP clustering. PMEI3[72] acted similarly as PMEI5 (Figure S5M). (I) Expression of OGOX1 inhibited RALF-triggered BRI1 and FLS2 co-clustering (arrowheads). Bottom rows (G)–(I) show pre-treatment of $OG_{DP10–15}$ prior to RALF application restored RALF-induced receptor clustering induced by PMEI5 (G) and OGOX1 (H and I). Figures S5N and S5O shows impacts on receptor endocytosis.

(J and K) In transgenic *Arabidopsis* seedlings, PMEI5oe suppressed (J) RALF1-triggered FER-GFP clustering and the inhibition was relieved by $OG_{DP10–15}$ application, and (K) RALF1-elevated FM4-64 uptake was suppressed in PMEI5ox seedlings. p (in red), most relevant comparative pairs; Figures S5P and S5Q shows image data. Figure S3C shows agroinfiltration workflow. Particle quantification and (*r*) analysis followed procedure described earlier. $^{**}p < 10^{-2}$, $^{***}p < 10^{-3}$, $^{****}p < 10^{-4}$; n.s., non-significant.

	Experiment	Samples
B	Root ROS response to RALF1	WT and FER signaling mutant seedlings
C	Root ROS response to OG	
D	FM4-64 uptake response to OG	
E	Receptor endocytosis response to high salt and temperature	Transgenic seedlings
F	Additioal cell surface regulator endocytosis response to high salt and temperature	Transgenic seedlings
G	FM4-64 uptake response to high salt and temperature	WT FER-signaling mutant seedlings
H,I	FM4-64 uptake and growth recovery responses to high salt and temperature	WT, seedlings +/- endoctyosis inhibitor
J,K	Growth recovery response to high salt and temperature	WT and endocytosis mutant seedlings
L	Growth recovery response to high salt and temperature	WT, FER-signaling mutant seedlings

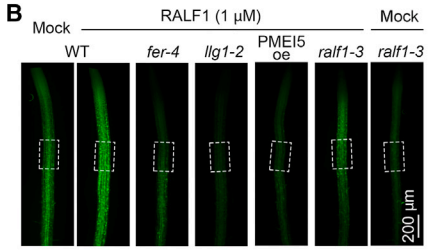

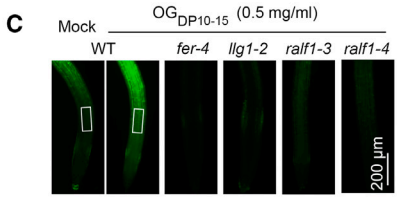

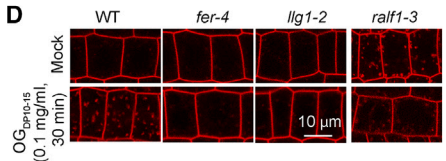

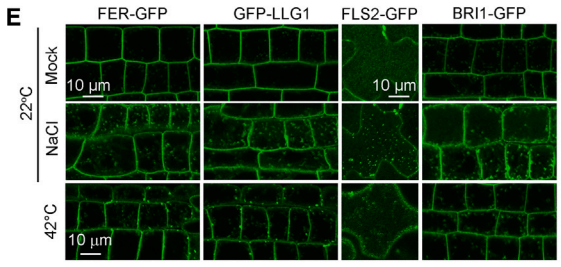

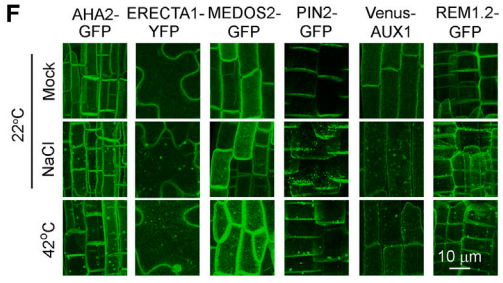

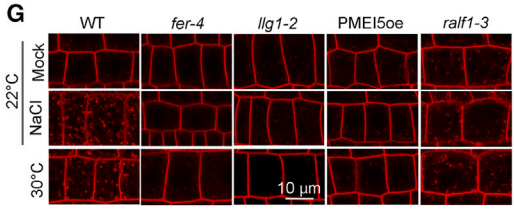

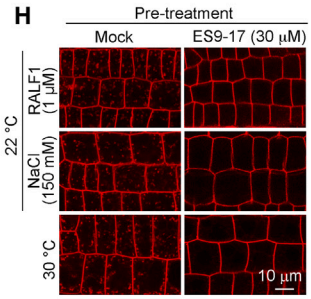

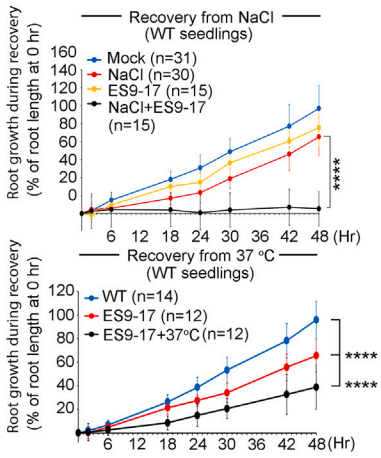

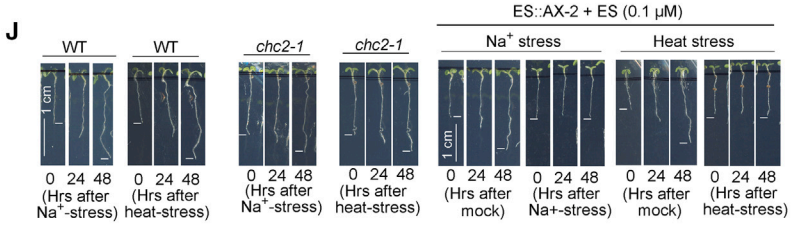

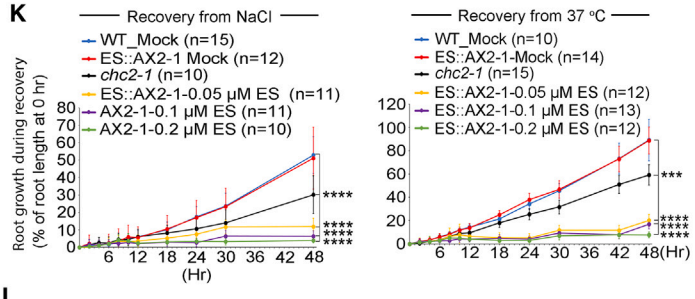

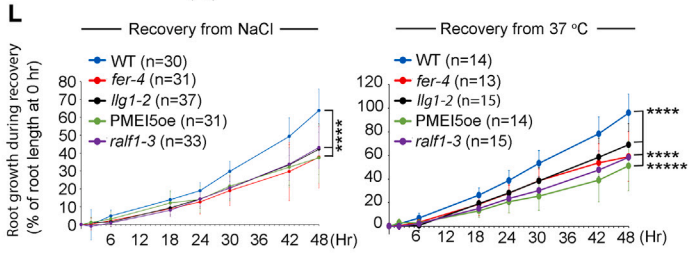

(legend on next page)

RALF and pectin conditions (Figures 6B, 6C, S6B, and S6C, lower data plot). Similar to RALF1-triggered elevation of general endocytosis being dependent on FER and LLG1 (Figure 1G), $OG_{DP10–15}$ also induced elevated levels of FM4-64 uptake, and the process was likewise dependent on FER and LLG1. *ralf1-3* mutant seedlings were also non-responsive to $OG_{DP10–15}$-induced FM4-64 uptake (Figures 6D and S6D). Together, these results established that RALF and pectin functioning in the same FER-LLG1 controlled signaling pathway.[9,10]

Stress suppresses plant growth and is recognized as an important coping strategy to better ensure survival.[2] Endocytosis facilitates the uptake of exogenous resources, and recycling of cell surface molecules, and is important for damage- and pathogen-triggered signaling.[43–45,78,79] Its capacity to rapidly alter cell membrane protein densities, thus expeditiously changing cellular dynamics, renders endocytosis well suited for a stress-coping strategy.[78–80] To test the hypothesis that pectin-RALF-FER-LLG1-mediated massive endocytosis functions as a coping mechanism against stress, we used high salt and elevated temperature, two often encountered environmental stressors, to explore the connection between the RALF-triggered cell surface processes and stress-induced responses (Figures 6E–6L). We observed that salt and heat stress-induced endocytosis of FER, LLG1, BRI1, and FLS2 as well as other cell surface regulators that responded to RALF1 (Figures 6E, 6F, and S6E). Internalization of FM4-64 revealed that general endocytosis in WT *Arabidopsis* seedlings was also significantly elevated by these stressors (Figures 6G and S6F). The augmented endocytic response was significantly impaired in *fer-4* and *llg1-2* mutant seedlings and in seedlings with perturbed pectin status (PMEI5oe) or reduced apoplastic RALF1 (*ralf1-3*, *ralf1-4, s1p*[34]; *s1p* is deficient in processing precursors into mature RALFs) (Figures 6G and S6F–S6H). These results evidenced a signal-response connection between salt and heat stress and widespread endocytosis. We note that the basal internalized FM4-64 levels in *ralf1-3*, *ralf1-4, s1p* were higher than in WT seedlings, suggesting the mutants were already in a state of stress. That these mutant seedlings were insensitive to the $OG_{DP10–15}$-, heat-, and salt-triggered response was consistent with a normal apoplastic RALF condition is critical for mediating environmental stress-induced response in the cell membrane.

FER guards against high salinity[20,21] and WT plants regained growth after acclimation to high salt conditions while the growth of *fer-4* remained arrested.[20] If massive endocytosis indeed underlies a stress-coping strategy for survival, inhibiting endocytosis would be detrimental. Monitoring growth recovery and endocytic uptake of FM4-64 (Figures 6H–6K and S6I–S6K), we observed that WT seedlings emerged from transient high salt and elevated temperature stress and recovered growth comparably relative to non-stressed control seedlings. However, inhibiting endocytosis chemically or genetically[44,45] reduced seedling capacity to emerge from these stressors, hampering growth recovery significantly (Figures 6H–6K, S6J, and S6K). Moreover, seedlings defective in any one of the components of the pectin-RALF-FERLLG1 ensemble were significantly hampered in their capacity to recover after salt and heat stress (Figure 6L). The reduced resilience of *fer-4*, *llg1-2*, PMEI5oe, and *ralf1-3* seedlings against these stressors was also reflected by their overall growth hypersensitivity under prolonged high salt and elevated growth conditions (Figure S6L). These results together provide compelling evidence for pectin-RALF-FER-LLG1 playing a concerted and crucial role in ensuring plant resilience to salt and heat stress by enabling massive endocytosis.

Stress triggers RALF-pectin phase separation and receptor clustering

We then explored whether stress triggers pectin-RALF phase separation in the cell surface and mediates the clustering of cognate and non-cognate targets as a prelude to stress-induced massive endocytosis (Figure 7A). We observed that high salt and elevated temperature induced clustering of RALF1-GFP in

Figure 6. Pectin-RALF interaction triggers FER-LLG1 signaling and induces massive endocytosis as a stress-coping strategy

(A) List of experiments.

(B–D) RALF1 and pectic fragments coordinately signaled the FER-LLG1 to ROS pathway. (B) RALF1 stimulated root ROS level in WT but not in *fer-4*, *llg1-2*, PMEI5oe, and *ralf1-3* seedlings; RALF1 treatment rescued *ralf1-3* and restored ROS level. (C) $OG_{DP10–15}$ stimulated ROS and (D) FM4-64 uptake in WT but not in *fer-4*, *llg1-2*, and *ralf1* mutants. Figures S6A–S6D shows mutation information on *ralf1* mutants, basal ROS levels in mutants, and data quantification.

(E–G) Salt and heat stress-induced endocytosis. 4-day-old seedlings were used. Normal growth was at 22°C, in 1/2 MS. Stress conditions were: 150 mM NaCl, an often-used condition[20,34]; 30°C–42°C (as indicated) determined after pilot experiments following various published conditions.[73–76]

(E and F) FP-tagged FER, LLG1, and other cell surface regulators in *Arabidopsis* seedlings.

(G) FM4-64 uptake in WT and mutants defective in one of the components of the pectin-RALF1-FER-LLG1 module. Salt or heat stress was applied for 15 min. For FM4-64 uptake, seedlings were pretreated with 1 μM FM4-64 for 15 min in 1/2 MS. Figures S6G and S6H show quantified and related data from *ralf1-4* and *s1p*.[34]

(H–K) Pectin-RALF-FER-LLG1-mediated endocytosis was required for growth recovery after stress-attenuated growth. High salt, elevated temperature conditions were with 150 mM NaCl for 3 h, 37°C for 2 h, respectively. After stress treatments, root growth recovery was monitored for 48 h. In growth recovery plots, growth is expressed as % of root lengths at the start of recovery (0 h) of individual seedling lines. Figure S6I details workflow for growth recovery experiments. (H) FM4-64 uptake without and with treatment by the clathrin-dependent endocytosis inhibitor ES9-17,[77] applied 30 min prior to stress-treatment.

(I) Growth recovery plots. Impact on growth recovery from stress under normal or ES9-17 treatment. See also Figure S6J.

(J and K) Growth recovery after stress-treatment in WT and mutants defective in endocytosis. *chc2-1* is compromised in clathrin-dependent endocytosis[45,46] and XVE >> AX2 conditionally expresses (induced by estradiol [ES]) AX2, an inhibitor of clathrin-mediated endocytosis.[44] Figure S6K shows ES treatment mock. (J) Representative WT, *chc2-1*, and XVE >> AX2 seedlings; distances between the white dashes represents growth since emergence from stress and are illustrated in the plots (K).

(L) Growth recovery after stress-treatment in WT and mutants defective in each of the components of the pectin-RALF-FER-LLG1 ensemble showed reduced capacity in growth recovery relative to WT. Figure S6L shows WT and mutant overall growth responses when kept under stress for 48 h.

Data quantification followed described above. ***$p < 10^{-3}$, ****$p < 10^{-4}$.

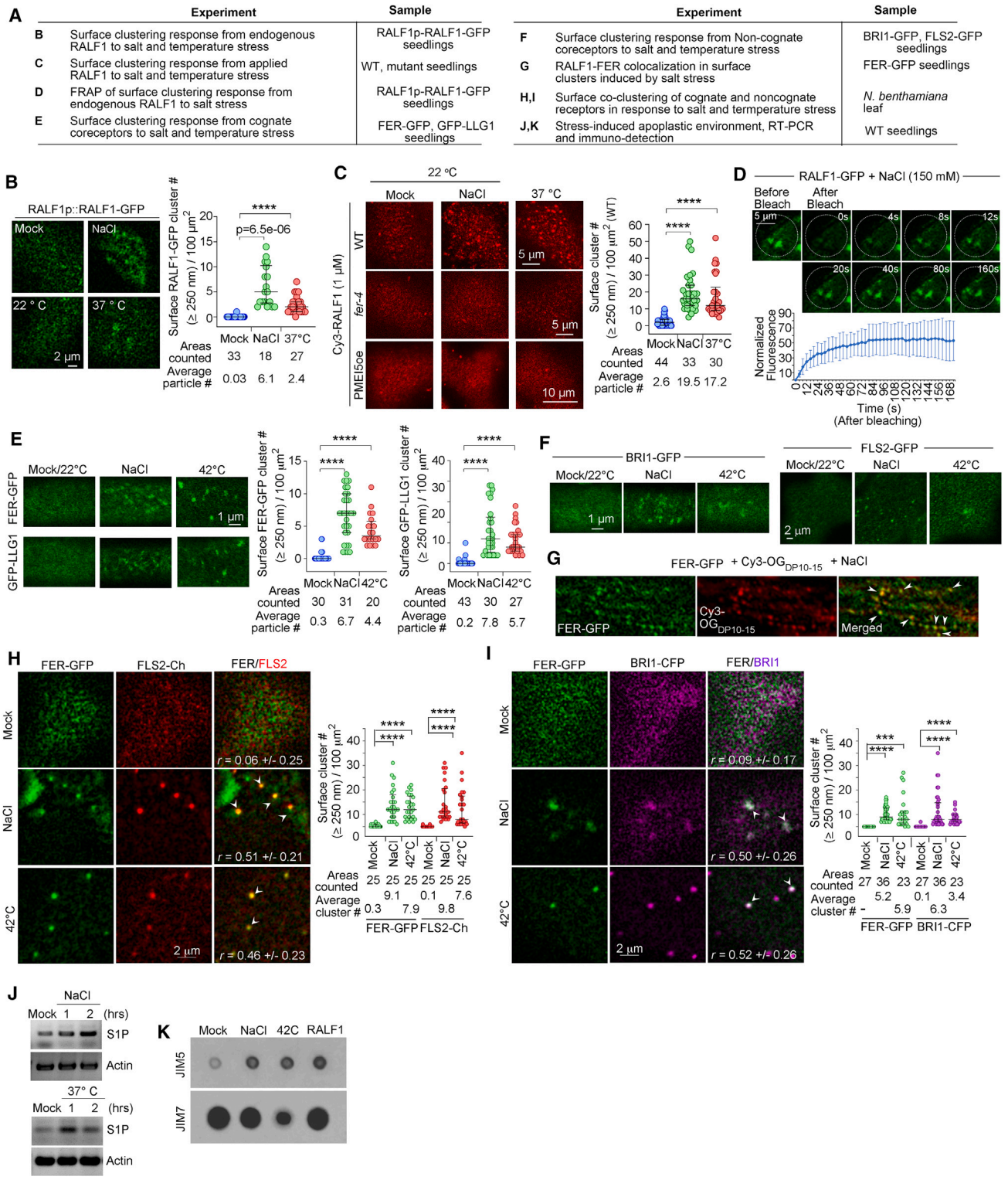

Figure 7. Salt and heat stresses promote RALF-pectin phase separation and nonselective receptor clustering

(A) List of experiments.

(B and C) High salt and temperature stimulated (B) clustering of endogenously produced RALF1 (from RALF1 promoter)- and (C) Cy3-RALF1-decorated clusters in WT but not in *fer-4* or PMEI5oe seedlings.

(legend continued on next page)

RALF1 promoter::RALF1-GFP transformed seedlings (Figure 7B). Application of Cy3-RALF1 to salt- or heat-stressed WT seedlings dramatically accentuated RALF clustering, and these responses were dependent on FER and a properly maintained level of de-esterified pectic environment (Figure 7C). These results were similar to RALF1-triggered receptor clustering (Figure 2) and mimicked PME5- and ADPG1-augmented Cy3-RALF1 clusters (Figures 5C and 5D), implying the involvement of elevated RALFs and pectin fragments in these stress responses. Salt stress-induced clustering of endogenously expressed RALF1-GFP was highly dynamic as demonstrated by rapid FRAP (Figure 7D; Video S6), thus consistent with it being an LLPS process. Elevated salt and temperature also triggered the clustering of FER-GFP, GFP-LLG1, BRI1-GFP, and FLS2-GFP (Figures 7E and 7F) in *Arabidopsis* seedlings. Applying Cy3-$OG_{DP10–15}$ showed that these pectic fragments were incorporated in salt-stress-triggered receptor clusters (Figure 7G), implying that endogenous pectic fragments would also be incorporated into these stress-induced clusters. Salt and heat also induced co-clustering of FER-GFP with FLS2-Ch and of FER-GFP and BRI1-CFP in *N. benthamiana* leaf cells (Figures 7H and 7I).

Abiotic and biotic stresses, such as high salt, elevated temperatures, and pathogen-derived elicitors, are known to induce cell wall remodeling.[31,32,61–63] Mining gene expression data[82] and our own transcription analysis provided results consistent with these stressors impacting the expression of ADPGs, RALF1, and S1P (Figures S6M–S6O). Along with augmenting S1P expression (Figure 7J), salt- and high-temperature-treated seedlings also maintained elevated levels of de-esterified pectin, as did RALF1 treatment (Figure 7K). Together, these results support the notion that high salt and temperature would create an altered apoplastic condition with elevated RALF and de-esterified pectin. Similarly, conditions that would elevate apoplastic RALF, such as exogenous application of RALF1, also stimulate de-esterified pectin accumulation (Figure 7K). These apoplastic conditions would enhance RALF-pectin condensation and the clustering of FER, LLG1, and other membrane targets. These events would simultaneously activate multiple signaling pathways as a rapid response to the stress signal and the ensuing massive endocytosis would moderate the activated processes and mediate a new cellular homeostasis for a more sustained response to ensure survival (Figure 7). The fact that the abiotic stressors would augment apoplastic RALFs (Figures 7J and S6O), which could downregulate flg22-triggered immunity signaling as demonstrated for RALF23,[23] also provide a means to integrate abiotic stress with immunity responses.

DISCUSSION

Our search for a cell surface mechanism that enables the diverse biological roles of FER led to the discovery of pectin-RALF phase separation at the cell wall-cell membrane interface and its role in mediating widespread clustering of cell surface regulators and their endocytosis (Figures 1, 2, 3, 4, and 5). Ligand-receptor binding on cell surface induces receptor clustering concentrating them into notable nano- and microdomains in the cell membrane is an important first step in the activation of a signal transduction. Receptor clustering also induces inward bending membrane curvatures and drives ligand-induced receptor endocytosis, which is important for modulating the activated pathways or participating in signaling events in the cytoplasm.[43,54,55,57,58] The RALF-triggered FER-LLG1-dependent promiscuous cell surface response is a fitting mechanism for enabling the diverse biological role of FER (Figure S7). Uncovering the reliance on de-esterified pectin and RALF in the FER-LLG1 to ROS signaling pathway (Figure 6) and that salt and heat stress triggers pectin-RALF phase separation, clustering of cell membrane-located regulators is a prelude to their endocytosis (Figure 7) elucidate physiological links for extracellular pectin-RALF interaction. Together, our results support that pectin-RALF phase separation-mediated responses at the cell surface is a crucial linkage that connects extracellular signal sensing to simultaneously impacting diverse response pathways and enabling the remarkable range of FER-LLG1 functions.

RALF-pectin driven phase separation uncovered here is distinct from many phase separation processes in biological systems studied thus far.[38–40] The involvement of a cell wall sugar polymer, a secreted disordered peptide that is a ligand for a receptor module in the biological compartment created by the cell wall-cell membrane continuum[29] is the perfect molecular and cellular combination to support an extracellular phase separation process that has thus far been elusive in biological systems.[38–40] Extracellular pectin-RALF phase separation at the cell wall-cell membrane interface provides a biologically powerful platform to orchestrate interwoven downstream signaling pathways.

The basal activity of the core FER to ROS signaling pathway[9,10] (Figure S1B) being dependent on pectin and RALF (Figures 6B, 6C, S6B, and S6C) is consistent with the assembly of pectin-RALF-FER-LLG1 into a functional ensemble being a phenomenon occurring under regular growth conditions. This was made notable at a low level when accentuated by applying Cy3-RALF1 in control cells (Figures 5C and 5D). Application of RALF (Figure 2), elevating the de-esterified pectin level in the cell wall (Figures 5C–5E), or altering the apoplastic environment

(D) FRAP of salt stress-triggered RALF1-GFP clusters revealed rapid recruitment of RALF1-GFP into these surface particles. See Video S6.
(E–G) High salt and temperature induced receptor clustering: FER-GFP and GFP-LLG1 (E), BRI1-GFP and FLS2-GFP (F). (G) Applied Cy3 $OG_{DP10–15}$ revealed pectic fragments was assembled into FER-GFP clusters. Arrowheads, colocalization.
(H and I) High salt and temperature induced co-clustering of FER-GFP with FLS2-Ch (H) and FER-GFP with BRI1-CFP (I).
(J and K) High salt and elevated temperature impact apolastic RALFs and pectin. (J) RT-PCR of S1P transcripts in stressed WT seedlings. (K) Immunodetection of de-esterified pectin (by JIM5)[81] and methyl-esterified pectin (by JIM7)[81] from control, NaCl and heat- stressed, and RALF1-treated WT seedlings. Same volumes (2 μL) of samples obtained from 20 seedlings were applied per dot. Methyl-esterified pectin was consistently low in elevated temperature treatments. Figures S6M–S6O shows related gene expression data.
Cluster quantification and (*r*) analysis followed methods described earlier. Data quantification followed described above. ***$p < 10^{-3}$, ****$p < 10^{-4}$.

by stress (Figure 7) augmented the phase-separation phenomenon to be readily notable, enabling the process to be biologically (Figure 6) and mechanistically examined (Figures 5 and 7). Observations made under the various experimental conditions used provide support for RALF-pectin collaboration in impacting cell wall property and receptor organization in the cell membrane and that pectin-RALF phase separation is biologically significant at the cell wall-cell membrane interface. RALF and pectic fragments being adequate for phase-separation *in vitro* and both are required to recruit FER and LLG1 to form pectin-RALF-FER-LLG1 condensates (Figure 3) support that the peptide-sugar interaction nucleates the phase separation process in the apoplast. In LLPS, specific and multivalent interactions are involved in nucleating the molecular assembly and supporting its propagation into notable molecular condensates of diverse biological molecules.[38–40] RALF-, salt-, and heat-triggered cell surface responses requiring FER and LLG1 (Figure 7) suggest that RALF-pectin interaction with FER-LLG1 provides specificity while multivalent interactions mediate promiscuous recruitment of diverse regulators into phase-separated membrane microdomains to trigger FER-LLG1-dependent signaling processes. Our results therefore align with the notion of RALF-pectic fragment condensates serving as scaffolds to assemble a biologically active exoskeleton to enable the multi-tasking ability of the FER-LLG1 signaling module.

The biological consequences triggered by endogenous demands or exogenous stimuli is rarely the outcome of any single pathway stimulated into action, but the sum of many collateral and compensating activities needed to engineer the optimum reaction to flourish or survive. The findings here suggest a molecular innovation that enables broad-based participation of diverse cellular processes in response to any single signal trigger. Phase-separation-mediated promiscuous responses would quickly and coordinately activate multiple, otherwise independently controlled signaling pathways. Plausibly, the ability to mobilize individual pathways into actions almost simultaneously provides a brief but critical time window for plants to orchestrate a more sustained downstream response to meet the need of changing cellular demands, cope with and survive challenges that threaten their well-being. FER, LLG1, and RALF from *Arabidopsis* are members of multi-membered protein families that are conserved across plant species.[5,7,83] Analogous extracellular phase-separation processes could be widespread, and a cell wall sugar-RALF-FER-LLG1-mediated mechanism could emerge as a common theme in orchestrating the coordination of diverse signaling pathways throughout the plant kingdom.

Limitations of the study

The structure of RALF-pectin condensates, the physicochemical bases of RALF-pectin phase separation and a high-resolution understanding of how pectin interacts with RALF and FER *in vitro* and on the plant cell surface are major challenges that need to be addressed. Biologically, how pectin-RALF condensates engage in multivalent interactions with diverse molecules in the cell wall-cell membrane interface and recruit them into active signaling complexes remains to be explained. Elucidating how fluctuations in apoplastic RALFs impact cell wall synthesis and remodeling will advance more precise mechanistic insights on how RALF-FER signaling affects the cell wall, which is intimately linked to growth and survival. How the pectin-RALF-FER-LLG1-mediated cell surface responses are translated into downstream consequences on individual pathways, and collective cytoplasmic and nuclear responses, will also need to be examined in detail. We plan to contribute efforts to tackle these challenges with multi-disciplinary collaborations in the next phase.

STAR★METHODS

Detailed methods are provided in the online version of this paper and include the following:

- KEY RESOURCES TABLE
- RESOURCE AVAILABILITY
  - Lead contact
  - Materials availability
  - Data and code availability
- EXPERIMENTAL MODEL AND STUDY PARTICIPANT DETAILS
- METHOD DETAILS
  - Plant material, growth, transformation
  - Recombinant DNA construction
  - Fusion protein expression and purification
  - Chemical labeling
  - Seedling growth assays
  - Aequorin-based calcium influx assay
  - Analyses of signal-triggered responses
  - Agroinfiltration
  - Stress-related analyses
  - Seedling ROS assay
  - Microscopy, image processing and data quantification
  - Protein–protein interaction assays
  - Protein-pectin interaction assays
  - Phase separation assays
- QUANTIFICATION AND STATISTICAL ANALYSIS

SUPPLEMENTAL INFORMATION

Supplemental information can be found online at https://doi.org/10.1016/j.cell.2023.11.038.

ACKNOWLEDGMENTS

This work has trained many undergraduate students, and we thank them, Khanhlinh Dinh, Amy Kwang, Theodore Lichoulas, Kara McNamara, Brook Sullivan, and Aamer Syed, for their participation in protein purification, seedling growth, and RALF growth-regulatory activity assays. For many gifts, we thank Alan Darville and colleagues (Complex Carbohydrate Research Center, Athens, Georgia) and D.S. Moura (Universidade de São Paulo) for initial gifts of OGs and RALF1 preparations, respectively; M. Sussman (U. Wisconsin), J. Chory (Salk Inst.), P. He (Texas A&M), K. Torii (U Texas in Austin), T. Ott (U Freiburg), B. Scheres (Wageningen U) and E. Russinova for various seed lines over the course of this work. We thank C. Anderson (Pennsylvania State University) and C. Xiao (Sichuan University, China) for the use of Figure S1E. Funding: research was supported by NSF (MCB-1715764, IOS-1645858, IOS-2101467) to A.Y.C. and H.-M.W., and support from the National Institute of Food and Agriculture, USDA, the Center for Agriculture, Food, and the Environment under project number MAS00525, which also supported K.S. The contents are solely the responsibility of the authors and do not represent the

official views of the USDA or NIFA. The Light Microscopy Facility is a Nikon Center of Excellence and receives support from the Massachusetts Life Science Center.

AUTHOR CONTRIBUTIONS

M.-C.J.L. and F.-L.J.Y. participated in all experiments, design, and data analysis, M.-C.J.L. more on cell biological and plant growth-related experiments, F.-L.J.Y. more on molecular, biochemical, and transient assay experiments. R.Y. initiated and contributed observations for the RALF-pectin assembly studies; K.S. contributed to stress response studies; S.J. contributed to *in vitro* RALF binding studies; J.C. advised and assisted in microscopy studies. All participated in data evaluation. H.-M.W. and A.Y.C. conceptualized the project, led the research strategy, acquired funding; H.-M.W. contributed molecular designs, piloted experiments, piloted and performed troubleshooting of various chemical and biochemical schemes; A.Y.C. contributed to plant and microscopy data acquisition. A.Y.C. and H.-M.W. led the writing process; all authors contributed to data analyses, manuscript preparation, and approve the manuscript.

DECLARATION OF INTERESTS

The authors declare no competing interests.

INCLUSION AND DIVERSITY

We support inclusive, diverse, and equitable conduct of research.

Received: May 23, 2023
Revised: October 1, 2023
Accepted: November 29, 2023
Published: December 28, 2023

REFERENCES

1. Wasserman, M.D., Wing, B., Bickford, N., Hobbs, K., Dijkstra, P., and Carr, J.A. (2022). Stress responses across the scales of life: toward a universal theory of biological stress. Integr. Comp. Biol. *61*, 2109–2118.
2. Zhang, H., Zhu, J., Gong, Z., and Zhu, J.K. (2022). Abiotic stress responses in plants. Nat. Rev. Genet. *23*, 104–119.
3. Cheung, A.Y. (2024). Feronia: a receptor kinase at the core of a global signaling network. Annu. Rev. Plant Biol.
4. Franck, C.M., Westermann, J., and Boisson-Dernier, A. (2018). Plant malectin-like receptor kinases: from cell wall integrity to immunity and beyond. Annu. Rev. Plant Biol. *69*, 301–328.
5. Yang, H., Wang, D., Guo, L., Pan, H., Yvon, R., Garman, S., Wu, H.M., and Cheung, A.Y. (2021). Malectin/malectin-like domain-containing proteins: A repertoire of cell surface molecules with broad functional potential. Cell Surf. *7*, 100056.
6. Blackburn, M.R., Haruta, M., and Moura, D.S. (2020). Twenty years of progress in physiological and biochemical investigation of RALF peptides. Plant Physiol. *182*, 1657–1666.
7. Abarca, A., Franck, C.M., and Zipfel, C. (2021). Family-wide evaluation of RAPID alkalinization FACTOR peptides. Plant Physiol. *187*, 996–1010.
8. Xiao, Y., Stegmann, M., Han, Z., DeFalco, T.A., Parys, K., Xu, L., Belkhadir, Y., Zipfel, C., and Chai, J. (2019). Mechanisms of RALF peptide perception by a heterotypic receptor complex. Nature *572*, 270–274.
9. Li, C., Yeh, F.-L., Cheung, A.Y., Duan, Q., Kita, D., Liu, M.-C., Maman, J., Luu, E.J., Wu, B.W., Gates, L., et al. (2015). Glycosylphosphatidylinositol-anchored proteins as chaperones and co-receptors for FERONIA receptor kinase signaling in Arabidopsis. eLife *4*, e06587.
10. Duan, Q., Kita, D., Li, C., Cheung, A.Y., and Wu, H.M. (2010). FERONIA receptor-like kinase regulates RHO GTPase signaling of root hair development. Proc. Natl. Acad. Sci. USA *107*, 17821–17826.
11. Dong, Q., Zhang, Z., Liu, Y., Tao, L.-Z., and Liu, H. (2019). FERONIA regulates auxin-mediated lateral root development and primary root gravitropism. FEBS Lett. *593*, 97–106.
12. Guo, H., Li, L., Ye, H., Yu, X., Algreen, A., and Yin, Y. (2009). Three related receptor-like kinases are required for optimal cell elongation in Arabidopsis thaliana. Proc. Natl. Acad. Sci. USA *106*, 7648–7653.
13. Yu, F., Qian, L., Nibau, C., Duan, Q., Kita, D., Levasseur, K., Li, X., Lu, C., Li, H., Hou, C., et al. (2012). FERONIA receptor kinase pathway suppresses abscisic acid signaling in Arabidopsis by activating ABI2 phosphatase. Proc. Natl. Acad. Sci. USA *109*, 14693–14698.
14. Escobar-Restrepo, J.-M., Huck, N., Kessler, S., Gagliardini, V., Gheyselinck, J., Yang, W.-C., and Grossniklaus, U. (2007). The FERONIA receptor-like kinase mediates male-female interactions during pollen tube reception. Science *317*, 656–660.
15. Liu, C., Shen, L., Xiao, Y., Vyshedsky, D., Peng, C., Sun, X., Liu, Z., Cheng, L., Zhang, H., Han, Z., et al. (2021). Pollen PCP-B peptides unlock a stigma peptide-receptor kinase gating mechanism for pollination. Science *372*, 171–175.
16. Zhang, L., Huang, J., Su, S., Wei, X., Yang, L., Zhao, H., Yu, J., Wang, J., Hui, J., Hao, S., et al. (2021). FERONIA receptor kinase-regulated reactive oxygen species mediate self-incompatibility in Brassica rapa. Curr. Biol. *31*, 3004–3016.e4.
17. Duan, Q., Kita, D., Johnson, E.A., Aggarwal, M., Gates, L., Wu, H.M., and Cheung, A.Y. (2014). Reactive oxygen species mediate pollen tube rupture to release sperm for fertilization in Arabidopsis. Nat. Commun. *5*, 3129.
18. Duan, Q., Liu, M.J., Kita, D., Jordan, S.S., Yeh, F.J., Yvon, R., Carpenter, H., Federico, A.N., Garcia-Valencia, L.E., Eyles, S.J., et al. (2020). FERONIA controls pectin- and nitric oxide-mediated male-female interaction. Nature *579*, 561–566.
19. Huang, J., Yang, L., Yang, L., Wu, X., Cui, X., Zhang, L., Hui, J., Zhao, Y., Yang, H., Liu, S., et al. (2023). Stigma receptors control intraspecies and interspecies barriers in Brassicaceae. Nature *614*, 303–308.
20. Feng, W., Kita, D., Peaucelle, A., Cartwright, H.N., Doan, V., Duan, Q., Liu, M.C., Maman, J., Steinhorst, L., Schmitz-Thom, I., et al. (2018). The FERONIA receptor kinase maintains cell-wall integrity during salt stress through Ca(2+) signaling. Curr. Biol. *28*, 666–675.e5.
21. Liu, X., Jiang, W., Li, Y., Nie, H., Cui, L., Li, R., Tan, L., Peng, L., Li, C., Luo, J., et al. (2023). FERONIA coordinates plant growth and salt tolerance via the phosphorylation of phyB. Nat. Plants *9*, 645–660.
22. Shin, S.Y., Park, J.S., Park, H.B., Moon, K.B., Kim, H.S., Jeon, J.H., Cho, H.S., and Lee, H.J. (2021). FERONIA confers resistance to photooxidative stress in Arabidopsis. Front. Plant Sci. *12*, 714938.
23. Stegmann, M., Monaghan, J., Smakowska-Luzan, E., Rovenich, H., Lehner, A., Holton, N., Belkhadir, Y., and Zipfel, C. (2017). The receptor kinase FER is a RALF-regulated scaffold controlling plant immune signaling. Science *355*, 287–289.
24. Shen, Q., Bourdais, G., Pan, H., Robatzek, S., and Tang, D. (2017). Arabidopsis glycosylphosphatidylinositol-anchored protein LLG1 associates with and modulates FLS2 to regulate innate immunity. Proc. Natl. Acad. Sci. USA *114*, 5749–5754.
25. Mittler, R. (2017). ROS Are Good. Trends Plant Sci. *22*, 11–19.
26. Lin, W., Tang, W., Pan, X., Huang, A., Gao, X., Anderson, C.T., and Yang, Z. (2022). Arabidopsis pavement cell morphogenesis requires FERONIA binding to pectin for activation of ROP GTPase signaling. Curr. Biol. *32*, 497–507.e4.
27. Wang, P., Clark, N.M., Nolan, T.M., Song, G., Bartz, P.M., Liao, C.Y., Montes-Serey, C., Katz, E., Polko, J.K., Kieber, J.J., et al. (2022). Integrated omics reveal novel functions and underlying mechanisms of the receptor kinase FERONIA in Arabidopsis thaliana. Plant Cell *34*, 2594–2614.
28. Zurzolo, C., and Simons, K. (2016). Glycosylphosphatidylinositol-anchored proteins: membrane organization and transport. Biochim. Biophys. Acta *1858*, 632–639.

29. McKenna, J.F., Rolfe, D.J., Webb, S.E.D., Tolmie, A.F., Botchway, S.W., Martin-Fernandez, M.L., Hawes, C., and Runions, J. (2019). The cell wall regulates dynamics and size of plasma-membrane nanodomains in Arabidopsis. Proc. Natl. Acad. Sci. USA *116*, 12857–12862.

30. Daněk, M., Angelini, J., Malínská, K., Andrejch, J., Amlerová, Z., Kocourková, D., Brouzdová, J., Valentová, O., Martinec, J., and Petrášek, J. (2020). Cell wall contributes to the stability of plasma membrane nanodomain organization of Arabidopsis thaliana FLOTILLIN2 and HYPERSENSITIVE INDUCED REACTION1 proteins. Plant J. *101*, 619–636.

31. Peaucelle, A., Braybrook, S., and Höfte, H. (2012). Cell wall mechanics and growth control in plants: the role of pectins revisited. Front. Plant Sci. *3*, 121.

32. Du, J., Anderson, C.T., and Xiao, C. (2022). Dynamics of pectic homogalacturonan in cellular morphogenesis and adhesion, wall integrity sensing and plant development. Nat. Plants *8*, 332–340.

33. Schallus, T., Jaeckh, C., Fehér, K., Palma, A.S., Liu, Y., Simpson, J.C., Mackeen, M., Stier, G., Gibson, T.J., Feizi, T., et al. (2008). Malectin: a novel carbohydrate-binding protein of the endoplasmic reticulum and a candidate player in the early steps of protein N-glycosylation. Mol. Biol. Cell *19*, 3404–3414.

34. Zhao, C., Zayed, O., Yu, Z., Jiang, W., Zhu, P., Hsu, C.C., Zhang, L., Tao, W.A., Lozano-Durán, R., and Zhu, J.K. (2018). Leucine-rich repeat extensin proteins regulate plant salt tolerance in Arabidopsis. Proc. Natl. Acad. Sci. USA *115*, 13123–13128.

35. Dünser, K., Gupta, S., Herger, A., Feraru, M.I., Ringli, C., and Kleine-Vehn, J. (2019). Extracellular matrix sensing by FERONIA and leucine-rich repeat extensins controls vacuolar expansion during cellular elongation in Arabidopsis thaliana. EMBO J. *38*, e100353.

36. Herger, A., Gupta, S., Kadler, G., Franck, C.M., Boisson-Dernier, A., and Ringli, C. (2020). Overlapping functions and protein-protein interactions of LRR-extensins in Arabidopsis. PLoS Genet. *16*, e1008847.

37. Liu, C., Yu, H., Voxeur, A., Rao, X., and Dixon, R.A. (2023). FERONIA and wall-associated kinases coordinate defense induced by lignin modification in plant cell walls. Sci. Adv. *9*, eadf7714.

38. Lyon, A.S., Peeples, W.B., and Rosen, M.K. (2021). A framework for understanding the functions of biomolecular condensates across scales. Nat. Rev. Mol. Cell Biol. *22*, 215–235.

39. Alberti, S., and Hyman, A.A. (2021). Biomolecular condensates at the nexus of cellular stress, protein aggregation disease and ageing. Nat. Rev. Mol. Cell Biol. *22*, 196–213.

40. Emenecker, R.J., Holehouse, A.S., and Strader, L.C. (2021). Biological phase separation and biomolecular condensates in plants. Annu. Rev. Plant Biol. *72*, 17–46.

41. Haas, K.T., Wightman, R., Peaucelle, A., and Höfte, H. (2021). The role of pectin phase separation in plant cell wall assembly and growth. Cell Surf. *7*, 100054.

42. Haruta, M., Sabat, G., Stecker, K., Minkoff, B.B., and Sussman, M.R. (2014). A peptide hormone and its receptor protein kinase regulate plant cell expansion. Science *343*, 408–411.

43. Irani, N.G., and Russinova, E. (2009). Receptor endocytosis and signaling in plants. Curr. Opin. Plant Biol. *12*, 653–659.

44. Ortiz-Morea, F.A., Savatin, D.V., Dejonghe, W., Kumar, R., Luo, Y., Adamowski, M., Van den Begin, J., Dressano, K., Pereira de Oliveira, G., Zhao, X., et al. (2016). Danger-associated peptide signaling in Arabidopsis requires clathrin. Proc. Natl. Acad. Sci. USA *113*, 11028–11033.

45. Mbengue, M., Bourdais, G., Gervasi, F., Beck, M., Zhou, J., Spallek, T., Bartels, S., Boller, T., Ueda, T., Kuhn, H., et al. (2016). Clathrin-dependent endocytosis is required for immunity mediated by pattern recognition receptor kinases. Proc. Natl. Acad. Sci. USA *113*, 11034–11039.

46. Yu, M., Li, R., Cui, Y., Chen, W., Li, B., Zhang, X., Bu, Y., Cao, Y., Xing, J., Jewaria, P.K., et al. (2020). The RALF1-FERONIA interaction modulates endocytosis to mediate control of root growth in Arabidopsis. Development *147*, dev189902.

47. Palmgren, M., and Morsomme, P. (2019). The plasma membrane H(+)-ATPase, a simple polypeptide with a long history. Yeast *36*, 201–210.

48. Dressano, K., Ceciliato, P.H.O., Silva, A.L., Guerrero-Abad, J.C., Bergonci, T., Ortiz-Morea, F.A., Bürger, M., Silva-Filho, M.C., and Moura, D.S. (2017). BAK1 is involved in AtRALF1-induced inhibition of root cell expansion. PLoS Genet. *13*, e1007053.

49. Lee, J.S., Kuroha, T., Hnilova, M., Khatayevich, D., Kanaoka, M.M., McAbee, J.M., Sarikaya, M., Tamerler, C., and Torii, K.U. (2012). Direct interaction of ligand-receptor pairs specifying stomatal patterning. Genes Dev. *26*, 126–136.

50. Huang, Y., Yin, C., Liu, J., Feng, B., Ge, D., Kong, L., Ortiz-Morea, F.A., Richter, J., Hauser, M.-T., Wang, W.-M., et al. (2020). A trimeric CrRLK1L-LLG1 complex genetically modulates SUMM2-mediated autoimmunity. Nat. Commun. *11*, 4859.

51. Raffaele, S., Bayer, E., Lafarge, D., Cluzet, S., German Retana, S., Boubekeur, T., Leborgne-Castel, N., Carde, J.-P., Lherminier, J., Noirot, E., et al. (2009). Remorin, a solanaceae protein resident in membrane rafts and plasmodesmata, impairs potato virus X movement. Plant Cell *21*, 1541–1555.

52. Jarsch, I.K., Konrad, S.S., Stratil, T.F., Urbanus, S.L., Szymanski, W., Braun, P., Braun, K.H., and Ott, T. (2014). Plasma membranes are subcompartmentalized into a plethora of coexisting and diverse microdomains in Arabidopsis and Nicotiana benthamiana. Plant Cell *26*, 1698–1711.

53. Rigal, A., Doyle, S.M., and Robert, S. (2015). Live cell imaging of FM4-64, a tool for tracing the endocytic pathways in Arabidopsis root cells. Methods Mol. Biol. *1242*, 93–103.

54. Irani, N.G., Di Rubbo, S., Mylle, E., Van den Begin, J., Schneider-Pizoń, J., Hniliková, J., Šíša, M., Buyst, D., Vilarrasa-Blasi, J., Szatmári, A.M., et al. (2012). Fluorescent castasterone reveals BRI1 signaling from the plasma membrane. Nat. Chem. Biol. *8*, 583–589.

55. Bücherl, C.A., Jarsch, I.K., Schudoma, C., Segonzac, C., Mbengue, M., Robatzek, S., MacLean, D., Ott, T., and Zipfel, C. (2017). Plant immune and growth receptors share common signalling components but localise to distinct plasma membrane nanodomains. eLife *6*, e25114.

56. McKenna, J.F. (2022). Quantifying the organization and dynamics of the plant plasma membrane across scales using light microscopy. Methods Mol. Biol. *2457*, 233–251.

57. Jaillais, Y., and Ott, T. (2020). The nanoscale organization of the plasma membrane and Its Importance in signaling: A proteolipid perspective. Plant Physiol. *182*, 1682–1696.

58. Kaksonen, M., and Roux, A. (2018). Mechanisms of clathrin-mediated endocytosis. Nat. Rev. Mol. Cell Biol. *19*, 313–326.

59. Salavessa, L., Lagache, T., Malardé, V., Grassart, A., Olivo-Marin, J.-C., Canette, A., Trichet, M., Sansonetti, P.J., and Sauvonnet, N. (2021). Cytokine receptor cluster size impacts its endocytosis and signaling. Proc. Natl. Acad. Sci. USA *118*, e2024893118.

60. Chinchilla, D., Shan, L., He, P., de Vries, S., and Kemmerling, B. (2009). One for all: the receptor-associated kinase BAK1. Trends Plant Sci. *14*, 535–541.

61. Denoux, C., Galletti, R., Mammarella, N., Gopalan, S., Werck, D., De Lorenzo, G., Ferrari, S., Ausubel, F.M., and Dewdney, J. (2008). Activation of defense response pathways by OGs and Flg22 elicitors in Arabidopsis seedlings. Mol. Plant *1*, 423–445.

62. Pontiggia, D., Benedetti, M., Costantini, S., De Lorenzo, G., and Cervone, F. (2020). Dampening the DAMPs: how plants maintain the homeostasis of cell wall molecular patterns and avoid hyper-immunity. Front. Plant Sci. *11*, 613259.

63. Voxeur, A., Habrylo, O., Guénin, S., Miart, F., Soulié, M.-C., Rihouey, C., Pau-Roblot, C., Domon, J.-M., Gutierrez, L., Pelloux, J., et al. (2019). Oligogalacturonide production upon Arabidopsis thaliana-Botrytis cinerea interaction. Proc. Natl. Acad. Sci. USA *116*, 19743–19752.

64. Gallego-Giraldo, L., Liu, C., Pose-Albacete, S., Pattathil, S., Peralta, A.G., Young, J., Westpheling, J., Hahn, M.G., Rao, X., Knox, J.P., et al. (2020). Arabidopsis DEHISCENCE ZONE polygalacturonase 1 (ADPG1) releases latent defense signals in stems with reduced lignin content. Proc. Natl. Acad. Sci. USA *117*, 3281–3290.

65. Benedetti, M., Verrascina, I., Pontiggia, D., Locci, F., Mattei, B., De Lorenzo, G., and Cervone, F. (2018). Four Arabidopsis berberine bridge enzyme-like proteins are specific oxidases that inactivate the elicitor-active oligogalacturonides. Plant J. *94*, 260–273.

66. L'Enfant, M., Domon, J.-M., Rayon, C., Desnos, T., Ralet, M.-C., Bonnin, E., Pelloux, J., and Pau-Roblot, C. (2015). Substrate specificity of plant and fungi pectin methylesterases: identification of novel inhibitors of PMEs. Int. J. Biol. Macromol. *81*, 681–691.

67. Wolf, S., Mravec, J., Greiner, S., Mouille, G., and Höfte, H. (2012). Plant cell wall homeostasis is mediated by brassinosteroid feedback signaling. Curr. Biol. *22*, 1732–1737.

68. Xu, F., Gonneau, M., Faucher, E., Habrylo, O., Lefebvre, V., Domon, J.-M., Martin, M., Sénéchal, F., Peaucelle, A., Pelloux, J., et al. (2022). Biochemical characterization of pectin methylesterase Inhibitor 3 from Arabidopsis thaliana. Cell Surf. *8*, 100080.

69. Müller, K., Levesque-Tremblay, G., Bartels, S., Weitbrecht, K., Wormit, A., Usadel, B., Haughn, G., and Kermode, A.R. (2013). Demethylesterification of cell wall pectins in Arabidopsis plays a role in seed germination. Plant Physiol. *161*, 305–316.

70. Li, Z., Sela, A., Fridman, Y., Garstka, L., Höfte, H., Savaldi-Goldstein, S., and Wolf, S. (2021). Optimal BR signalling is required for adequate cell wall orientation in the Arabidopsis root meristem. Development *148*, dev199504.

71. Mravec, J., Kračun, S.K., Rydahl, M.G., Westereng, B., Miart, F., Clausen, M.H., Fangel, J.U., Daugaard, M., Van Cutsem, P., De Fine Licht, H.H., et al. (2014). Tracking developmentally regulated post-synthetic processing of homogalacturonan and chitin using reciprocal oligosaccharide probes. Development *141*, 4841–4850.

72. Peaucelle, A., Braybrook, S.A., Le Guillou, L., Bron, E., Kuhlemeier, C., and Höfte, H. (2011). Pectin-induced changes in cell wall mechanics underlie organ initiation in Arabidopsis. Curr. Biol. *21*, 1720–1726.

73. Oyoshi, K., Katano, K., Yunose, M., and Suzuki, N. (2020). Memory of 5-min heat stress in Arabidopsis thaliana. Plant Signal. Behav. *15*, 1778919.

74. Silva-Correia, J., Freitas, S., Tavares, R.M., Lino-Neto, T., and Azevedo, H. (2014). Phenotypic analysis of the Arabidopsis heat stress response during germination and early seedling development. Plant Methods *10*, 7.

75. Suter, L., and Widmer, A. (2013). Phenotypic effects of salt and heat stress over three generations in Arabidopsis thaliana. PLoS One *8*, e80819.

76. Wu, J.-R., Wang, L.-C., Lin, Y.-R., Weng, C.-P., Yeh, C.-H., and Wu, S.-J. (2017). The Arabidopsis heat-intolerant 5 (hot5)/enhanced response to aba 1 (era1) mutant reveals the crucial role of protein farnesylation in plant responses to heat stress. New Phytol. *213*, 1181–1193.

77. Dejonghe, W., Sharma, I., Denoo, B., De Munck, S., Lu, Q., Mishev, K., Bulut, H., Mylle, E., De Rycke, R., Vasileva, M., et al. (2019). Disruption of endocytosis through chemical inhibition of clathrin heavy chain function. Nat. Chem. Biol. *15*, 641–649.

78. Zhang, L., Xing, J., and Lin, J. (2019). At the intersection of exocytosis and endocytosis in plants. New Phytol. *224*, 1479–1489.

79. López-Hernández, T., Haucke, V., and Maritzen, T. (2020). Endocytosis in the adaptation to cellular stress. Cell Stress *4*, 230–247.

80. Couchoud, M., Der, C., Girodet, S., Vernoud, V., Prudent, M., and Leborgne-Castel, N. (2019). Drought stress stimulates endocytosis and modifies membrane lipid order of rhizodermal cells of Medicago truncatula in a genotype-dependent manner. BMC Plant Biol. *19*, 221.

81. Pattathil, S., Avci, U., Baldwin, D., Swennes, A.G., McGill, J.A., Popper, Z., Bootten, T., Albert, A., Davis, R.H., Chennareddy, C., et al. (2010). A comprehensive toolkit of plant cell wall glycan-directed monoclonal antibodies. Plant Physiol. *153*, 514–525.

82. Hruz, T., Laule, O., Szabo, G., Wessendorp, F., Bleuler, S., Oertle, L., Widmayer, P., Gruissem, W., and Zimmermann, P. (2008). Genevestigator v3: a reference expression database for the meta-analysis of transcriptomes. Adv. Bioinformatics *2008*, 420747.

83. Noble, J.A., Bielski, N.V., Liu, M.-C.J., DeFalco, T.A., Stegmann, M., Nelson, A.D.L., McNamara, K., Sullivan, B., Dinh, K.K., Khuu, N., et al. (2022). Evolutionary analysis of the LORELEI gene family in plants reveals regulatory subfunctionalization. Plant Physiol. *190*, 2539–2556.

84. Geldner, N., Hyman, D.L., Wang, X., Schumacher, K., and Chory, J. (2007). Endosomal signaling of plant steroid receptor kinase BRI1. Genes Dev. *21*, 1598–1602.

85. Robatzek, S., Chinchilla, D., and Boller, T. (2006). Ligand-induced endocytosis of the pattern recognition receptor FLS2 in Arabidopsis. Genes Dev. *20*, 537–542.

86. Petrásek, J., Mravec, J., Bouchard, R., Blakeslee, J.J., Abas, M., Seifertová, D., Wisniewska, J., Tadele, Z., Kubes, M., Covanová, M., et al. (2006). PIN proteins perform a rate-limiting function in cellular auxin efflux. Science *312*, 914–918.

87. Clough, S.J., and Bent, A.F. (1998). Floral dip: a simplified method for Agrobacterium-mediated transformation of Arabidopsis thaliana. Plant J. *16*, 735–743.

88. Morato do Canto, A., Ceciliato, P.H., Ribeiro, B., Ortiz Morea, F.A., Franco Garcia, A.A., Silva-Filho, M.C., and Moura, D.S. (2014). Biological activity of nine recombinant AtRALF peptides: implications for their perception and function in Arabidopsis. Plant Physiol. Biochem. *75*, 45–54.

89. Matthus, E., Wilkins, K.A., Swarbreck, S.M., Doddrell, N.H., Doccula, F.G., Costa, A., and Davies, J.M. (2019). Phosphate starvation alters abiotic-stress-induced cytosolic free calcium increases in roots. Plant Physiol. *179*, 1754–1767.

90. Li, R., Raikhel, N.V., and Hicks, G.R. (2012). Chemical effectors of plant endocytosis and endomembrane trafficking. In Endocytosis in Plants, J. Šamaj, ed. (Springer), pp. 37–61.

91. Van Damme, D., Gadeyne, A., Vanstraelen, M., Inzé, D., Van Montagu, M.C.E., De Jaeger, G., Russinova, E., and Geelen, D. (2011). Adaptin-like protein TPLATE and clathrin recruitment during plant somatic cytokinesis occurs via two distinct pathways. Proc. Natl. Acad. Sci. USA *108*, 615–620.

92. Ortiz-Zapater, E., Soriano-Ortega, E., Marcote, M.J., Ortiz-Masiá, D., and Aniento, F. (2006). Trafficking of the human transferrin receptor in plant cells: effects of tyrphostin A23 and brefeldin A. Plant J. *48*, 757–770.

93. Boutté, Y., Frescatada-Rosa, M., Men, S., Chow, C.-M., Ebine, K., Gustavsson, A., Johansson, L., Ueda, T., Moore, I., Jürgens, G., et al. (2010). Endocytosis restricts Arabidopsis KNOLLE syntaxin to the cell division plane during late cytokinesis. EMBO J. *29*, 546–558.

94. Norkunas, K., Harding, R., Dale, J., and Dugdale, B. (2018). Improving agroinfiltration-based transient gene expression in Nicotiana benthamiana. Plant Methods *14*, 71.

95. Zhang, Y., Chen, M., Siemiatkowska, B., Toleco, M.R., Jing, Y., Strotmann, V., Zhang, J., Stahl, Y., and Fernie, A.R. (2020). A highly efficient Agrobacterium-mediated method for transient gene expression and functional studies in multiple plant species. Plant Commun. *1*, 100028.

96. Adler, J., and Parmryd, I. (2010). Quantifying colocalization by correlation: the Pearson correlation coefficient is superior to the Mander's overlap coefficient. Cytom. A *77*, 733–742.

STAR★METHODS

KEY RESOURCES TABLE

REAGENT or RESOURCE	SOURCE	IDENTIFIER
Antibodies		
mouse monoclonal anti-His antibody	Santa Cruz	Sc-8036; RRID:AB_627727
mouse monoclonal anti-HA antibody	Santa Cruz	Sc-7392; RRID:AB-627809
Rat monoclonal anti-JIM5 antibody	University of Georgia, Complex Carbohydrate Research Center	JIM5 (ref. 82)
HRP-conjugated secondary anti-mouse antibodies	ImmunoReagents	Cat # GTxMu-003-DHRPX
Bacterial and virus strains		
Agrobacterium tumefaciens: GV3101	Gold Biotechnology	Cat # CC-207
Escherichia coli: BL21	New England Biolab	Cat # C2530H
Biological samples		
Arabidopsis thaliana	Taxonomy ID: 3702	N/A
Nicotiana benthamiana	Taxonomy ID: 4100	N/A
Chemicals, peptides, and recombinant proteins		
Alexa Fluor647 Cadaverine	ThermoFisher	Cat #A30679
Cyanine 3 hydrazide	Lumiprobe	Cat #11070
Sulfo-Cy3 hydrazide	Lumiprobe	Cat #11370
Sulfo-Cy3-amine	Lumiprobe	Cat #113C0
Sulfo-Cy5-amine	Lumiprobe	Cat #133C0
Sulfo-Cyanine5 NHS Ester	Lumiprobe	Cat #13320
FAM-amine	Lumiprobe	Cat# 151C0
Sulfo-Cyanine3 NHS Ester	Lumiprobe	Cat #11320
FAM-maleimide	Lumiprobe	Cat #44180
CF™ 640R aminooxy	Sigma	Cat #SCJ4600041
EDC	CreoSalus	RC8102
Sulfo-NHS	Pierce	PG82071
FM4-64	Life. Technologies	Cat #1365565
Coelenterazine-H	Research Products International	Cat #C61500
Wortmannin	Invitrogen	Cat #PHZ1301
Tyrphostin A23	MP Biomedicals	Cat #158820
ES9-17	Sigma	Cat #SML2712
H2DCF-DA	Cayman	Cat #85155
Lipid acid free Bovine Serum Albumin (BSA)	Gold Biotechnology	Cat #A-421-10
Polygalacturonic acid sodium salt	Sigma	Cat #P3850
Galacturonan oligosaccharides DP25-DP50	BioSynth	Cat #OG59705
Galacturonan DP10-DP15	BioSynth	Cat #OG59704
Chitosan oligomer DP12-DP20	BioSynth	Cat #OC168673
1,6-Hexanediol	Alfa Aesar	Cat #12439
(-)-Epigallocatechin Gallate	Selleckchem	Cat #S2250
Estradiol	Cayman	Cat #10006315
RALF1 peptide	Biomatik	Custom made
HIS_6-HA-RALF1	This paper	N/A
HIS_6-HA-RALF23	This paper	N/A

(*Continued on next page*)

Continued		
REAGENT or RESOURCE	SOURCE	IDENTIFIER
Cherry-RALF1-HIS_6	This paper	N/A
HIS_6-HA-RALF1(I6A)	This paper	N/A
HIS_6-HA-RALF1(AAA_{6-8})	This paper	N/A
HIS_6-HA-RALF1(AA25-26)	This paper	N/A
HIS_6-HA-RALF1(AAA37-39)	This paper	N/A
HIS_6-HA-RALF1(K43D)	This paper	N/A
HIS_6-HA-RALF1(AA46,48)	This paper	N/A
HIS_6-HA-RALF1(C18A)	This paper	N/A
HIS_6-HA-RALF1(C41A)	This paper	N/A
MBP-LLG1	This paper	N/A
MBP-FERecd	This paper	N/A
LLG1-HIS_6	This paper	N/A
FERecd-HIS_6	This paper	N/A
Critical commercial assays		
Bac-to-Bac™ Baculovirus Expression System	Gibco	Cat # 10359016
PureLink ™ RNA Mini Kit	Invitrogene	Cat # 12183018A
Experimental models: Cell lines		
Insect cell: SF9	Expression Systems	94-001F
Insect cell: Tni	Expression Systems	94-002S
Experimental models: Organisms/strains		
WT$^{FERp:FER-GFP}$	Duan et al.[10]	N/A
PMEI5OE$^{FERp:FER-GFP}$	This paper	N/A
llg1-2 $^{35S:LLG1-GFP}$	This paper	N/A
WT $^{REM1.2:REM1.2-YFP}$	Jarsch et al.[52]	N/A
fer-4 $^{REM1.2:REM1.2-YFP}$	This paper	N/A
llg1-2 $^{REM1.2:REM1.2-YFP}$	This paper	N/A
WT $^{35S:AHA2-GFP}$	This paper	N/A
fer-4 $^{35S:AHA2-GFP}$	This paper	N/A
llg1-2 $^{35S:AHA2-GFP}$	This paper	N/A
WT $^{35S:BRI1-GFP}$	Geldner et al.[84]	N/A
fer-4 $^{35S:BRI1-GFP}$	This paper	N/A
llg1-2 $^{35S:BRI1-GFP}$	This paper	N/A
WT $^{FLS2:FLS-GFP}$	Robatzek et al.[85]	N/A
er105 $^{ERECTA:ERECTA-YFP}$	Lee et al.[49]	N/A
WT $^{35S:MEDOS2-GFP}$	This paper	N/A
WT $^{PIN2:PIN2-GFP}$	Petrásek et al.[86]	N/A
fer-4 $^{PIN2:PIN2-GFP}$	This paper	N/A
llg1-2 $^{PIN2:PIN2-GFP}$	This paper	N/A
WT $^{VENUS-AUX1}$	ABRC	CS67173
WT $^{35S:LTI1.6-YFP}$	Feng et al.[20]	N/A
WT $^{35S:PMEI5}$	Wolf et al.[67]	N/A
WT $^{35S:AEQUORIN}$	Haruta et al.[42]	N/A
fer-4 $^{35S:AEQUORIN}$	Haruta et al.[42]	N/A
$WT^{E2;\ XVE>>AX2}$	Ortiz-Morea et al.[44]	N/A
WT $^{RALF1:RALF1-GFP}$	This paper	N/A
ralf1-3	ABRC	SALK_205367C
ralf1-4	ABRC	GABI969810

(*Continued on next page*)

Continued

REAGENT or RESOURCE	SOURCE	IDENTIFIER
s1p	Zhao et al.[34]	N/A
chc2-1	Ortiz-Morea et al.[44]	N/A
fer-4	Duan et al.[10]	N/A
llg1-2	Li et al.[9]	N/A
Recombinant DNA		
p1352-FER:FER-CFP	This paper	N/A
p1352-FER:FER-GFP	Duan et al.[10]	N/A
p1352-35S:LLG1-cYFP-LLG1gpi	This paper	N/A
p1352-35S:BRI1-GFP	This paper	N/A
pCAMBIA1390-FLS2p:FLS2-myc-Ch	This paper	N/A
pCAMBIA1390-35S:BRI1-CFP	This paper	N/A
pCAMBIA1390-35S:PMEI5-HA	This paper	N/A
pCAMBIA1390-35S:PMEI3-HA	This paper	N/A
pCAMBIA1390-35S:ADPG1-HA	This paper	N/A
pCAMBIA1390-35S:P19	This paper	N/A
pCAMBIA1390-35S:OGOX1-HA (OGOX1oe)	This paper	N/A
pCAMBIA1390-RALF1p:RALF1-GFP	This paper	N/A
pCAMBIA1390-35S:PME5-GFP	This paper	N/A
pET21a-HA-RALF1	Li et al.[9]	N/A
pET21a-HA-RALF23	This paper	N/A
pET28a-mcherry-RALF1	This paper	N/A
pET21a-HA-RALF1(I6A)	This paper	N/A
pET21a-HA-RALF1(AAA6-8)	This paper	N/A
pET21a-HA-RALF1(AA25-26)	This paper	N/A
pET21a-HA-RALF1(AAA37-39)	This paper	N/A
pET21a-HA-RALF1(K43D)	This paper	N/A
pET22a-HA-RALF1(AA46,48)	This paper	N/A
pET28a-HA-RALF1(C18A)	This paper	N/A
pET28a-HA-RALF1(C41A)	This paper	N/A
pMALc-MBP-LLG1	Li et al.[9]	N/A
pMALc-MBP-FERecd	Duan et al.[10]	N/A
pFastBacTOPO-LLG1	This paper	N/A
pFastBacTOPO-FERecd	This paper	N/A
Software and algorithms		
FIJI	NIH	https://fiji.sc/
Prism	Prism software	https://www.graphpad.com/features
Nikon NIS-Elements AR	NIKON	https://www.microscope.healthcare.nikon.com/en_AOM/products/software/nis-elements
Others	None	N/A
Oligonucleotides		
Primer	**Sequence**	
p1352-FER:FER-CFP-F	CCGCGCGGATCCATGAAGATCACAGAGGGACGATTCC	
p1352-FER:FER-CFP-R	CGCCGTCGACACGTCCCTTTGGATTCATGATCTG	
p1352-FER:FER-GFP-F	CCGCGCGGATCCATGAAGATCACAGAGGGACGATTCC	
p1352-FER:FER-GFP-R	CGCCGTCGACACGTCCCTTTGGATTCATGATCTG	
p1352-35S:LLG1-cYFP-LLG1gpi-F	CGCAGATCTAGTTTCATTTCAGATGGGGTCTTC	
p1352-35S:LLG1-cYFP-LLG1gpi-R	CGTCGACCGAGGTAGTTGCTGCGTTTACCTC	

(*Continued on next page*)

Continued

REAGENT or RESOURCE	SOURCE	IDENTIFIER
p1352-35S:BRI1-GFP-F	GGATCCATGAAGACTTTTTCAAGCTTCTTTCTC	
p1352-35S:BRI1-GFP-R	CGTCGACTAATTTTCCTTCAGGAACTTCTTTTAT	
pCAMBIA1390-FLS2p:FLS2-myc-Ch-F	CGCGCGGATCCATGAAGTTACTCTCAAAGACC	
pCAMBIA1390-FLS2p:FLS2-myc-Ch-R	CGGCTAGTCGACAACTTCTCGATCCTCGTTACG	
pCAMBIA1390-35S:PMEI5-HA-F	CGGATCCATGGCCACAATGCTAATAAACCAC	
pCAMBIA1390-35S:PMEI5-HA-R	CGTCGACGGTCACAAGCTTGTTGAAAATAAG	
pCAMBIA1390-35S:PMEI3-HA-F	CCGCGGATCCACGGCTCCTACACAAAATCTCTTC	
pCAMBIA1390-35S:PMEI3-HA-R	CCGCGTCGACAAGATGTACGTCGTGGGGTTTGCC	
pCAMBIA1390-35S:ADPG1-HA-F	CGCCGGATCCATGGCCCGTTGTTGCAGACATCTTGC	
pCAMBIA1390-35S:ADPG1-HA-R	CGCCGTCGACAGAGCATTTAGGAGAAACGGTGCC	
pCAMBIA1390-35S:OGOX1-HA (OGOX1oe)-F	CCGGCGGATCCATGCTCACGACACCTCCACGAACC	
pCAMBIA1390-35S:OGOX1-HA (OGOX1oe)-R	CCGCGGTCGACGAAGACATGTAAGACCACCGTCGC	
pCAMBIA1390-RALF1p:RALF1-GFP-F	AGCGGCCGCTAGGAAGATTTTGATCACCGG	
pCAMBIA1390-RALF1p:RALF1-GFP-R	CGGATCCTTTCTTGCCTTTCTTTGGGTTC	
pET21a-HA-RALF1-F	CGGATCCGCGACCACAAAATACATAAGC	
pET21a-HA-RALF1-R	CGTCGACCTAACTCCTGCAACGAGCAAT	
pET21a-HA-RALF23-F	CGGATCCGCTACGAGGAGGTACATCAGC	
pET21a-HA-RALF23-R	CCTCGAGTGAGCGCCGGCAGCGAGTGATGG	
pET28a-mcherry-RALF1-F	CGGATCCGCGACCACAAAATACATAAGC	
pET28a-mcherry-RALF1-R	CGTCGACCTAACTCCTGCAACGAGCAAT	
pET21a-HA-RALF1(I6A)-F	ACAAAATACGCTAGCTATCAGTCT	
pET21a-HA-RALF1(I6A)-R	CTGATAGCTAGCGTATTTTGTGGA	
pET21a-HA-RALF1(AAA6-8)-F	CGGATCCGCGACCACAAAATACGCTGCAGCTCAGTCTTTGAAACGGAAC	
pET21a-HA-RALF1(AAA6-8)-R	CGTCGACCTAACTCCTGCAACGAGCAAT	
pET21a-HA-RALF1(AA25,26)-F	GGTGCGTCTGCAGCCAATTGTCAGAACGGA	
pET21a-HA-RALF1(AA25,26)-R	CTGACAATTGGCTGCAGACGCACCTCTTCTTGA	
pET21a-HA-RALF1(AAA37-39)-F	CGGATCCGCGACCACAAAATACATAAGC	
pET21a-HA-RALF1(AAA37-39)-R	CGTCGACCTAACTCCTGCAACGAGCAATTTTGCTGCAACCTGCTGCAGC	
pET21a-HA-RALF1(K43D)-F	CGGATCCGCGACCACAAAATACATAAGC	
pET21a-HA-RALF1(K43D)-R	CGTCGACCTAACTCCTGCAACGAGCGATATCGCTGCAACCACGACTATA	
pET21a-HA-RALF1(AA46,48)-F	CGGATCCGCGACCACAAAATACATAAGC	
pET21a-HA-RALF1(AA46,48)-R	CGGTCGACCTAGCTAGCGCAAGCAGCGATATCGCTGCAACCACG	
pET21a-HA-RALF1(C18A)-F	CCTCGAGCTAGTCGACGGTATCGATAAGCTTGATATC	
pET21a-HA-RALF1(C18A)-R	ACCTCTTCTGCTAGCAGGCACACTGTTCCGTTTC	
pET21a-HA-RALF1(C41A)-F	AGTCGTGGTGCTAGCAAAATTGCTCGTTGC	
pET21a-HA-RALF1(C41A)-R	AATTTTGCTAGCACCACGACTATAAGG	
pMALc-MBP-LLG1-F	CGCAGATCTAGTTTCATTTCAGATGGGGTCTTC	
pMALc-MBP-LLG1-R	CGTCGACCGAGGTAGTTGCTGCGTTTACCTC	
pMALc-MBP-FERecd-F	CCGCGGGATCCGCTGCTGATACTCTCCAACA	
pMALc-MBP-FERecd-R	CCGCGGTCGACAGCCGTATTGCTTTTGCATTTCC	
pFastBacTOPO-LLG1-F	CGCAGATCTAGTTTCATTTCAGATGGGGTCTTC	
pFastBacTOPO-LLG1-R	CGTCGACCGAGGTAGTTGCTGCGTTTACCTC	
pFastBacTOPO-FERecd-F	CCGCGGGATCCGCTGCTGATACTCTCCAACA	
pFastBacTOPO-FERecd-R	CCGCGGTCGACAGCCGTATTGCTTTTGCATTTCC	
RALF1-RT-F	ATGGACAAGTCCTTTACTCTG	
RALF1-RT-R	CTAACTCCTGCAACGAGCAAT	
S1P-RT-F	GGCATTGATTTGGGTAGAGGC	
S1P-RT-R	GGCTAATCGATTCGACCCTGATGC	

(*Continued on next page*)

Continued

REAGENT or RESOURCE	SOURCE	IDENTIFIER
ADPG1-RT-F	GGATCAGCAACTGCCAAGAAC	
ADPG1-RT-R	AGAGCATTTAGGAGAAACGGTGCC	
ADPG2-RT-F	TGCGAAGACCAAGAGTCGGCA	
ADPG2-RT-R	AGTGGAGTTGCACTGAGGCAG	
Actin-RT-F	CGTACAACCGGTATTGTGCTGG	
Actin-RT-R	GGAGATCCACATCTGCTGGAATG	

RESOURCE AVAILABILITY

Lead contact

Further information and requests for resources and reagents should be directed to and will be fulfilled by the lead contact, Alice Y. Cheung (acheung@biochem.umass.edu).

Materials availability

Constructs and plant seeds generated in this study will be available from the lead contact upon request.

Data and code availability

All data reported in this paper are available from the lead contact upon request.

Any additional data required to reanalyze the data reported in this paper is available from the lead contact upon request.

This study did not generate any code or additional information.

EXPERIMENTAL MODEL AND STUDY PARTICIPANT DETAILS

- *Arabidopsis thaliana* Col-0, seedlings
- *Nicotiana benthamiana*, leaves
- *In vitro*

METHOD DETAILS

Plant material, growth, transformation

Wild-type *Arabidopsis thaliana* ecotype Columbia (*A. thaliana* Col-1), *fer-4*,[10] *llg1-2*,[9] *ralf1-3 (SALK_205367C)*, *ralf1-4 (GABI969810)*, *chc2-1*,[45,46] *s1p*[34] and various transformed *A. thaliana* lines were used in this study. For tissue culture-grown plants, seeds were germinated on Gamborg's B5 (B5) or ½-strength Murashige and Skoog (½ MS) medium supplemented with 1% sucrose, 0.7 % agar, pH 5.7. After stratification at 4° C for 2 days, plates were transferred to 22 °C for germination and growth in a growth chamber under a 12-h/12-h light-dark cycle.[6,7] Three or four-days-old seedlings were used for root growth and cell biological assays, respectively. Arabidopsis transformation was performed using the floral dip method.[87] *Nicotiana benthaminan* plants were grown at 28°C for transient transformation by Agroinfiltration according to Bücherl et al.[55]

Recombinant DNA construction

Recombinant constructs for fusion proteins were generated following basic molecular cloning procedures. RALFs are processed from pre-pro proteins; mature RALF1 and RALF23 from Arabidopsis span positions 72–120 and 89–138 of their respective full-length precursor proteins[6,7] (Figure S1C); the first amino acid of mature RALF1 is designated position 1, aligned with designations in the crystallographic study.[8] Recombinant mature RALFs were N-terminally tagged by HIS_6 for affinity purification; unless the HIS_6 tag was used for immunodetection, only the secondary tag, such as HA, also on the N-terminus is indicated in the text or figures. Oligonucleotide primers were synthesized by Sigma-Aldrich.

Fusion protein expression and purification

Every RALF preparation (in 100 mM NaCl, 50 mM sodium acetate, pH 5.7) was examined for quality on SDS-PAGE and tested in root growth assays[7,42,88] (see Figure S1) prior to use in functional analyses. For recombinant LLG1 fusion proteins, the core region (amino acids 24–149, i.e. without the C-terminal signature region for GPI-anchor modification)[9] was used. Immunodetection of insect cell-produced FERecd-HIS_6 and LLG1-HIS_6 was carried out on PVDF membranes (Millipore). Ponceau S-staining to assess sample loading was followed by immunodetection using anti-His (Santa Cruz) (Figure S1N). Signal was detected by chemiluminescence using the PXi image documentation system (Syngene).

E. coli produced HIS_6-tagged and maltose-binding protein (MBP)-tagged recombinant proteins were prepared as described.[9,10] LLG1-HIS_6 and $FERecd^9$-HIS_6 were expressed in Sf9 or Hi5 insect cells using the BAC-to-Bac Baculovirus Expression System (Invitrogen) according to the manufacturer's instructions. Proteins from insect cell culture supernatants was affinity-purified on Ni-Sepharose Excel resin (GE) according to the manufacturer's instructions. Spectra/Por 3 dialysis tubing (Spectrum) was used for dialysis. Purified proteins were examined by SDS-PAGE (Figure S1) to assess their quality and confirm the quantification results. All recombinant proteins contained a secondary tag for immunodetection or fluorescence imaging, including HA, GFP, citrine-YFP (cYFP), cerulean-CFP (cCFP), mCherry (Ch) or a small flurochrome (see below).

Chemical labeling

Chemical labeling was carried out according to manufacturer procedures Fluorochromes used included Alexa Fluor647 Cadaverine, a sulfonylated probe as used in Rigal et al.[53] (ThermoFisher Cat# A30679), Cyanine3 (Cy3) hydrazide (Lumiprobe Cat# 11070), Sulfo-Cy3 hydrazide (Lumiprobe Cat# 11370) and Sulfo-Cy3-amine (Lumiprobe Cat# 113C0). Sulfo-Cyanines were used unless indicated otherwise. Sulfo-Cy5 NHS Ester (Lumiprobe Cat# 13320) and Sulfo-Cy3 NHS Ester (Lumiprobe Cat# 11320) were used for LLG1-His; FAM-maleimide (Lumiprobe Cat# 44180) was used for FERecd-His labeling. Bioactivity of labeled RALF1 was assessed after each preparation on root growth assays and determined to be comparable to before labeling samples (Figures S1K and S1L).

Sulfo-Cy5-amine (Lumiprobe Cat# 133C0) or Sulfo-Cy3-amine (Lumiprobe Cat# 113C0) or FAM-amine (Lumiprobe, Cat# 151C0) were used to label $OG_{DP10\text{-}15}$. Carboxyl groups of OG were activated by mixing with freshly made EDC (CreoSalus RC8102) and Sulfo-NHS (Pierce PG82071) according to manufacturer's instructions, followed by adding a five-time volume of 100% ethanol to precipitate OG to remove free Sulfo-NHS. OG pellet was dried and resuspended with 200 μl of 0.1 M Sodium bicarbonate, pH 8.3. 10 μl of Sulfo-Cy5-amine (Lumiprobe Cat# 133C0) was added to the reaction mixture, incubated at room temperature for 2 hrs. After labeling, OG was precipitated with 100% ethanol to remove free dye, then washed twice with 100% ethanol. The OG pellet was dried and resuspended in ~100 μl ddH_2O to a 20 mg/ml final concentration. For chitosan[71] labeling, the aldehyde group at the C-terminal end of oxidative carbohydrate sugar was labeled with CF™640R aminooxy (Sigma Cat# SCJ4600041). 10 μl of CFTM640R aminooxy (Sigma Cat# SCJ4600041) was added to the reaction mixture in 50 mM sodium acetate, pH5.7, incubated in the dark at 37 °C for overnight (~16 hr). After labeling, chitosan was precipitated with 100% ethanol to remove free dye, then washed twice with 100% ethanol. The chitosan pellet was dried and resuspended in ~100 μl ddH_2O to a 20 mg/ml final concentration.

Seedling growth assays

Seedling root growth and medium alkalinization were assessed as described previously.[9,42,88] RALF1 and RALF23 showed comparable activity in root growth assays (Figures S1F and S1G). Three-days-old light-grown seedlings were treated in growth medium under treatment or control (mock) condition for 2 days. For growth medium pH and primary root growth assays, samples were measured at the beginning and end of treatments. For root growth, growth plates were scanned at the beginning and end, or intermittently, for measurement by FIJI at the end of experiments. All experiments were repeated at least three times with similar results.

Aequorin-based calcium influx assay

The luminescence assays followed.[89] 3-4 days-old seedlings were preincubated in 96-well plates overnight (~16 hrs) in 200 μl of 1/2MS liquid media with 2.5 μM coelenterazine cp (Sigma). The assays were initiated by adding 50 μl of 50 mM Sodium phosphate (pH7.4) containing signal molecules. Luminescence was monitored every 2 seconds for one minute by microplate reader (Synergy H1) immediately after the application of treatment solution.

Analyses of signal-triggered responses

Various RALF peptides (Figure S1) were used. Each RALF preparation was tested for its efficacy in endocytosis assays. Dose–response and time course-dependent responses (Figures S2A–S2D) established optimum treatment conditions to be 1-4 μM peptide, for 15-40 mins. flg22 treatment followed.[55] Treatment conditions are indicated in figures or their legends. When chemically labeled fluorescent RALF1 was used, seedlings were rinsed extensively in growth medium prior to observation. Controls (mock samples) were treated similarly except for treatment reagents added.

Treatments with various chemicals followed published[53,90–93] and manufacturers' recommendations. For FM4-64[53] (Life Technologies, #1365565) labeling of endocytic membrane, seedlings were pre-treated with FM4-64 (1 μM, 15 mins) prior to RALF1 (1 μM, 30 mins), $OG_{DP10\text{-}15}$ (0.1 mg/ml, 30 mins), salt (150 mM NaCl, 15mins), or heat (30 °C, 15 mins) treatment. For Wortmannin[90] (Invitrogen, Cat# PHZ1301) treatment to inhibit endocytosis, seedlings were pretreated with or without wortmannin for 30 min, followed by RALF1 treatment for 30 min. For clathrin-dependent endocytosis inhibitors, seedlings were co-treated with RALF1 and Tyrphostin A23 [TyrA23][91,92] (MP Biomedicals, Cat#158820), and ES9-17[77] (Sigma Cat #SML2712) as indicated in the figure panels. Estradiol treatment followed.[44] Concentrations of estradiol used were pre-determined not to significantly impact growth for the duration of experiments (see Figure S6K).

Samples were microscopically examined.

Agroinfiltration

Figure S3C provides a workflow for Agroinfiltration experiments carried out in *N. benthamiana* performed generally following published procedures.[55] Agrobacteria carrying various transgenes resuspended in 10 ml infiltration buffer (10 mM $MgCl_2$, 10 mM MES, pH 5.6, 0.5% glucose) with 100 μM acetosyringone. 1 ml of bacteria (adjusted to OD_{600} = 0.4 to 0.8) was syringe-infiltrated into the adaxial sides of *N. benthamiana* leaves. When needed, Agrobacteria containing *35S::P19*[94] were co-infiltrated to augment the expression of some constructs. Transfected samples were examined 48–72 h after infiltration. Bacteria dosage and transfection times were pre-assessed in pilot experiments to determine working conditions. When $OG_{DP10\text{-}15}$ was used, it was syringe-infiltrated for an hour before RALF infiltration.

Arabidopsis seedling Agroinfiltration to transiently express receptor-FP proteins in wild type, *fer-4* and *llg1-2* Arabidopsis leaves followed the procedure.[95] Briefly, Agrobacteria carrying transgenes of interest were resuspended with wash solution (500 μl, 10 mM MgCl2, 100 μM acetosyringone), then diluted ten-fold into wash buffer for OD_{600} measurement and adjustment to OD_{600} = 0.3 to 0.4 using infiltration solution (1/4 MS, pH6.0, 1% sucrose, 100 μM acetosyringone, 0.005% Silwet L-77) and 50 μl of bacteria suspension was syringe-infiltrated into the adaxial sides of *Arabidopsis thaliana* leaves. For RALF treatments, the peptides were syringe-infiltrated (~100–200 μl of 1 μM peptide in Agroinfiltration buffer) or vacuum-infiltrated. Responses were monitored by confocal microscopy starting from ~10 min to 60 mins as indicated in figures.

Stress-related analyses

For growth-related studies, 3 or 4-day-old seedlings [*fer-4, llg1-2, 35S-PMEI5*,[67] *and ralf1-3, ralf1-4*, *chc2-1*, *XVE>>AX2*[44] and *s1p*[34]] were germinated on ½ MS agar. For growth under heat stress, seedlings were transferred to 37°C to continue growth for 48 hrs. For salt stress, seedlings were transferred to ½ MS agar with 150 mM NaCl for continued growth for 48 hrs. Root lengths were measured at 0, 24 and 48 hrs of treatments as indicated in figures. For root growth recovery after transient salt stress, seedlings were treated with 150 mM NaCl with for 3 hours, washed with ½ MS twice and transferred to ½ MS agar plates. For recovery from heat stress, seedlings were treated at 37 °C for 2 hours and returned to 22 °C. For endocytosis inhibitor treatments, WT seedlings were pre-treated with inhibitors (30 μM TyrA23, 30 μM ES9-17) for 30 mins, treated with 150 mM NaCl for 3 hours or heat (37 °C) for 2 hours. Seedlings were returned to normal growth conditions for recovery and monitored for 48 hrs. Primary root lengths were measured by FIJI. Figure S6I shows the experimental workflow.

For stress-induced receptor responses in transiently transformed *N. benthamiana* leaves, samples (at ~48 hrs after Agroinfiltration) were either vacuum-infiltrated with NaCl (150 mM) for 5 min at 22 °C and left for 30 minutes prior to observation, or with elevated temperature (indicated in figures) for 30 mins and observed immediately after treatment. Surface clusters were monitored between 10-60 minutes; endocytic responses were recorded between 40-60 minutes. For OG application, $OG_{DP10\text{-}15}$ was applied at 0.1 mg/ml $OG_{DP10\text{-}15}$ by injection or vacuum infiltration. Images from comparative samples was acquired at similar times between 25-30 mins after treatment.

For salt stress-induced cell surface responses in seedlings, 3-4 days old wild-type or transformed Arabidopsis seedlings expressing various fluorescent protein-tagged target membrane proteins were treated either with NaCl (150 mM) for five minutes, left at 22 °C for another 30 min prior to observation. For heat-stress, seedlings were treated with elevated temperature (42 °C) for 30 mins, followed by observation. To track general endocytosis, wild-type and mutant seedlings were pre-treated with 1 μM FM4-64[53] for 15 mins, followed by either 150 mM NaCl for 15 mins at 22 °C or elevated temperature (30 °C) for 15 mins.

For stress-induced cell surface response in seedlings, wild-type, *fer-4* and PMEI5oe seedlings were pre-treated with 150 mM NaCl for 3 hours at 22 °C or with elevated temperature (37 °C) for 2 hours, followed by treatment with 1 μM Cy3-RALF1 for 10 mins before observation.

For RT-PCR analysis of stress-induced gene expression, 7 to 8-days-old wild type seedlings were treated with 150 mM NaCl or heat (37 °C) for 1 and 2 hours, total RNA was extracted with PureLink™ RNA Mini Kit (Invitrogene, Cat #. 12183018A). 3 μg RNA was used for RT-PCR. Data from stress experiments was also extracted from Genevestigator[82] for comparison.

For stress- and RALF1-induced changes in de-esterified pectin, 20 8-days old wild type seedlings were treated with 150 mM NaCl, 42 °C for 3.5 hours, or 1 μM HA-RALF1 for 30 min. Treated seedlings were collected, ground, and extracted with 150 μl buffer (50 mM CDTA, 50 mM ammonium oxalate, 50 mM ammonium acetate, pH 5.5). After 20 min, samples were centrifuged with at top speed (13.3k rpm) and the supernatants were transferred to the new microfuge tubes. Then, 150 μl of 3M NaOAc, pH5, and 750 μl 100 % ethanal were added. Samples were kept at -80°C for 1hr to precipitate the pectin. Samples were centrifuged at full speed (13.3k rpm), then the pellet was washed with 75% ethanol and dried. The dry pellet was resuspended with 50 μl ddH2O. For immunodetection of pectins, 2 μl of the samples was spotted on the nitrocellulose filter paper, dried for 30 minutes, followed by a standard filter binding assay with JIM5 and JIM7 antibodies for detection of de-esterified and methylesterified pectins.[81]

Seedling ROS assay

ROS assays followed.[9,10] 4-days-old seedlings were treated with 1 μM RALF1 and 5 μM H2DCF-DA (2',7'-dichlorofluorescein diacetate) (Cayman, Cat#85155) for 30 mins or 0.5 mg/ml $OG_{DP10\text{-}15}$ and 10 μM H2DCF-DA for 30 mins in ½ MS liquid medium, followed by washing twice with ½ MS liquid medium before observation. Comparative images were taken under the same exposure time, and signals were quantified with the same ROI by FIJI.

Microscopy, image processing and data quantification

Laser scanning confocal microscopy was performed on a NIKON A1. Images were acquired using default settings (GFP and FAM with 488ex; cYFP with 514ex, Ch, RFP and Cy3 with 561ex, Alexa647 and Cy5 with 640ex). Total internal reflection fluorescence microscopy (TIRFm) was carried out on a Nikon Ti using a 100x TIRF objective; images were acquired by a sCMOS camera. Widefield fluorescence microscopy was carried out on a Nikon Ti.

For colocalization analysis, GFP/Ch signals were acquired with 488 nm ex/525 nm em (GFP) and 561 nm ex/595 nm em (Ch); CFP colocalization with GFP or YFP, signals were acquired with 445 nm ex/540 nm em for CFP, and 514 nm ex/617.5 nm em for GFP and YFP. Images were displayed using Nikon NIS-Elements AR Analysis Software (V 5.02) or FIJI and assembled in Photoshop. Identical imaging conditions were used for comparative samples. Where images are shown with brightness and/or contrast adjustments, comparative images were modified identically. Quantitative analyses of particle numbers and Pearson's correlation coefficient of colocalization[96] were performed with Nikon NIS-Elements AR Analysis Software; particle size $\geq$ 0.1 μm, $\geq$ 0.25 μm or $\geq$ 0.5 μm used for quantifications as indicated in figure legends. For seedling root data, puncta from 100 μm^2 regions in single optical sections (0.5 or 0.25 μm) of five representative cells per seedling were counted with identical fluorescence intensity thresholds for all lines compared. Three to five roots were counted for each condition. For Agroinfiltration studies, fluorescently labeled puncta with diameters $\geq$ 0.25 μm was counted in 100 μm^2 or 500 μm^2 (25 x 20 μm) ROI as indicated in figure legends from single optical sections (0.25 μm) using identical fluorescence intensity thresholds for comparative samples.

Co-localization analysis was carried out with FIJI as described in Bücherl et al.[55] The acquired images were 'mean' filtered with a radius of 2 pixels. Background was subtracted using the 'rolling ball' method with a radius of 20 pixels. Equally-sized regions of interest were manually selected for co-localization analysis, and quantification was performed using the plugin Intensity Correlation Analysis in FIJI. Random sampling by NIS analysis software produced similar results. For quantifications. Pearson's correlation coefficients, -1 to 1, indicate increasingly higher confidence for signal colocalization.[96]

Protein–protein interaction assays

In vitro protein–protein interactions were detected using *E. coli*- or insect cell-produced recombinant proteins (Figure S1; key resources table).

Protein pull-down assays used *E. coli*-expressed target proteins according to Li et al.[9] and Duan et al.[10] For filter-binding assays, different amounts of bait proteins were applied (2 μl from a concentration series) to nitrocellulose membrane (Bio-Rad, Cat #162-0112) by direct spotting onto membranes for dot blots. For immunodetection, membranes were blocked with 5% fatty acid free bovine serum albumin (BSA) (GoldBio; #A-412-10) in 1x TBST (TBS [20 mM Tris-HCl pH 7.5, 150 mM NaCl], with 0.1% Tween-20) for 1 h, followed by incubation for 1 h with target proteins. After three washes in 1x TBST buffer, 10 min each, immunodetection was carried out as described above.

For microscale thermophoresis (MST) of RALF1 interaction with LLG1, Cy5-LLG1-HIS_6 was dialyzed extensively into buffer (50 mM sodium phosphate, pH 7.5, 200 mM NaCl) after labeling and adjusted to 100 nM in MST buffer (25 mM sodium acetate, pH 6.0, 100 mM NaCl, and 0.001% Tween-20) and HIS_6-HA-RALF1 (25 μM to 0.000763 μM in MST buffer) was added. The samples were loaded into Monolith NT.115 Premium Capillaries (MOK025), and molecular interactions were monitored by the Monolith NT.115 system (NanoTemper Technologies) at medium MST power, 20–30% LED power. The data were further analyzed using MO Affinity Analysis software (V2.3).

For fluorescence anisotropy assays for interactions between RALF1 and mutant RALF1s with OG, FAM-$OG_{DP10-15}$ was adjusted to 5 μM in buffer [50 mM Sodium acetate, pH5.7, pH5.7, 100 mM NaCl] containing 0.001% Tween-20. FAM-$OG_{DP10-15}$ was titrated with 35 μM to 0.003418 μM of HIS_6-HA-peptides. The samples were loaded into a 96-well plate (black-bottomed plate) for fluorescence anisotropy measurement with ex485/em528 in the SYNERGY 2 microplate reader (Bio-Tek). Fluorescence anisotropy values (r) were calculated with the equation: $r = (I_{VV} - G \times I_{VH})/ (I_{VV} + 2G \times I_{VH})$ where I_{VV} and I_{VH} are the parallel fluorescence intensities and perpendicular fluorescence intensities, respectively, and G is a correction factor for instrument differences in emission detections Three independent measurements were made for each reaction, their averages were used for the data and the anisotropy titration curves were analyzed with nonlinear curve-fitting analysis.

Protein-pectin interaction assays

For protein-pectin fragment (f-PGA) interaction, filter binding assays followed previous procedures.[20] f-PGA [from sonicated polygalacturonic acid (SIGMA, Cat#P3850] in 10 mM Tris-HCl, pH8 buffer was used in binding for 1 h, followed by immunodetection by JIM5, monoclonal antibody against low-methylesterified pectin.[81] For the filter binding of RALF1 with $OG_{DP10-15}$ and RALF1 with $OG_{DP25-50}$, 1 μM RALF1 in 50 mM sodium acetate, pH5.7, 100 mM NaCl buffer was used in binding for 1 h, followed by immunodetection by mouse-anti-HA (Santa Cruz, #C0419) primary antibody and then anti-Mouse-IgG-HRP (ImmunoReagents, #80-94-052021) secondary antibody. Signal was detected by chemiluminescence using the PXi image documentation system (Syngene).

For MST assays, Cy5-$OG_{DP25-50}$ and Cy5-$OG_{DP10-15}$ [BioSynth, # OG59705, #OG59704] were adjusted to 4 μM and 10 μM, respectively, in MST-Tween (0.001% Tween-20) buffer. Each was titrated with 50 μM to 0.001526 μM of HIS_6-HA-RALF1. For OG-FERecd MST assay, Cy5-$OG_{DP25-50}$ (4 μM) in MST-Tween (0.001% Tween-20) buffer containing 1 mM $CaCl_2$ and titrated with 45 μM to 0.001373 μM of FERecd-HIS_6. The samples were loaded into Monolith NT.115 Capillaries; MOK022 and molecular interactions

were monitored using medium (10% LED) MST power. The data were analyzed by plotting dosage of protein against Cy5-OG-induced fluorescence changes (change in raw fluorescence). Curve fitting was performed, and the Kd values were calculated with 95% confidence level by the Prism 9 (GraphPad Software).

Phase separation assays

In vitro, f-PGA, $OG_{DP25-50}$, $OG_{DP10-15}$ (gifts from CCRC, Athens, Georgia, and Biosynth; Figure S4A), and recombinant proteins were used. Cy5-$Chitosan_{DP12-20}$ (SIGMA, Cat #SCJ4600041) was used as a probe for de-esterified pectin. OG, chitosan[71] and protein labeling were described above. Proteins and pectic fragments used in each experiment were mixed (as indicated in the figure/legends) in 50 mM sodium acetate, pH 5.7, incubated for 5 mins. 4 μl of the mixture was transferred to a glass slide for image acquisition by confocal, widefield fluorescence or DIC. For 1, 6-Hexanediol (Alfa Aesar, Cat#12439) treatment *in vitro*, 0.01 mg/ml $OG_{DP10-15}$ was premixed with 1,6-hexanediol in 50 mM Sodium Acetate, pH5.7, then Cy3-RALF1 (5 μM) was added for 5 mins, followed by imaging. For *in vivo* 1, 6-Hexanediol treatment in seedlings, 4-days-old transgenic seedlings were treated with 1,6-hexanediol together with 1 μM RALF1 for 30 mins, then observed by confocal microscopy.

For fluorescence recovery after photobleaching (FRAP) analysis of *in vitro* assembled condensates, 5 μM Cy3-RALF1 and 0.1 mg/ml $OG_{DP10-15}$ were mixed in 50 mM sodium acetate, 100 mM NaCl, pH 5.7. Individual Cy3-RALF1/OG particle was chosen for initial photobleaching by laser 561ex for 2 seconds with laser power 10, and the fluorescence recovery was imaged at 2s intervals for a total of about 5 mins. For *in vitro* FAM-FERecd FRAP experiment, 5 μM FAM-FERecd was mixed with 5 μM Cy3-RALF1 and 0.1 mg/ml $OG_{DP10-15}$ in 50 mM sodium acetate, 150 mM NaCl, pH 5.7. Individual FAM-FERecd/RALF1/OG particle was chosen for initial photobleaching by laser 488ex for 2 seconds with laser power 15, and the fluorescence recovery was imaged at 2s intervals for a total of about 5 mins.

For the *in vivo* FRAP experiments of RALF1-triggered receptor clustering, FERp-FER-GFP seedlings were treated with 1 μM RALF1 for 30 mins. Region of interest of RALF1-induced FER-GFP surface particles was chosen for initial photobleaching by laser 488ex for 3 seconds with laser power 20, and the fluorescence recovery was imaged at 4s intervals for 5 mins. RALF1p-RALF1-GFP seedlings were used for stress-trigger receptor clustering. Seedlings were treated with 150 mM NaCl for 30 mins. Regions of interest of salt-induced RALF1-GFP surface particles were chosen for initial photobleaching by laser 488ex for 3 seconds with laser power 20, and the fluorescence recovery was imaged at 4s intervals for about 3 mins.

QUANTIFICATION AND STATISTICAL ANALYSIS

Statistical analysis was performed with Student's *t*-tests (two-tailed, paired). Significance values are indicated on data plots. The statistical details, including n for each measurement, were presented in figure legends and figures. The significant differences were indicated as following: ****, $p < 0.0001$; ***, $p < 0.001$; **, $p < 0.01$; *, $p < 0.05$; ns, not significant, $p > 0.05$. Quantitative data are shown in column-scattered plots (Prism). The center, top and bottom lines show the median, upper, and lower quartiles.

CellPress

Supplemental figures

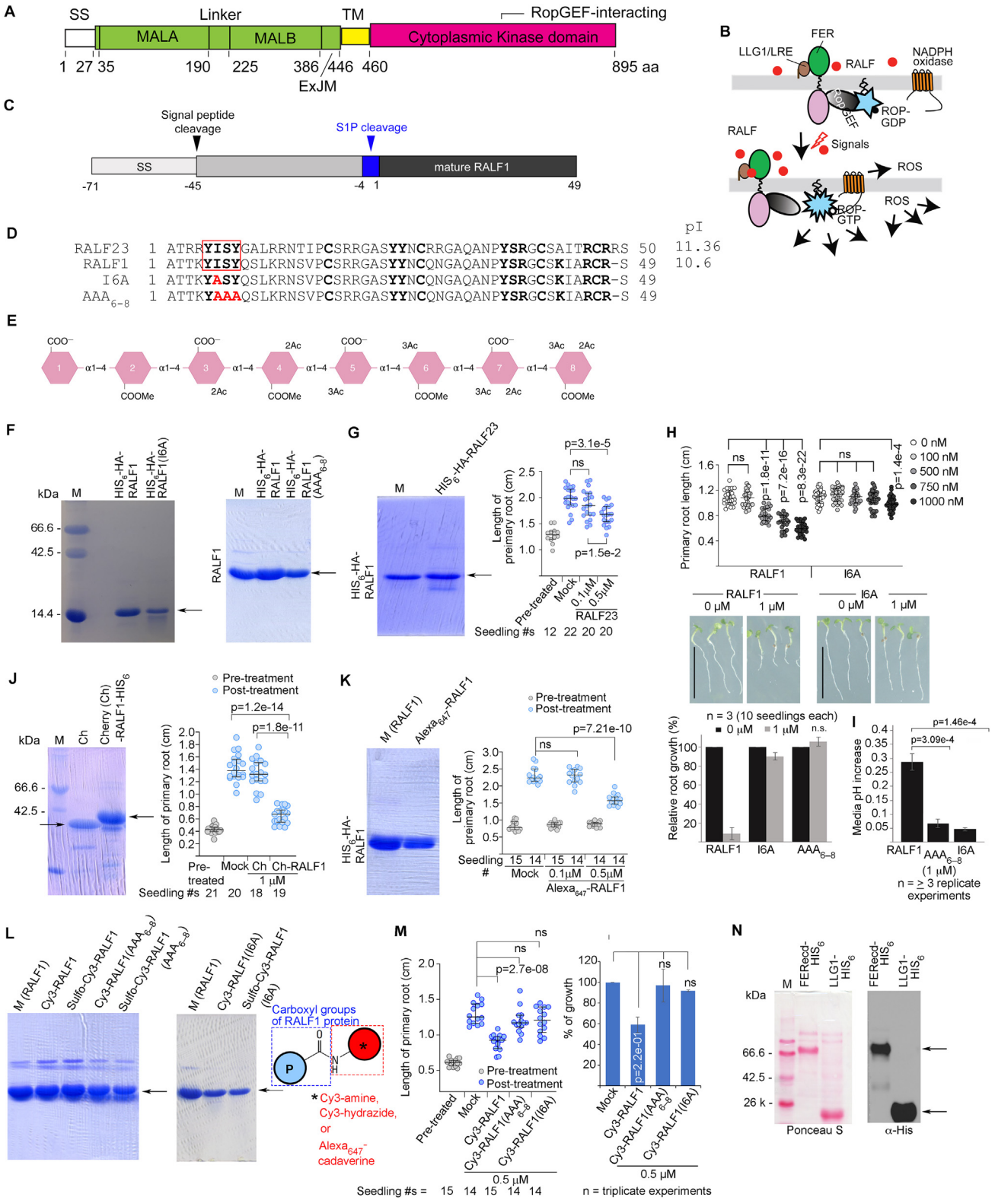

(legend on next page)

Figure S1. FER, RALF1, and related peptides and representative purified proteins used in this study, related to introduction and applicable to Figures 1, 2, 3, 4, 5, 6, and 7

(A) Domain map of FER receptor kinase. SS, signal sequence; MalA, MalB, malectin domains A, B[3,5]; exJM, extracellular juxtamembrane[9]; TM, transmembrane. Numbers, amino acid (aa) positions. MalA, MalB bind pectin[4,17,30]; exJM interacts with LLG1.[9] FER is one of 17 closely related receptor kinases in *Arabidopsis*.[2]

(B) A schematic illustrating the FER-LLG1-ROPGEF-RAC/ROP-NADPH oxidase-dependent ROS signaling pathway. RALFs are the ligands for FER-LLG1 and, with signals that impact their presence in the apoplast, these peptides regulate FER-LLG1 signaling.

(C) Domain map (top) of RALF1 precursor protein. Arrowheads, signal peptide cleavage and S1P[34] cleavage sites to remove pro-peptide region.

(D) Amino acid sequences of RALF23, RALF1 (numbering starts with 1 for the first amino acid of the mature RALF) and two N-terminal region variants I6A and $ISY_{6-8} \rightarrow AAA_{6-8}$ (designated AAA_{6-8}). The N-terminal $YISY_{5-8}$ motif, boxed, is conserved in most RALFs and important for their medium alkalinization activity.[6] RALF1 and RALF23 are closely related,[7] and ligands of FER-LLG1[6,7,23,42]; the identity and similarity between RALF1 and RALF23 are 74% and 86%, respectively. RALF1 is the predominant root-expressed RALF; RALF23 is expressed more strongly in shoot tissues. Their activities in whole plant growth and root growth assays are similar[7] (see below also). Here, RALF1 was used predominantly in *Arabidopsis* seedling root-based assays; RALF23 in leaf-based assays. RALF1 and RALF23 were used and acted similarly in *N. benthamiana*.

(E) Pectin molecular structure (adapted from Du et al.[32]). Pectins are modified homopolymer of α-1,4-linked galacturonides and can have one of eight different modification states of the backbone polysaccharide chain as shown. They are produced in methyl-esterified form (COOMe) and become de-esterified (COO–) in the cell wall.

(F and G) Representative Coomassie-blue-stained SDS-PAGE gels of *E. coli* produced RALF1 and mutants I6A and AAA_{6-8} (F) and RALF23 (G). Every RALF1 preparation was tested for its root growth inhibition and FER-GFP endocytosis activity to determine working peptide concentrations (between 1 and 4 μM).

(H and I) RALF growth-related assays. (H) Root growth assay shows a dose-dependent inhibition profile typical of RALF1; N-terminal I6A and AAA_{6-8} mutants lacked the capacity. (I) Medium alkalinization assays showed typical RALF1 alkalinization activity, but I6A and AAA_{6-8} lacked the capacity.

(J–M) Cherry (Ch)-RALF1, $Alexa_{647}$-RALF1, various Cy3-RALF1, I6A, and AAA_{6-8} mutants. Data plots show root growth inhibition assays, demonstrating that activities were comparable between unlabeled and fluorescent RALF1s. Sulfonylated fluorochromes imposed less solubility issues rendering, e.g., $Alexa_{647}$, is sulfonylated and an often-used tag in similar studies where ligands were monitored.[54] Sulfonulyated and non-sulfonylated fluorochroms acted comparably. Unless indicated otherwise, sulfonylated fluorochromes were used for chemical labeling.

(N) A Ponceau S-stained protein blot and its corresponding immunoblot of insect cell-produced HIS_6-tagged FER extracellular domain (FERecd) and LLG1.

For scatter-dot plots (G, H, and J–M), data are from a representative experiment repeated at least three times with similar results; histograms (H, I, and M) show the average of at least three replica experiments (each with $n \geq 10$ seedlings). p values, determined by Student's t tests, two-tailed, paired, are as indicated; n.s, non-significant. M, marker lanes; purified HIS_6-HA-RALF1 was sometimes used as marker. For simplicity, HIS_6 and HA were not included for designations in the text, unless the tags were used for immunodetection.

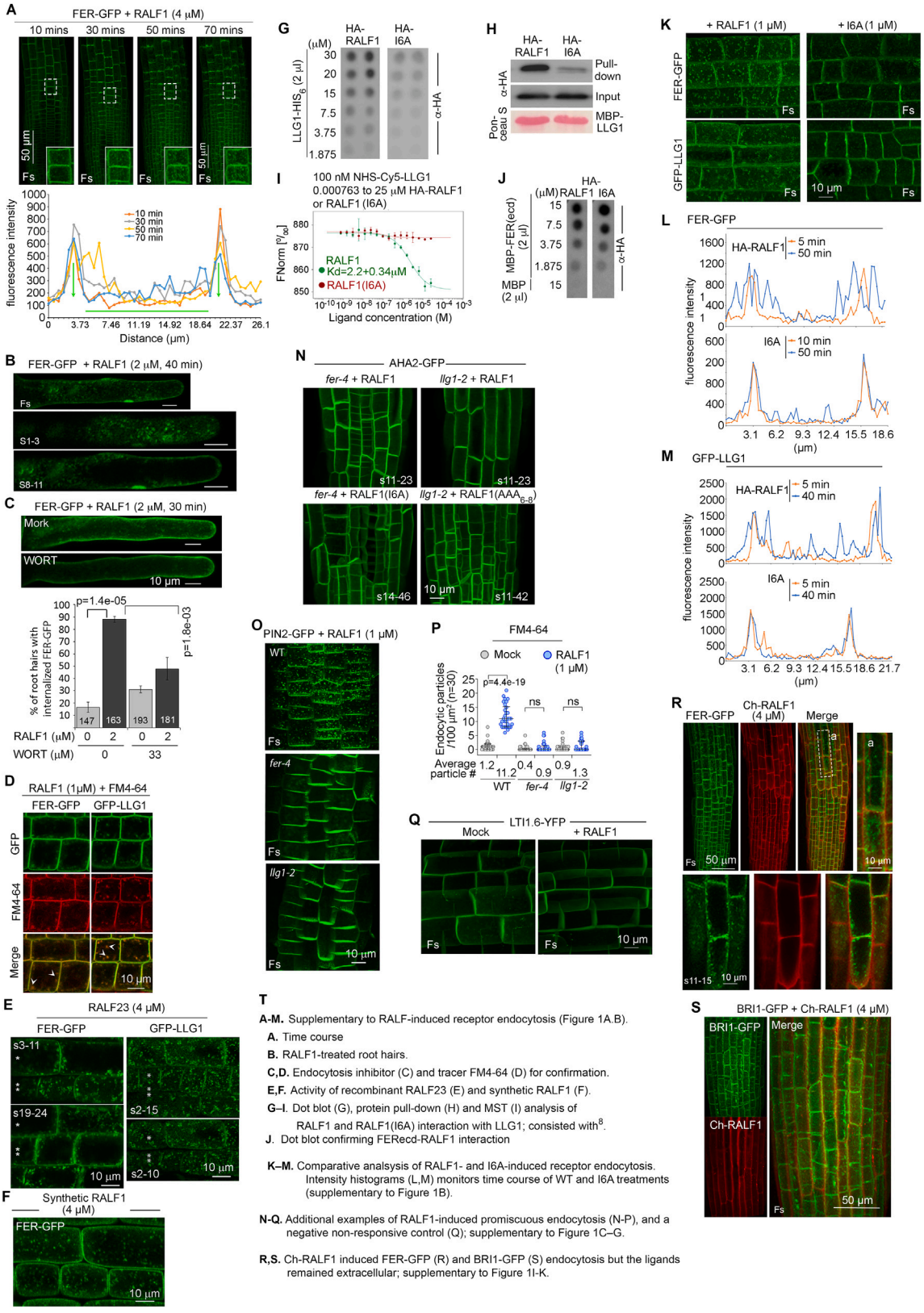

T

A-M. Supplementary to RALF-induced receptor endocytosis (Figure 1A.B).

A. Time course

B. RALF1-treated root hairs.

C,D. Endocytosis inhibitor (C) and tracer FM4-64 (D) for confirmation.

E,F. Activity of recombinant RALF23 (E) and synthetic RALF1 (F).

G–I. Dot blot (G), protein pull-down (H) and MST (I) analysis of RALF1 and RALF1(I6A) interaction with LLG1; consisted with[8].

J. Dot blot confirming FERecd-RALF1 interaction

K–M. Comparative analsysis of RALF1- and I6A-induced receptor endocytosis. Intensity histograms (L,M) monitors time course of WT and I6A treatments (supplementary to Figure 1B).

N-Q. Additional examples of RALF1-induced promiscuous endocytosis (N-P), and a negative non-responsive control (Q); supplementary to Figure 1C–G.

R,S. Ch-RALF1 induced FER-GFP (R) and BRI1-GFP (S) endocytosis but the ligands remained extracellular; supplementary to Figure 1I-K.

(legend on next page)

Figure S2. RALF-induced promiscuous endocytosis, related to Figure 1

Methods are as described for Figure 1 and in STAR Methods section.

(A–E) Pilot experiments on RALF1-induced FER and LLG1 endocytosis studies.

(A) Time course of RALF1-triggered FER-GFP endocytosis in root meristematic and transition zones. Boxed areas are shown in insets, enlarged 2.5×, contrast and brightness adjusted equally to highlight increasing levels of internalized FER-GFP with time. Typically, cytoplasmic FER-GFP particles were evident starting from ~10 min upon treatment, comparable to similar endocytosis detection time course in plant ligand-induced receptor endocytosis studies.[34,44–46,55] Endocytosis became robust between 20 and 30 min and continued to increase till saturation at about 50–60 min. Routinely, observations were made between 15 and 60 min after ligand application, most data shown were collected between 30 and 40 min, a time frame often used in other ligand-induced receptor endocytosis experiments, e.g., for BRI1, FLS2.[34,44–46,55] Fs, maximum intensity projection of a full stack; s#s, range of sections covering similar tissue thickness used for the maximum projection image shown.

(B) RALF1-induced FER-GFP endocytosis in root hairs.

(C) RALF1 treatment of root hairs with or without wortmannin (WORT), a commonly used inhibitor of endocytosis.[90] Typically, WORT treatment alone induced a low level of intracellular particles. Despite this, its counter effect on RALF1-induced intracellular particles was evident. Data = average ± SD (n = 3 replicates, ≥50 root hairs per replicate; # in data bars = total root hairs. p values by Student's t tests (two-tailed, paired) as indicated.

(D) RALF1 and endocytic membrane stain FM4-64[53] co-treatment of root cells, showing colocalization of RALF1-induced FER-GFP- and GFP-LLG1-labeled cytoplasmic particles and FM4-64 (arrowheads, representative), consistent with the GFP- puncta being endocytic particles. All image panels were brightness adjusted equally. These pilot experiments (A–D) guided experimental conditions used in the bulk of the studies presented here. Every preparation of RALF peptides were tested first for their biological efficacy (Figure S1). 1–4 μM RALFs were used depending on preparations, without qualitative differences.

(E and F) RALF23- and synthetic RALF1 peptide-induced FER-GFP endocytosis.

(G–J) Comparative RALF1 and mutant I6A interaction with LLG1 (G–I). Dot blot (G), protein pull-down assay (H), and microscale thermophoresis (MST) (I) showed I6A with compromised capacity to bind LLG1. Dot blots had immobilized receptor proteins and ligands in solution (500 nM). MST uses Cy5-LLG1 as a target for RALF1 and I6A. Results were consistent with previous reports.[8] (J) Dot blot showing RALF1 and I6A with comparable capacity to bind immobilized FERecd. Data shown are representative of at least three independent experiments with comparable results.

(K–M) Comparative RALF1- and mutant I6A-induced FER and LLG1 endocytosis. Supplementary to Figure 1A data plot (K). Histograms of FER-GFP (L) and GFP-LLG1 (M) signal intensity across cells treated with WT RALF1 (upper) or mutant I6A (lower). Results show RALF1 induced increasing intracellular receptor signals with time relative to plasma membrane signals while I6A did not affect plasma membrane signals. Data supplements Figure 1B, which shows quantified data of total intracellular signal: plasma membrane signal over the entire time course.

(N–P) RALF-induced endocytosis of non-cognate targets, AHA2-GFP (N), PIN2-GFP (O), and FM4-64 uptake (P) in WT but not *fer-4* or *llg1-2*. Data supplements Figures 1C–1H.

(Q) LTI1.6-YFP, a commonly used cell membrane marker protein,[20] did not respond to RALF1.

(R) Ch-RALF1 induced receptor endocytosis but itself remained extracellular. Box (a) is shown magnified to highlight the extracellular Ch-RALF1 signal. S# in bottom row indicates maximum projection of five 0.25 μm optical sections.

(S) Ch-RALF1-treated BRI1-GFP expressing seedling root showing robust BRI1-GFP endocytosis with Ch-RALF1 remained extracellular. Similar observations were made for Ch-RALF1 induced PIN2-GFP endocytosis (see Figure 1E).

(T) A list providing an experimental flow for the results reported in this figure.

Ligand concentrations were as indicated; where not indicated, treatment time was 40 min. In images where Fs or s# are not indicated, single optical sections are shown. Maximal intensity projections of comparative samples cover similar tissue thickness. Intracellular signal and cytoplasmic particle quantification was as described in Figure 1 and in STAR Methods. In each experiment, ≥3 replicate seedlings per treatment and 3–5 100 μm^2 from each seedling were quantified for particles ≥0.25 μm. p values by Student's t tests (two-tailed, paired) are as indicated; n.s., non-significant. All experiments were repeated at least three times with comparable results.

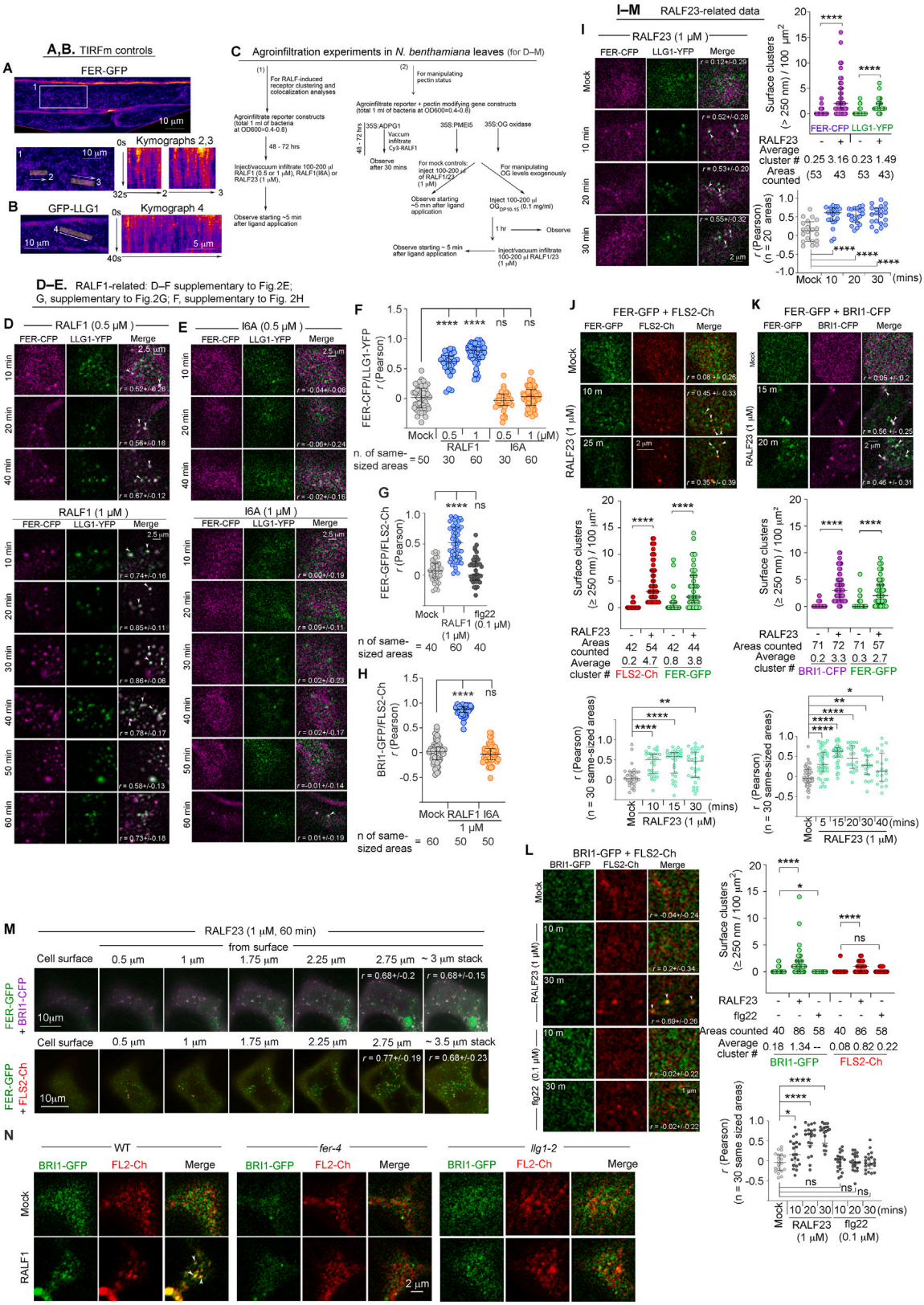

(legend on next page)

Figure S3. RALF-induced FER and LLG1 clustering and endocytosis, related to Figure 2

(A and B) TIRFm imaging of mock-treated *Arabidopsis* seedling root cells expressing FER-GFP (A) or GFP-LLG1 (B). Enlarged Box 1 highlights FER-GFP signal along the cell membrane. Arrows 2, 3, and 4 mark locations and directions for kymographs, showing that FER-GFP and GFP-LLG1 signals remained relatively stable in locations, not displaying significant lateral displacements or internalization beyond TIRF range, contrary to receptor clustering and endocytosis observed in RALF1-treated samples shown in Figures 2C and 2D and Videos S1, S2, S3, and S4.

(C–M) Analysis in agroinfiltration transiently transformed *N. benthamina* leaf epidermal cells.

(C) Workflow for agroinfiltration experiments. (1) For RALF-induced receptor clustering and endocytosis; (2) for manipulating pectin status in the cell wall reported later (in Figure 5).

(D–F) RALF1 data. RALF1 (D) but not RALF1(I6A) (E) induced clustering of cognate receptors FER-CFP and LLG1-YFP. Responses to two ligand concentrations (0.5 and 1 μM) were monitored between 10 and 60 min. Results summary: with 1 μM RALF1, notable receptor clusters were routinely observed by 10 min after ligand application whereas they were just beginning to gather in 0.5 μM RALF1-treated samples. Robust receptor clusters were typical by 30–40 min after ligand application, their extent correlated with RALF1 dosage (see Figure 2E). Quantitative analysis showed that by 30–40 min after ligand application, receptor clusters ($\geq$250 nm) were significantly more prevalent in RALF1-treated samples than in the mock or I6A-treated samples (see Figure 2E). These parameters also informed on the regime of experimental conditions for later agroinfiltration experiments. Arrowheads highlight representative co-clusters. (F) Pearson's correlation coefficient (r) analysis demonstrating RALF1 but not I6A induced significant colocalization of the cognate co-receptor pairs; average *r* is indicated in corresponding image panels.

(G–H) RALF1 data. (G and H) Full data from Pearson's correlation coefficient (r) analysis of ligand-induced co-clustering of cognate and non-cognate receptors shown in Figures 2G and 2H. RALF1 but not flg22 induced significant co-clustering of FER-GFP and FLS2-Ch (G). Mutant I6A had a significantly diminished capacity to induce BRI1-GFP and FLS2-Ch co-clustering relative to RALF1 (H).

(I–M) RALF23 acted similarly as RALF1 (shown in Figure 2). (I) RALF23 induced FER and LLG1 co-clustering showing time-dependence; results were comparable to that by RALF1 treatment. (J and K) RALF23 induced FER-GFP and FLS2-Ch co-clustering (J) and FER-GFP and BRI1-CFP co-clustering (K). Pearson's correlation coefficients (*r*) show considerable levels of colocalization of FER-GFP with each of the other two receptors.

(L) RALF23 induced co-clustering of non-cognate targets BRI1-GFP and FLS2-Ch (2nd and 3rd rows); flg22 treatment was similar to mock, few in number of receptors clusters and they did not colocalize (4th and 5th rows). Two single cell surface sections (each 0.25 μm) are shown in (J)–(L).

(M) RALF23 induced endocytosis of FER-GFP and BRI1-CFP (upper) and FER-GFP and FLS2-Ch (lower). Images are stacks of two contiguous 0.25 μm sections (from the cell surface to progressively more cytoplasmic regions (indicated as increasing μm from the cell surface in the image panels). The last image of each row shows maximum intensity projection of images covering 3–3.5 μm cell thickness, showing an abundance of endocytosed receptor particles.

(N) RALF1-induced co-clustering of non-cognate receptors BRI-GFP and FLS2-Ch in WT but not *fer-4* or *llg1-2* seedling leaf cells, demonstrating FER and LLG1 dependence.

Data quantification was as detailed in Figure 2 legend. For quantification of cluster numbers, clusters $\geq$0.25 μm in 100 μm^2 areas were analyzed according to Bücherl et al.[55] (NIS analysis software); Pearson's correlation coefficient of colocalization (r) (arrowheads show represented clusters) used FIJI according to Bücherl et al.[55] and were from $\geq$20 equal-sized regions of interest from three replicate samples for each treatment in one experiment. Random sampling of equal-sized areas of interest (by Nikon NIS analytical software) yielded comparable results. p values were by Student's t tests (two-tailed, paired); *$p < 0.05$, **$p < 10^{-2}$, ****$p < 10^{-4}$; n.s., non-significant difference. Each experiment was repeated at least three times with comparable results.

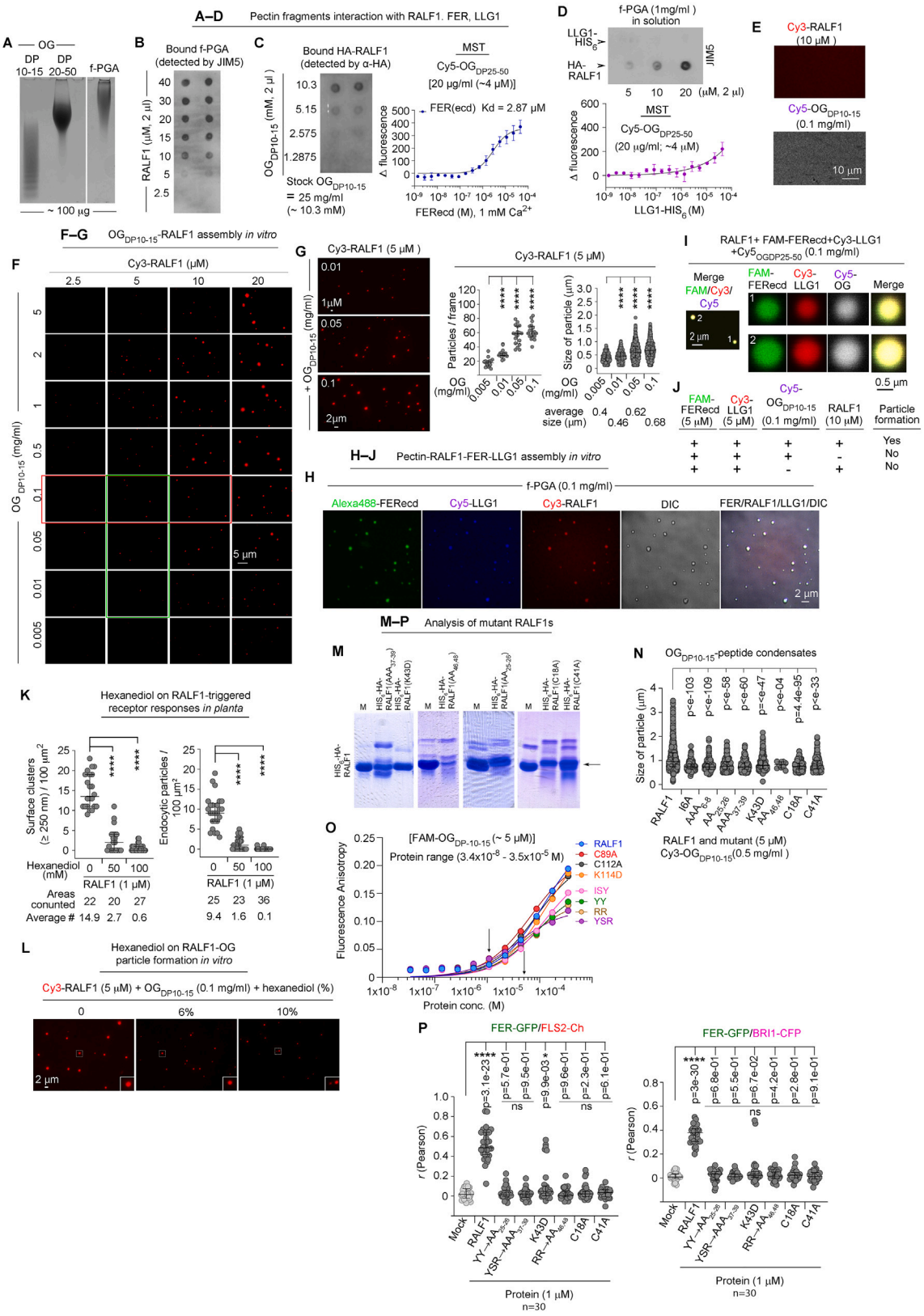

(legend on next page)

Figure S4. Pectin-RALF interaction drives phase separation formation of pectin-RALF-FER-LLG1condensates *in vitro*, related to Figures 3 and 4

(A–D) Pectin interacts with RALF1, FERecd but not LLG1.

(A) OG and pectic fragments used. $OG_{DP10–15}$ and $OG_{DP25–50}$ was from Biosynth; fragmented PGA (f-PGA) was from PGA (Sigma-Aldrich) after sonication.

(B) Dot blot of immobilized RALF1 binding to f-PGA (in solution, 2 mg/mL) and signal quantification.

(C) Dot blot of immobilized $OG_{DP10–15}$ interaction with HA-RALF1 (1 μM in solution) and MST for Cy5-$OG_{DP25–50}$ and FERecd binding.

(D) Immobilized LLG1-His_6 interaction with f-PGA (1 mg/mL in solution) and MST of LLG1-His_6 and Cy5-$OG_{DP25–50}$ interaction, both showing no LLG1-RALF1 interaction. On dot blots, bound pectic fragments were detected by JIM5, monoclonal antibody for de-esterified pectin,[81] and bound HA-RALF1 by anti-HA antibody.

(E) Cy3-RALF1 and Cy5-$OG_{DP25–50}$ alone remained in solution.

(F) Concentration dependence for $OG_{DP10-15}$ and RALF1 assembly *in vitro*. Images are representative of data used for the phase map in Figure 3H.

(G) Representative data of $OG_{DP10–15}$ and RALF1 assembly dependence on OG concentration.

(H and I) Pectic fragments of variant sizes, f-PGA (H) and Cy5-$OG_{DP25-50}$ (I) support *in vitro* assembly of pectic-RALF-FER-LLG1 particles. (1, 2 in I) are representative particles assembled from unlabeled RALF1 and other labeled components shown in a merged panel and three single channels for the other labeled components.

(J) Summary data showing assembly of FER and LLG1 required both pectic fragments and RALF.

(K) Data quantification hexanediol inhibition of RALF1-triggered FER-GFP clustering *in vivo*.

(L) Impact of hexanediol on $OG_{DP10–15}$-RALF1 assembly *in vitro*.

(M–P) Characterization of mutant RALF1s. RALF1 amino acid sequence and substitutions in mutant RALF1s are shown in Figure 4A. (M) Mutant RALF1 preparations. (N) Full quantification data for particle sizes. (O) Fluorescence anisotropy of $OG_{DP10–15}$ interaction with WT and mutant RLAF1s, data cover the entire peptide concentration range. Data between the arrows are shown in Figure 4D. (P) Full Pearson's coefficient of colocalization for FER co-clustering with FLS2 (left) and BRI1 (right).

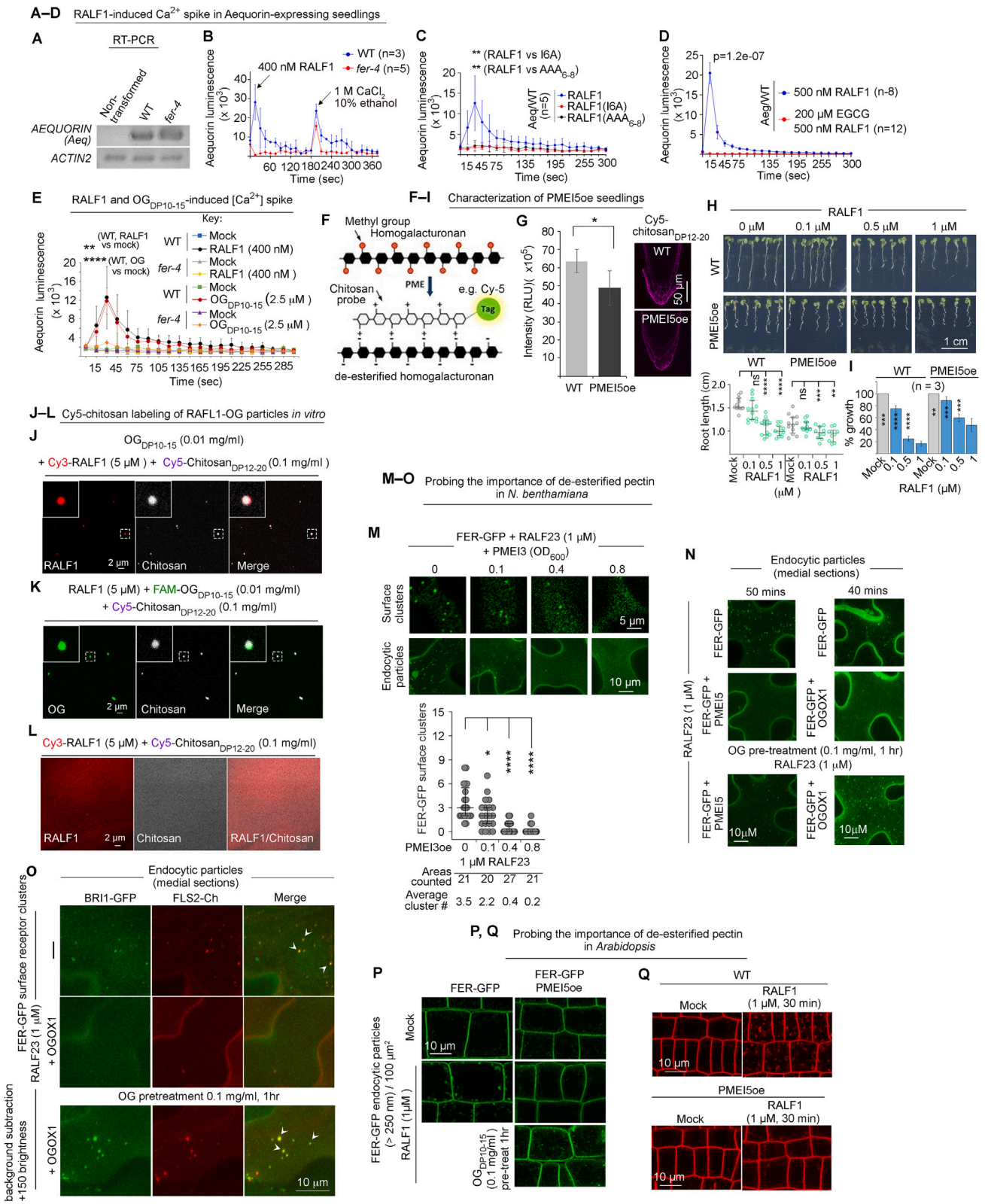

(legend on next page)

Figure S5. RALF-triggered RALF-pectin assembly and pectin-RALF-receptor clusters in the cell surface, related to Figures 3 and 5

(A–D) RALF-triggered rapid increase in cytosolic [Ca^{2+}]. (A) RT-PCR for aequorin expression in WT and *fer-4* seedlings. (B) RALF1-triggered cytosolic [Ca^{2+}] spike in WT but not *fer-4*.

Gene expression (A) and the response to terminal discharge of $CaCl_2$ (according to Matthus et al.[89]) (B) confirmed aequorin expression in both WT and *fer-4* seedlings, ascertaining Ca^{2+} influx dependence on FER. (C) RALF1 but not N-terminal YISY motif mutants (I6A, $AAA_{6–8}$) triggered Ca^{2+} influx. (D) RALF1-triggered [Ca^{2+}] spike was blocked by EGCG, which inhibits PMEI activity,[66,67,70] thus reducing de-esterified pectin in the cell wall.[66–68] The result demonstrates an intact cell wall is critical for the early RALF-signaled response.

(E) $OG_{DP10–15}$ induced [Ca^{2+}] spike in WT but not *fer-4*, similar to RALF1.

(F–I) Characterization of PMEI5oe seedlings.[67] (F) Chitosan-de-esterified pectin interaction. Cy5-$Chitosan_{DP10–20}$ was used here as a diagnostic for de-esterified pectin. The positively charged amino groups in chitosan align with the negatively charged carboxyl groups in de-esterified homogalacturonan, rendering fluorescence-labeled chitosan a good reporter for de-esterified pectin, including for its status in plants.[68,71]

(G–I) Analysis of 35S::PMEI5 expressing (PMEI5oe) seedlings.[67,69] (G) WT and PMEI5oe seedlings were treated with Cy5-chitosan according to Mravec et al.[71] and Xu et al.,[68] showing reduced Cy5-chitosan signal in PMEI5oe, confirming lower level of de-esterified pectin in these seedlings relative to WT as established previously.[67,69] (H and I) PMEI5oe seedlings were less sensitive to RALF1-inhibited root growth. Seedlings were treated with RALF1 for 2 days. Root lengths were measured before and after RALF1 treatment. Under normal growth condition, PMEI5oe roots were shorter than WT and they were significantly less sensitive to RALF1-induced root growth inhibition, implying that de-esterified pectin is important for RALF1 activity. (H) From one representative experiment. (I) Averaged from three replicate experiments, showing RALF1 dose-dependent growth inhibition relative to mock-treated controls. Growth data quantification followed that described in Figure S1 legend and in STAR Methods.

(J–L) Cy5-chitosan binding as a reporter for de-esterified pectin in *in vitro* phase-separated RALF1-OG condensates. Data supplements Figures 5C–5E, which shows *in planta* results. (J and K) Cy5-chitosan colocalized with *in vitro* assembled Cy3-RALF1-$OG_{DP10-15}$ particles (J) and FAM-$OG_{DP10–15}$-RALF1 particles (K).

(L) Cy3-RALF1 and Cy5-chitosan in the absence of OG remained in solution.

(M–Q) De-esterified pectin was important for RALF-induced receptor clustering.

(M–O) Agroinfiltration experiments.

(P and Q) *Arabidopsis* seedling experiments.

(M) Over-expression of PMEI3 inhibited RALF1-triggered FER-GFP surface clustering and endocytosis; results were similar to those from PMEI5 treatment (Figure 5G). The response showed a typical dose-dependent response to input PMEI3 (as indicated by Agrobacterium OD_{600}).

(N) RALF23 induced FER-GFP endocytosis (top row) was suppressed by PMEI5 and OGOX1 (middle row) and reversed by OG application (bottom row), similar to results on their clustering shown in Figures 5G and 5H.

(O) RALF23 induced endocytosis of BRI1-GFP and FLS2-GFP (top row) was suppressed by OGOX1 (middle row), and reversed by OG application (bottom row), similar to results on their clustering shown in Figure 5I.

(P) FERp::FER-GFP in PMEI5oe transformed *Arabidopsis* showed RALF1-induced FER-GFP endocytosis was suppressed by PMEI5 over-expression, but restored by OG application, similar to that observed in *N. benthamiana* experiments.

(Q) FM4-64 uptake showing that RALF1-elevated general endocytosis was suppressed in PMEI5oe transformed seedlings. Images supplements quantified data shown in Figures 5J and 5K.

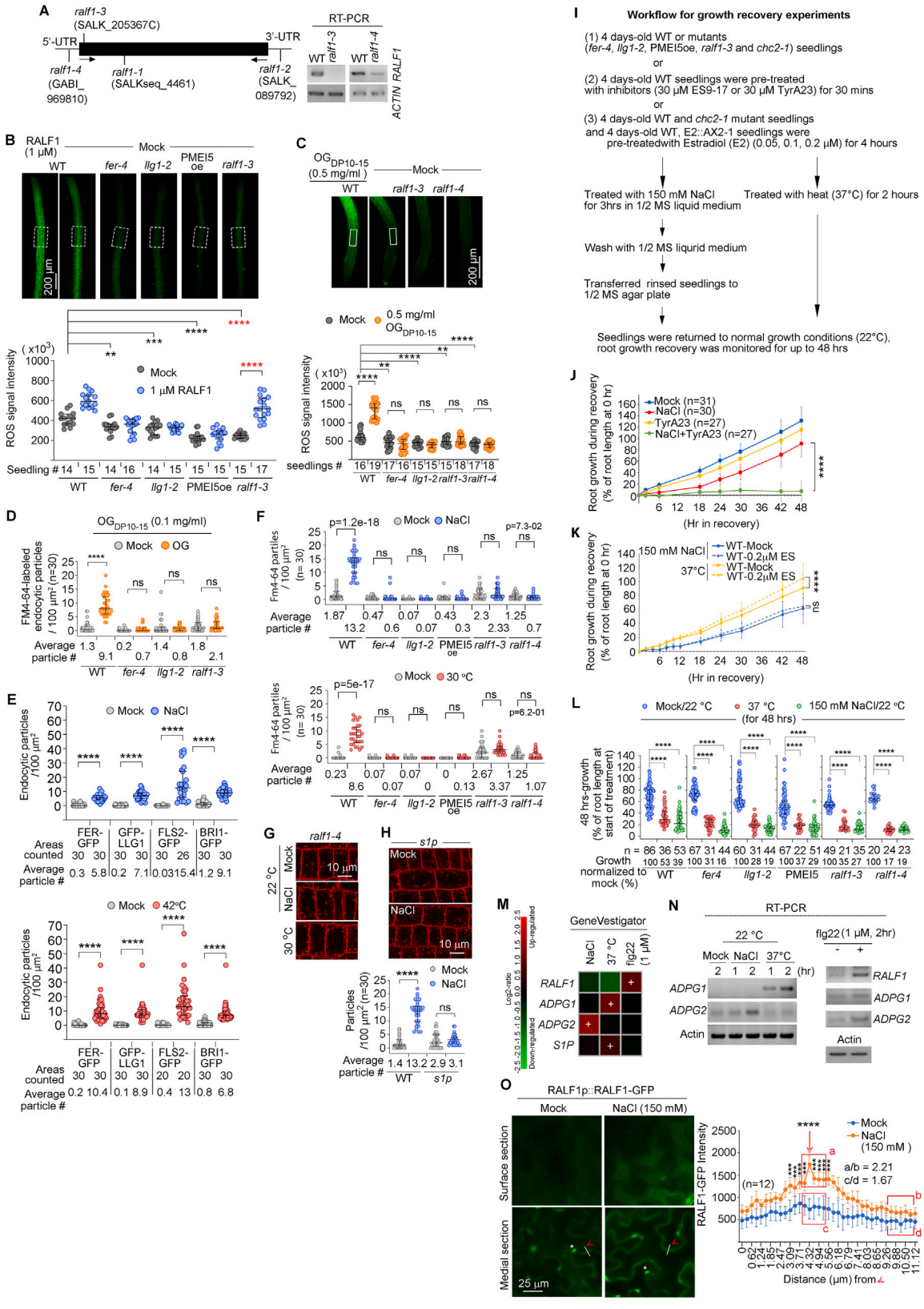

(legend on next page)

Figure S6. Biological impact of pectin-RALF-FER-LLG1 signaling, related to Figures 6 and 7

(A) T-DNA insertion mutations in RALF1 and RT-PCR analysis of RALF1 expression levels in *ralf1-3* (null) and *ralf1-4* (strongly suppressed).

(B and C) H_2DCF-DA detection of ROS in the roots of WT and mutant seedlings defective in each of the components of the pectin-RALF-FER-LLG1 ensemble. Results show reduced levels of ROS in mutant roots. Data supplements results from RALF1 and $OG_{DP10–15}$-treatment in Figures 6B and 6C.

(D) Quantification of FM4-64 uptake in response to $OD_{DP10–15}$ in WT and mutants defective in the RALF1, FER, or LLG1. Data supplements Figure 6D.

(E) Quantification of RALF-induced endocytosis of multiple fluorescent protein-tagged cell surface regulators, FER, LLG1, BRI1, and FLS2, in *Arabidopsis* seedlings. Data supplements Figure 6E.

(F) Quantified data for salt and heat stress-induced FM4-64 internalization in WT and seedlings defective in individual components of the pectin-RALF1-FER-LLG1 ensemble. Data supplements Figure 6G.

(G) FM4-64 uptake in *ralf1-4* showing a higher basal level of internalized FM4-64 under control conditions but was insensitive to RALF-stimulation of FM4-64 uptake as shown by quantified data (Figure S6F). Results were similar to those from *ralf1-3* (in Figure 6G) and *s1p*[34] (in H).

(H) FM4-64 uptake in salt-stressed WT and *s1p* seedlings. Seedling were pretreated with FM4-64 then maintained under normal growth or salt-stressed (150 mM NaCl for 15 min) conditions. Loss of S1P, the protease that generates pre-RALFs facilitating their secretion,[34] rendered higher basal levels of internalized FM4-64 relative to WT, similar to observed in *ralf1* mutants (G and Figure 6G). Importantly, salt stress-stimulated FM4-64 internalization was suppressed in *s1p* seedlings, similar to *ralf1* mutants being insensitive to heat- and high salt-stimulated FM4-64 uptake (Figures 6G, S6F, and S6G). These results support that secreted mature RALFs are required for salt- and heat-stress-stimulated endocytosis and underscore that reduced levels of apoplastic RALFs are generally stressful.

(I) Workflow for plant growth recovery after stress followed by studies shown in Figures 6I–6L, S6J, and S6K.

(J) Inhibiting clathrin-dependent endocytosis inhibitor TyrA23 suppressed growth recovery from high salt- and elevated temperature. While ES9-17 is currently the gold standard,[77] TyrA23 has been classically used in many endocytosis studies, including in plant cells. Similar to ES9-17, TyrA23 had mild influence on growth recovery under normal growth conditions but significantly inhibited growth recovery after salt stress. Together with results from ES9-17, mutations impacting clathrin-dependent encotytosis (Figures 6I–6K), the TyrA23 results provide an additional set of observations as support.

(K) Control growth recovery experiments showing estradiol (ES) treatment of WT seedlings after salt- and heat-stress were comparable. Data supplements Figures 6J and 6K.

(L) Salt- and heat-induced growth suppression in WT and seedlings defective in individual components of pectin-RALF1-FER-LLG1 ensemble. 3-day-old seedlings were transferred from normal (22°C, no supplemental NaCl) to stress conditions (150 mM NaCl, or 37°C) for 48 h. Root lengths were measured at the start and end of stress treatments. Results showed that *fer-4*, *llg1-2*, *ralf1-3*, *ralf1-4*, and PMEI5oe lines were all hypersensitive to stress-induced root growth inhibition, consistent with their participation in coping mechanisms to survive stress. Growth (y axis) during treatment is expressed as % of the root lengths at 0 h for individual seedling lines. The approximate averaged % growth for each line under stress normalized to non-stressed seedlings is also shown (below x axis) for each seedling lines.

(M–O) Salt and heat stresses variably impact RALF1 and pectic fragment production. (M) Gene expression data from Genevestogator[79] showing that high salt, high temperature, and the immunity elicitor flg22 augment expression of RALF1, *SIP* which encodes the protease required for RALF maturation and secretion,[34] and ADPG1,2, which produce pectic fragments.[62] (+) on heatmap indicates stress induces increase. (N) RT-PCR data showing similar impacts. (O) Salt-stress-augmented secretion of RALF1-GFP to the cell surface. *N. benthamiana* pavement cells were transformed by RALF1p::RALF1-GFP. (Images) Tangential images across the pavement cell surfaces (top row) show RALF1-GFP signal was notably higher in NaCl-treated than control mock-treated cells. Medial sections (bottom row and quantified data plot) show relatively higher cell surface to intracellular RALF1-GFP signal in NaCl-treated cells relative to mock samples. Quantified signals across the cell boundary of two neighboring cells (white lines) are shown in the data plot. Signals in the histogram are averaged from twelve neighboring pairs of cells. Ratios of average cell surface signal/average cytoplasmic signals (a/b for stressed seedlings; c/d for mock seedlings) reflect higher levels of secreted RALF1-GFP in stressed versus control seedlings, consistent with results showing salt stress stimulated the expression of SIP (Figure 7J), which are secreted to the apoplast after processing by the protease S1P,[34] enhancing the production of mature RALF peptides. Together, these results are consistent with salt and heat stresses stimulate the expression of genes whose products elevate the presence of mature RALFs and pectic fragments on the cell surface.

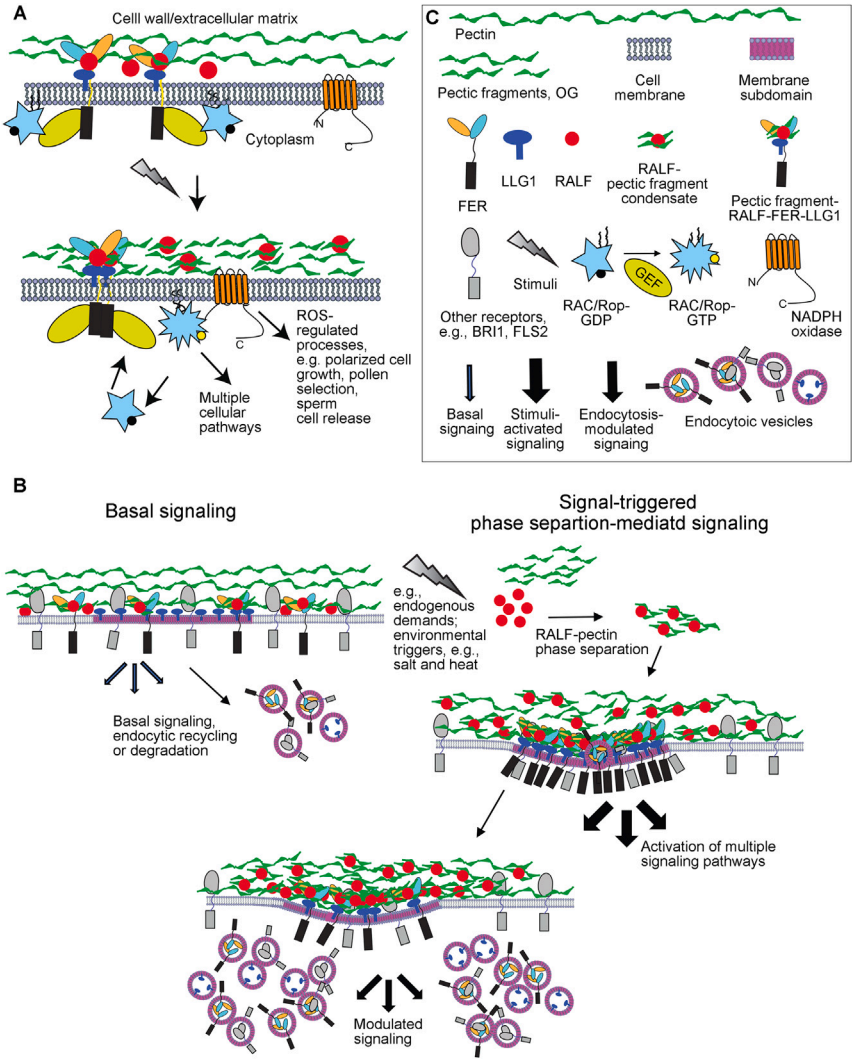

Figure S7. A model for RALF-pectin phase-separation-mediated FER- and LLG1-dependent global signaling, related to all findings in Figures 1, 2, 3, 4, 5, 6, and 7

(A) The FER-LLG1 to RAC/ROP-signaled NADPH oxidase-dependent ROS production pathway.[9,10,15,19] Results in this study demonstrated RALF and de-esterified pectin jointly regulate the FER to ROS pathway (Figures 6B and 6C) and that the pectin-RALF-FER-LLG1 module is crucial for RALF- and OG-triggered [Ca^{2+}] spike within seconds of treatment (Figure S5E), and important for regulating FER-LLG1 dependent cell surface regulator clustering and endocytosis.

(B) Basal and signaled-triggered RALF-pectin phase separation-mediated signaling. (Left) Under normal growth conditions, a basal level of pectic fragments and RALFs in the extracellular matrix maintains a homeostatic level of pectin-RALF-FER-LLG1 ensembles, mediating e.g., a house-keeping level of activities from FER-LLG1 (thin block arrows). (Right) Results here support that elevating RALF or pectic fragments facilitates RALF-pectin phase separation driving the formation of pectin-RALF-FER-LLG1 ensembles as well as recruiting other cell surface regulators into the phase-separated molecular condensates. Increases in pectic fragments and apoplastic RALFs could be induced by endogenous needs, e.g., to support cell expansion and morphogenesis, or exogenously, e.g., when plants encounter environmental stresses such as heat and salinity (Figures 7J, 7K, and S6M–S6O). Increased concentrations of these regulators in the cell surface clusters would trigger the activation of FER-LLG1 signaling as well as that from diverse regulators also recruited into these phase-separated cell surface clusters (thick block arrows). The widespread cell surface responses (Figures 6E–6G) would enable the broad FER-LLG1 functional range, including coping with environmental stresses demonstrated here. Ligand-induced receptor clustering induces membrane bending and triggers the recruitment of cytoplasmic factors to initiate endocytosis.[57,58] The consequential massive endocytosis after RALF-triggered receptor clustering would moderate the activated pathways to sustain the needed signal-triggered responses (medium-sized block arrows).

(C) Key for symbols used. Note: thickness of block arrows signify differential signaling strengths from basal (thinnest) to signal activated (thickest) to endocytosis modulated (intermediate).